

## PERSONNEL

Dr. James D. Patterson, Principal Investigator  
Professor and Head  
Physics and Space Sciences Department  
Florida Institute of Technology

*James D. Patterson*

Dr. Weigang Li, Post-Doctoral Research Associate  
Physics and Space Sciences Department  
Florida Institute of Technology

*Weigang Li*

# Electronic Characterization of Defects in Narrow Gap Semiconductors

## ABSTRACT

We use a Green's function technique to calculate the position of deep defects in narrow gap semiconductors. We consider substitutional (including antisite), vacancy, and interstitial (self and foreign) deep defects. We also use perturbation theory to look at the effect of non-parabolic bands on shallow defect energies and find non-parabolicity can increase the binding by 10% or so. We consider mercury cadmium telluride (MCT), mercury zinc telluride (MZT) and mercury zinc selenide (MZS). For substitutional and interstitial defects we look at the situation with and without relaxation.

For substitutional impurities in MCT, MZT, and MZS, we consider  $x$  (the concentration of Cd or Zn) in the range  $0.1 < x < 0.3$  and also consider appropriate  $x$  so  $E_g = 0.1$  eV for each of the three compounds. We consider several cation site s-like deep levels and anion site p-like levels. For  $E_g = 0.1$  eV, we also consider the effects of relaxation. Similar comments apply to the interstitial deep levels whereas no relaxation is considered for the ideal vacancy model. Relaxation effects can be greater for the interstitial than the substitutional cases.

Specific results are given in figures and tables and comparison to experiment is made in a limited number of cases. We find, for example, that I, Se, S, Rn, and N are possible cation site, s-like deep levels in MCT and Zn and Mg are for anion site, p-like levels; both levels for substitutional cases. The corresponding cation and anion site levels for interstitial deep defects are (Au, Ag, Hg, Cd, Cu, Zn) and (N, Ar, O, F). For the substitutional cases we have some examples of relaxation moving the levels into the band gap, whereas for the interstitial case we have examples where relaxation moves it out of the band gap. Future work involves calculating the effects of charge state interaction and seeing the effect of relaxation on vacancy levels.

# ELECTRONIC CHARACTERIZATION OF DEFECTS IN NARROW GAP SEMICONDUCTORS

I.	Introduction .....	1
II.	Deep Levels of Point Defects in Semiconductors .....	1
A.	Green's Function Method .....	1
B.	Ideal Vacancy Model .....	2
C.	Band Structure .....	2
D.	Lattice Relaxation and Molecular Dynamics Approach .....	2
E.	Interstitial Defects .....	3
F.	Summary of Results for MCT, MZT, and MZS .....	5
1.	Results for Substitutional Defects (including antisite defects) .....	5
a.	Deep levels as a function of the composition $x$ ...	5
b.	Predicted deep levels with no relaxation .....	6
c.	Effects of lattice relaxation .....	7
d.	Effects of lattice relaxation on deep levels .....	8
2.	Results for Vacancies .....	9
3.	Results for Interstitial Impurities .....	9
a.	Predicted deep levels with no relaxation .....	9
b.	Effects of lattice relaxation .....	10
4.	Comparison with Experiment .....	10
5.	Comparison with Other Theories .....	11
a.	Lattice relaxation of substitutional impurities in HgTe .....	11
b.	Interstitial impurities in MCT .....	11
III.	Work to be Done Later .....	12
IV.	Results for Shallow Levels in II-VI Materials .....	20
V.	Appendices .....	52
A.	References .....	52
B.	Publications and Reports Prepared for this Work .....	54
a.	Semi-Annual Report .....	54
b.	March APS Meeting .....	54
c.	Space Grown Crystals .....	54
d.	Narrow Gap Semiconductors .....	54

## TABLES

1.	Effects of Lattice Relaxation on Substitutional Deep Levels .....	16
2.	Effects of Lattice Relaxation on Interstitial Deep Levels .....	17
3.	Comparison of the Predicted Deep Levels from the Present Theory with Experimental Data .....	19
4.	Results for Shallow Levels in II-VI Materials .....	21

## FIGURES

1.	Substitutional Deep Levels in MCT as a Function of x	(cation-site, s-like)	23
2.	Substitutional Deep Levels in MCT as a Function of x	(anion-site, p-like)	24
3.	Substitutional Deep Levels in MZT as a Function of x	(cation-site, s-like)	25
4.	Substitutional Deep Levels in MZT as a Function of x	(anion-site, p-like)	26
5.	Substitutional Deep Levels in MZS as a Function of x	(anion-site, p-like)	27
6.	Substitutional Deep Levels in MCT for $E_g = .1$ eV	(cation-site, s-like)	28
7.	Substitutional Deep Levels in MCT for $E_g = .1$ eV	(anion-site, p-like)	29
8.	Substitutional Deep Levels in MZT for $E_g = .1$ eV	(cation-site, s-like)	30
9.	Substitutional Deep Levels in MZT for $E_g = .1$ eV	(anion-site, p-like)	31
10.	Substitutional Deep Levels in MZS for $E_g = .1$ eV	(anion-site, p-like)	32
11.	Substitutional Deep Levels in MCT for $E_g = .1$ eV with Lattice Relaxation		
	(cation-site, s-like)		33
12.	Substitutional Deep Levels in MCT for $E_g = .1$ eV with Lattice Relaxation		
	(anion-site, p-like)		34
13.	Substitutional Deep Levels in MZT for $E_g = .1$ eV with Lattice Relaxation		
	(cation-site, s-like)		35
14.	Substitutional Deep Levels in MZT for $E_g = .1$ eV with Lattice Relaxation		
	(anion-site, p-like)		36
15.	Substitutional Deep Levels in MZS for $E_g = .1$ eV with Lattice Relaxation		
	(anion-site, p-like)		37
16.	Vacancy Deep Levels	(cation-site, s-like)	38
17.	Vacancy Deep Levels	(anion-site, p-like)	39
18.	Interstitial Deep Levels in MCT	(cation-site, s-like)	40
19.	Interstitial Deep Levels in MCT	(anion-site, p-like)	41
20.	Interstitial Deep Levels in MZT	(cation-site, s-like)	42
21.	Interstitial Deep Levels in MZT	(anion-site, p-like)	43
22.	Interstitial Deep Levels in MZS	(cation-site, s-like)	44
23.	Interstitial Deep Levels in MZS	(anion-site, p-like)	45
24.	Interstitial Deep Levels in MCT with Lattice Relaxation	(cation-site, s-like)	46
25.	Interstitial Deep Levels in MCT with Lattice Relaxation	(anion-site, p-like)	47
26.	Interstitial Deep Levels in MZT with Lattice Relaxation	(cation-site, s-like)	48
27.	Interstitial Deep Levels in MZT with Lattice Relaxation	(anion-site, p-like)	49
28.	Interstitial Deep Levels in MZS with Lattice Relaxation	(cation-site, s-like)	50
29.	Interstitial Deep Levels in MZS with Lattice Relaxation	(anion-site, p-like)	51

## I. INTRODUCTION

In the semi-annual report<sup>(a1)</sup>, we have already presented the background for this work so this report will mainly focus on results.

The main defects we will look at are deep defects caused by short range potentials. We will include substitutional (including antisite), vacancy, and interstitial (self and foreign) deep defects. Some brief results will be given for shallow defects caused by long range potentials, where perturbation theory will be used to look at the effects of non-parabolic bands.

We will consider mercury cadmium telluride, mercury zinc telluride and mercury zinc selenide. They have non-parabolic bands, but are interesting because they have large mobilities, tunable band gaps, are candidates for microgravity growth and are potentially important materials to make infrared detectors<sup>(a2-a4)</sup>.

As is standard, the Green's function technique will be used to calculate the positions of the deep defects.

Note that deep defects may or may not be near the band edge. They are often very important as recombination centers. Shallow defects are near the band edge and in narrow gap semiconductors are often assumed to be fully ionized. Their importance is to supply carriers, but like all defects they may also scatter carriers.

## II. DEEP LEVELS OF POINT DEFECTS IN SEMICONDUCTORS

### A. Green's Function Method

For substitutional defects we showed in the semi-annual report<sup>(a1)</sup> that the Schrodinger wave equation and the definition of Green's Functions lead to

$$\det \left[ I_i - G_i^0(E) V_i \right] = 0 \quad (1)$$

which determines the defect energy levels. This equation is true for both  $A_1$  (s-like) and  $T_2$  (p-like) states, with appropriate choice of  $V_i$  and  $G_i^0(E)$  as discussed in the semi-annual report. The relevant Green's Functions are  $G_i^0(E)$  and the potential of the defect determines the  $V_i$ .

It turns out that the energy bands can be written in terms of diagonal matrix elements as

$$A_1 \text{ levels: } G_{aa}^s = U_s^{-1} \quad (2a)$$

$$T_2 \text{ levels: } G_{aa}^p = U_p^{-1} \quad (2b)$$

where  $U_s$  and  $U_p$  are impurity potentials determined by  $V_s$  and  $V_p$ .

#### B. Ideal Vacancy Model

For the ideal vacancy model  $U_s$  and  $U_p$  can be assumed infinite which equivalently cuts all the bonds, and so

$$G_{aa}^s(E) = 0 \quad (3a)$$

$$G_{aa}^p(E) = 0 \quad (3b)$$

#### C. Band Structure

In order to do our calculations we need to know the band structure, because  $G^0$ , the Green's functions of the perfect crystal, depends on the band structure. For II-VI semiconductors, in principle we also need to include spin orbit interactions. When they can be ignored, which may happen, the presence of spin just doubles the degeneracy.

#### D. Lattice Relaxation

Lattice relaxation, particularly for the substitutional case, has been discussed in the semi-annual report. We showed that differing host and impurity body lengths, due to relaxation, determined the off diagonal elements of the defect potential. The amount of relaxation was computable by molecular dynamics. The ideal vacancy model does not allow relaxation, and the peculiarities of relaxation due to interstitials will be discussed in the next section.

## E. Interstitial Defects

Interstitial impurities play an important role, as point defects, in semiconductors. In fact, self-interstitial impurities and vacancies are the most important native defects in semiconductors. From experiment, it is found that Li, Mg, and the transition metals in Si prefer to occupy the interstitial sites. Furthermore, in the II-VI materials, it is believed that substitutional group-I acceptors may spontaneously move to an interstitial site<sup>(b1)</sup>. In this section, we study tetrahedral - site interstitial s - and p - bonded impurities in MCT, MZT, and MZS. We believe that hexagonal interstitial impurities can also be calculated using a similar model to that described below.

For a substitutional defect in zincblende structure semiconductors, the defect has a tetrahedral symmetry in the materials. That is, there are four nearest-neighbor atoms and twelve second-nearest-neighbor atoms around the defect. If the distance between the defect and the nearest neighbors is  $d$ , then the distance between the defect and its second neighbors is  $1.64d$ . However, the situation of tetrahedral-site interstitial impurities is quite different. In this case, there are four nearest neighbors around an interstitial impurity with a distance  $d$ , but six second neighbors around it with an only slightly greater distance  $1.15d$ . Hence, the nearest-neighbor approximation, which is often used for substitutional defects, is not acceptable for interstitial impurities. In contrast, in a crude approximation the interstitial may be thought of as tenfold coordinated. That is, we may assume that there are ten nearest neighbors around the interstitial impurity.

Sankey and Dow<sup>(b1)</sup> proposed a model to calculate deep levels introduced by a s- and p-bonded impurity occupying an interstitial site of tetrahedral symmetry in Si. This model can be easily extended for II-VI materials. The main points of this model are as follows: The host Hamiltonian  $H_0$  is determined by the Vogl's

$10N \times 10N$   $sp^3s^*$  band structure theory, where  $N$  is the number of unit cells, and the ten states are  $s\uparrow, s\downarrow, px\uparrow, px\downarrow, py\uparrow, py\downarrow, pz\uparrow, pz\downarrow, s^*\uparrow$ , and  $s^*\downarrow$ . The use of excited  $s^*$  orbitals allows a description of the conduction bands that is flexible enough to treat both direct and indirect band gap semiconductors. The interstitial impurity is treated by the  $10N$  host basis orbitals and includes one s orbital and three p orbital centered at the interstitial site. Hence the Hamiltonian matrix for the host plus interstitial impurity is a direct sum  $H_0$  and  $H_I$ , where  $H_I$  is the diagonal  $4 \times 4$  interstitial Hamiltonian.



Therefore, the modeled Hamiltonian takes the schematic block form

$$H = \begin{pmatrix} H_0 & W \\ W^+ & H^I \end{pmatrix}, \quad (4)$$

where  $W$  denotes the coupling matrix elements between the interstitial atom and the host.

The calculation of  $H_0$  is exactly same as that in the case of substitutional defects.  $H^I$  is a 4 x 4 diagonal matrix which has a form as

$$H^I = \begin{pmatrix} \epsilon_s & & & \\ & \epsilon_p & & \\ & & \epsilon_p & \\ & & & \epsilon_p \end{pmatrix}, \quad (5)$$

where  $\epsilon_s$  and  $\epsilon_p$  are the orbital energies of the interstitial impurities. For example, for a neutral self-interstitial impurity in Si,  $\epsilon_s$  and  $\epsilon_p$  are the orbital energies of Si. The elements of the transfer matrix  $W$  are taken to be zero except those between the interstitial atom and its first and second neighbors. The elements coupling the interstitial and the nearest neighbors,  $W_{nn1}$ , are taken to be those of the Vogl et al.<sup>(b2)</sup> tight - binding model and the elements coupling the interstitial and the second neighbors,  $W_{nn2}$ , are taken to be a fraction of  $W_{nn1}$ . In the case of Si, Sankey and Dow assumed that

$$W_{nn2} = 0.4W_{nn1} \quad (6)$$

The deep levels are calculated using the Green's function method as usual. Therefore, they are determined by the determinantal equation

$$\det[1 - G_{\text{ref}}(E) V] = 0, \quad (7)$$

where  $G_{\text{ref}}(E) = (E - H_{\text{ref}})^{-1}$ , and  $H_{\text{ref}}$  is the Hamiltonian of eq (4) with  $H^I = H_{\text{ref}}^I$ . Here  $H_{\text{ref}}^I$  is the Hamiltonian of the neutral, self-interstitial impurity.  $V$  is the

defect potential matrix which has the same form and meaning as that in Hjalmarson's theory. Since the interstitial atom occupies a site of tetrahedral symmetry, the point group symmetry is  $T_d$ . The condition for a deep level in the band gap simply reduces to the familiar conditions as below:

$$\begin{aligned} [G_{\text{ref}}(E)]_{ss} &= (U_s)^{-1}, \\ [G_{\text{ref}}(E)]_{pp} &= (U_p)^{-1}. \end{aligned} \quad (8)$$

To extend this model to be used for II-VI materials, we just need to include the spin-orbital coupling in the calculations. In the new model, the host Hamiltonian  $H_0$  is now determined by the  $20N \times 20N$   $sp^3s^*$  (spin with spin orbit coupling doubles the number of states) band structure theory proposed by Kobayashi<sup>(b3)</sup>, and the rest of the model will be the same as Sankey's model.

## F. Summary of Results for MCT, MZT, and MZS

### 1. Results for Substitutional Impurities (including antisite defects)

#### (a) Deep levels as a function of the composition $x$

The results for the chemical trends of deep levels produced by various impurities in MCT, MZT, and MZS as a function of the alloy composition  $x$  are summarized in Fig. 1 - Fig. 5. Fig. 1 shows the cation - site, s - like deep levels produced by N, S, and I impurities in MCT as the function of  $x$  in the range of 0.1 to 0.3. Fig. 2 shows the anion - site, p - like deep levels produced by Mg, Zn, and Cd impurities in MCT for  $x$  in the same range. Fig. 3 to Fig. 5 show deep levels in MZT and MZS for  $x$  from 0.1 to 0.3. It is worth mentioning that there are no cation-site, s-like deep levels predicted in MZS.

One of the most important conclusions from these figures is that the slopes of the deep levels  $dE/dx$  are always smaller than  $dE_{\text{gap}}/dx$ . This usually has the consequence that, if a deep level exists for  $x = 1$ , then this deep level will remain in the band gap for a very large range of  $x$ . It is also worthy to note that the slopes of the anion - site deep levels are very small, these levels, thus, are "attached" to the valence band. These two results are very useful in practice. For example, detecting impurity energy levels in narrow gap alloys is much more difficult than that in wide gap alloys. However, following the results above, instead of detecting the deep

levels in the narrow gap alloy, we can try to detect the same deep levels in the same alloy with a wider gap. If we find an anion - site deep level in a wide gap alloy, we can be almost sure that this level will be found in the same alloy with a narrow gap.

(b) Predicted deep levels with no relaxation

The results of the predicted deep levels produced by various impurities in MCT, MZT, and MZS are summarized in Fig. 6 to Fig. 10. The effect of lattice relaxation on deep levels is not included in the present predictions but will be included later. The energy band gap of the materials is specified as 0.1 eV. Thus, the compositions of MCT, MZT, and MZS considered here are approximately 0.22, 0.15, and 0.08 respectively, which will give the desired band gap at  $T = 0$  K (approximately). Fig. 6 and Fig. 8 show the cation -site, s - like deep levels, and Fig. 7, Fig. 9, and Fig. 10 show the anion - site, p - like deep levels. In these figures, besides the deep levels within the band gap we also show the deep levels resonant near the band gap edges.

Inspecting these figures, we can see that all impurities substituted for cation atoms (Hg, Cd, and Zn) in MCT (Fig. 6) and MZT (Fig. 8) are donor - like impurities. That is, they are all from the rows at the right side of the cation atoms in the Periodic Table. Therefore they are more electro- negative than the cation atoms in MCT and MZT. On the other hand, all impurities substitutional for anion atoms (Te and Se) of MCT (Fig. 7), MZT (Fig. 9), and MZS (Fig. 10) are acceptor - like impurities. They are all from the rows at the left side in the Periodic Table, and they are, thus, more electropositive than the anion atoms in MCT, MZT, and MZS. This result also has its practical use. Typically, if we find an impurity level produced by substitution for cation atoms in MCT and MZT, then this impurity level is donor - like. On the other hand, if we find an impurity level produced by substitution for anion atoms, then this level is acceptor - like.

It can be also seen from these figures that even though the same impurities will form different energy levels in different materials, the order of these levels in the materials is the same. For example, the order of deep levels produced by impurities of Mg, Zn, and Cd substituted for anion atom Te

in MCT is  $E_{Mg} < E_{Zn} < E_{Cd}$ . The same order is found in MZT and MZS. Therefore if we can determine one deep level produced by a specific impurity from experiments, we can then guess the positions of deep levels produced by other impurities. This illustrates what we mean when we say our calculation is very good for predicting chemical trends.

(c) Effects of lattice relaxation

The results of the deep levels in the band gap as functions of the appropriate on - site defect potential,  $U_{A1}$  or  $U_{T2}$  (see section IIA ), denoted as "impurity potential", and the appropriate off - diagonal parts of the defect potentials,  $\alpha_{A1}$  or  $\alpha_{T2}$  ( see a1), are summarized in Fig. 11 to Fig. 15 in MCT, MZT, and MZS. The curves in these figures correspond to the various values of  $\alpha$  shown in the figures. As mentioned before, the effects of lattice relaxation are included in parameter  $\alpha$ , and  $\alpha = 0$  corresponds to the case of no lattice relaxation. In the case of MCT in Fig.11, where we consider the cation - site, s - like (  $A_1$  ) deep levels,  $\alpha_{A1} = 0.5$  corresponds a 27% outward relaxation, and  $\alpha_{A1} = -0.5$  corresponds a 15% inward relaxation. In Fig. 12, where we consider the anion - site, p -like (  $T_2$  ) deep levels,  $\alpha_{T2} = 0.2$  corresponds a 12% inward relaxation and  $\alpha_{T2} = -0.2$  corresponds a 18% outward relaxation. It is worthy to note that the relaxation directions are opposite for  $A_1$  and  $T_2$  states. Similar calculations can be done for MZT and MZS in Fig. 13 to Fig.15.

The deep levels for a particular impurity with a particular value of  $\alpha$  can be obtained from these figures by finding the intersections with the curve for that value of  $\alpha$  with a vertical line drawn from the value of " impurity potential " for that impurity. If there is no intersection for a particular case, then no deep level of the appropriate symmetry is predicted in the band gap for the impurity with that value of  $\alpha$ .

Inspection of these figures reveals the qualitative effects of lattice relaxation on deep levels. First, these effects are very

small for cation - site, s - like deep levels in MCT and MZT. They can be totally neglected in the calculations of deep levels for specific impurities. It can be also seen that the  $\alpha \neq 0$  curves all have chemical trends which are similar to the  $\alpha = 0$  ( no lattice relaxation ) curves. From Fig. 12 we can see that an inward relaxation ( $\alpha_{T2} > 0$ ) moves deep levels toward the valence band and an outward relaxation ( $\alpha_{T2} < 0$ ) moves deep levels toward the conduction band. Since the band gap we consider here is only 0.1 eV, the effects of lattice relaxation on deep levels are very important. Including these effects may move deep levels out of the band gap or move deep levels into the band gap. For example, in Fig. 14, an impurity with "impurity potential" = 2.9 eV (Mg) has a deep level in the middle of the band gap for  $\alpha = 0$  (no relaxation). However, a 10% inward relaxation will move this energy level out of the band gap, the energy level will resonate in the valence band. On the other hand, a 15% outward relaxation will move this energy level to the conduction band.

(d) Effects of lattice relaxation on deep levels

In order to determine a deep level for a particular impurity in MCT, MZT, and MZS with appropriate symmetry,  $\alpha$  must be specified. To specify  $\alpha$   $d_I$  and  $d_H$  must be determined first. The host bond length  $d_H$  as a function of the composition in MCT, MZT, and MZS can be calculated using  $d_H = r_H^a + r_H^c$ , and the impurity bond length  $d_I$  can be determined by molecular dynamics technique discussed in section IID. The effects of lattice relaxation on deep levels produced by various impurities in MCT, MZT, and MZS are summarized in Table 1. Since these effects on cation-site, s-like levels can be ignored, only the results on anion-site, p-like levels are shown in Table 1.

It can be seen from Table 1 that the percentage of lattice relaxation is in the range of 4% - 6.5%. The shift of deep levels after considering the relaxation is less than  $E_g/2$  or 0.05 eV. Therefore, if a deep level with no relaxation is in the middle of the gap, this level will stay in the gap after relaxing. However, if a deep level with no relaxation is near

the gap edges, this level may move out of the gap after relaxing, or move in the gap from the conduction band or the valence band. For example, antisite defect Zn in Te site in MCT is predicted to produce a deep level in the middle of the band gap ( $E_g/2$ ) without relaxation, and including the effects this level is predicted to move to near the conduction band ( $0.9 E_g$ ). When Tl and In are substituted for Se in MZS, they are predicted to form deep levels just below the valence band without relaxation, but including the effects, these two levels move into the band gap.

## 2. Results for Vacancies

The deep levels produced by vacancies in MCT, MZT, and MZS are summarized in Fig. 16 and Fig. 17. Fig. 16 shows the cation-site, s-like vacancies levels of MCT, MZT, and MZS. The vacancy levels of MCT and MZT are resonant in the valence band and the vacancy level of MZS is in the middle of the band gap. Fig. 17 shows the anion-site, p-like vacancy levels. These levels are slightly below the corresponding levels in Fig. 16. These levels are calculated by "the ideal vacancy model" mentioned in Sec. IIB. Since the effects of lattice relaxation are not included in the calculation, the accuracy of these levels need to be improved. This problem will be discussed in the last chapter.

## 3. Results for Interstitial Impurities

### (a) Predicted deep levels with no relaxation

The results of the predicted deep levels produced by interstitial impurities in MCT, MZT, and MZS are summarized in Fig. 18 to Fig. 23. Fig. 18, Fig. 20, and Fig. 22 show the cation-site, s-like deep levels, and Fig. 19, Fig. 21, and Fig. 23 show the anion-site, p-like deep levels in these materials. Here, cation-site means that the nearest neighbors of the interstitial are anion atoms, and anion-site means that the neighbors of the interstitial are cation atoms.

Inspecting these figures, we can find some interesting properties of the deep levels. First, one can find that cation-site, self-interstitial impurities often produce deep levels in the energy band gap. In the case of MCT, both self-interstitial impurities Hg and Cd produce deep levels well within the band gap. Hg interstitial in MZT also produces a deep level within the band gap and Zn interstitial in MZT produces a deep level just below the valence band edge (this level will move into the band gap after considering the effects of lattice relaxation). Hg interstitial and Zn

interstitials also produce deep levels in MZS. In contrast with the deep levels produced by substitutional impurities, the cation-site deep levels produced by interstitials are often acceptor-like. For example, in the case of MCT, the deep levels produced by Cu, An, Ag, Mg, and Zn interstitials are all acceptor-like. This conclusion holds for MZT and MZS. On the other hand, the anion-site interstitial deep levels can be donor-like or acceptor-like. For example, in the case of MCT, N and O interstitials introduce acceptor-like deep levels in the band gap, and F and Ar introduce donor-like levels in the band gap.

#### (b) Effects of lattice relaxation

The results of the effects of lattice relaxation on interstitial deep levels in MCT, MZT, and MZS are summarized in Fig. 24 to Fig. 29. Most of discussions in section IIF (c) for substitutional impurities are also suitable here. For example, we can see from these figures that the effects on cation-site, s-like levels are much smaller than those on anion-site, p-like levels. An outward relaxation ( $\alpha < 0$ ) moves anion-site, p-like levels toward the conduction band, and an inward relaxation ( $\alpha > 0$ ) moves these levels toward the valence band. On the other hand, the cation-site, s-like deep levels will move the other way under the lattice relaxation.

The effects of lattice relaxation on deep levels produced by various interstitial impurities are summarized in Table 2. It can be seen that the percentage of the relaxation in all the cases is in the range of 0.0% - 16%. N interstitial in MZS causes almost no relaxation, and Zn interstitial in MCT will introduce only 0.3% relaxation. On the other hand, F interstitial in MZT introduces a 16% relaxation. It can be also seen that Mg interstitial in MCT, O and Ar interstitial in MZT, and Hg and O interstitial in MZS will move out of the band gap after considering the effects of lattice relaxation. But Zn interstitial in MZT may move into the band gap after considering the effects.

#### 4. Comparison with Experiments

Many experimental techniques can be used to study the properties of defects in narrow gap semiconductors, especially to detect the defect energy levels in the band gap. These techniques include

photoluminescence (PL), deep level transient spectroscopy (DLTS), admittance spectroscopy (AS), thermally stimulated current (TSC), magnetic optical spectroscopy (MOS), electron paramagnetic resonance (EPR) and so on. Detecting the defect energy levels and identifying them are not an easy work to do. For the last two decades, many efforts have been made by experimentalists on MCT<sup>(c1)</sup>. However, to our knowledge, except for one or two cases<sup>(c2)</sup>, very little work has been done for MZT and MZS. Some experimental data which are firmly identified for MCT are shown and compared with our predicted deep levels in Table 3. These are the only data available to us at the moment.

It can be seen from Table 3 that our predicted deep levels produced by Hg interstitial and Au interstitial are almost the same as the experimental data. In other cases, our predicted deep levels are more or less in agreement with the data. The differences between the data and the predicted levels are less than 0.15 eV. We believe that this discrepancy can be explained by our neglecting the effects of charge state splitting in the calculations. From this comparison, we have reason to believe that our predicted deep levels for MZT and MZS are reliable to an accuracy on the order of 0.1 to 0.2 eV. The calculations are a considerable improvement over the 0.5 eV uncertainty typical of other results.

## 5. Comparison with Other Theories

### (a) Lattice relaxation of substitutional impurities in HgTe

The problem of lattice relaxation introduced by substitutional impurities in MCT has also been studied by other research groups using different theories. For example, Berding and Sher use a total energy method to calculate the defect formation energy in MCT which can be used to predict the relaxation about the defect site<sup>(c3)</sup>. In their approach, defect formation energies are calculated from the difference in total energies of the compound with and without the defect. They found that for the composition  $x=0$ , a Hg antisite defect (in a Te site) and a Te antisite defect (in a Hg site) in HgTe introduce 0.06 Å and 0.2 Å outward relaxation, respectively. In our calculation we found that the corresponding relaxations are 0.05 Å and 0.13 Å which are reasonably close to their results.

### (b) Interstitial impurities in MCT

The problem of interstitial impurities in MCT is also studied by Morgan-Pond, Goettig, and Schick using a total energy



method<sup>(c4-c6)</sup>. In order to calculate the lattice relaxation induced by an interstitials, they use a supercell approach in which there are 64 atoms in the bulk crystal supercell and one more for the interstitial. They predict that Cd, Hg, and In interstitials in MCT may have 3% to 4% relaxation. From Table 3 we can see that Cd and Hg interstitials in MCT are predicted by our calculation to have 4.3% and 3.6% respectively, which are in agreement with their predictions. Morgan - Pond et al. also calculate deep levels produced by Indium and self interstitials (Hg, Cd, and Te) in MCT using a cluster method. They found that a Hg interstitial may form a s - like level in the band gap, and an In interstitial may produce a s - like level resonant just below the valence band. From Fig. 19 we can see that the Hg interstitial is predicted to form a s - like deep level at about 0.8  $E_g$ , and a s - like In interstitial deep level is predicted to resonate in the valence band. Essentially, our predictions agree with theirs.

### III. Work can be Done Later

In the present work, we developed a formalism for investigating deep defect states in narrow gap semiconductors. With the formalism, we can study the electronic properties of either impurities or native defects (including antisite defects, vacancies, and interstitials). Specifically, the deep levels produced by these impurities and defects in the band gap of these materials can be predicted. The major advantage of this formalism is that different types of defects can be easily studied for alloys of various compositions of one or more types of materials. In comparison to other calculations, the accuracy of our calculations is much improved by including the effects of lattice relaxation on deep levels. One can see from Table 3 that the uncertainties of our predicted deep levels are less than 0.15 eV in comparison with the experimental data.

We note that, however, our formalism has neglected the effects of charge state splittings on deep levels produced by ionized impurities and defects. This formalism can, thus, be used only for neutral impurities and defects. In most cases where data are available, the charge state splittings of deep levels are of the order of 0.1 eV to 0.3 eV. For example, the measured splittings of S, Se, and Te in Si are 0.295, 0.286, and 0.212 eV<sup>(d1)</sup>. Myles predicted that the splittings of deep levels in Hg<sub>1-x</sub>Cd<sub>x</sub>Te are of the order of 0.1 eV to 0.2 eV<sup>(d2)</sup>. A sophisticated deep level theory also predicted that a neutral Ga vacancy in GaP has its energy level to be 0.2 eV lower than the negatively charged vacancy<sup>(d3)</sup>. Since the band gap of a narrow gap semiconductor is typically 0.1 eV, the effects of charge state splitting are very important in the calculations of deep levels. Based on these facts, we have reason to believe that the remaining uncertainties in our predicted deep levels can be explained by the effects of charge state splitting. The formalism can, thus, be further improved by including these effects.

We also note that our formalism failed to study the effects of lattice relaxation on deep levels produced by *vacancies*. The reason of this failure is that we use the "ideal vacancy model" in the calculations of *vacancy* deep levels. That is, when we calculate vacancy deep levels based on this model, we assume that the diagonal elements of the defect potential matrix are infinity. This is equivalent to remove an atom from the crystal, but leaving all other atoms in the same position. Thus, the effects of lattice relaxation which are represented in the off-diagonal elements of the defect potential matrix have no affect on vacancy deep levels. A more sophisticated theory, however, indicated that a 10% lattice relaxation may cause a 0.3 eV shift of a deep level with no relaxation<sup>(d3)</sup>. It is worthy to note that a Cd vacancy may form a deep level at about 0.4 eV above the valence band edge in CdTe<sup>(d4)</sup>, but our formalism predicted this level at about 0.1 eV above the valence band edge in CdTe. We believe that this conflict can be explained by the effects of lattice relaxation. Obviously, in order to improve the accuracy of the calculations of *vacancy* deep levels we must construct a better model than the "ideal vacancy model".

The charge state effects can be included in the calculations of deep levels in an approximate manner, using a self - consistent procedure. Following Haldane and Anderson<sup>(d5)</sup>, the atomic - orbital energies, or ionization potential, in different charge states are approximated by

$$\begin{aligned}
 E_{s\sigma}(\{n\}) &= E_s^0 + \sum_{\sigma} n_{s\sigma} U_{ss} + \sum_{j,\sigma} n_{p\sigma} U_{sp} \\
 E_{p\sigma}(\{n\}) &= E_p^0 + \sum_{j,\sigma} n_{p\sigma} U_{pp} + \sum_{\sigma} n_{s\sigma} U_{sp}
 \end{aligned} \tag{9}$$

where  $\sigma$  is the spin. Here  $n_{s\sigma}$  and  $n_{p\sigma}$  are the occupation numbers ( 0 or 1) of the s orbital and p orbital of spin  $\sigma$ , respectively. The collective set of occupation number is denoted by  $\{n\}$ . The quantities  $E_s^0$ ,  $E_p^0$ ,  $U_{ss}$ ,  $U_{sp}$ , and  $U_{pp}$  are empirical parameters chosen so that they reproduce i) the Hartree - Fock occupied s and p orbital energies for the neutral free atom and ii) the experimental s and p ionization potentials. Sankey and Dow have determined them for numerous atoms<sup>(d6)</sup>. The diagonal matrix elements of the defect potential will now be

$$U_{s\sigma} = \beta_{s\sigma}[E_{s\sigma}(\text{imp}) - E_{s\sigma}(\text{host})], \tag{10a}$$

and

$$U_{p\sigma} = \beta_{p\sigma}[E_{p\sigma}(\text{imp}) - E_{p\sigma}(\text{host})]. \tag{10b}$$

The spin - orbit occupation number  $n_\alpha$  ( $\alpha = s\uparrow, s\downarrow, p_i\uparrow, p_i\downarrow, i = x, y, \text{ or } z$ ) can be written as<sup>(d7)</sup>

$$n_\alpha = \int_{-\infty}^0 F(E) D(E) dE, \quad (11)$$

where  $F(E)$  is the Fermi function,  $D(E)$  is the local spectral density of states which can be written as

$$D(E) = \langle \mu | \rho(E) | \mu \rangle = -(1/\pi) \text{Im} \langle \mu | G(E) | \mu \rangle = -(1/\pi) \text{Im} \langle \mu | [1 - G_0 V]^{-1} | \mu \rangle, \quad (12)$$

where  $G_0$  is the host Green's function and  $V$  is the defect potential matrix.

For a particular impurity, a scheme for obtaining self - consistent solutions is implemented as follows. For an input defect potential  $V$ , the deep level energy  $E$  can be calculated by Eq(1). With this  $E$  and  $V$ , the spin - orbit occupation numbers  $n_\alpha$  are computed from Eq(11). The  $n_\alpha$  are then used to compute the spin - orbit energies  $E_{s\sigma}$  and  $E_{p\sigma}$  from Eq(9). These energies are then used to compute new potential matrix elements from Eq(10). Finally, the resulting  $V$  is used in Eq(1) to calculate a new deep level energy  $E$ . This procedure is repeated iteratively until self - consistency is obtained.

The effects of lattice relaxation on vacancy deep levels can be considered following Singh and Madhukar's model<sup>(d8)</sup>. To simplify the problem, let's consider a cluster with two atoms per unit cell and one  $s$  orbital per atom. We use the subscripts 0 and 1 to denote these atoms. The Hamiltonian of the perfect crystal can then be written as

$$H_0 = \sum_{i,\mu} |i_\mu\rangle \epsilon_\mu \langle i_\mu| + \sum_{i,j} |i\rangle V \langle j| \quad (13)$$

where  $\mu$  takes 0 and 1, and  $i$  and  $j$  are nearest neighbors. If a defect is at 0 site, then the interactions describing the defect are given by

$$\begin{aligned} \langle 0, s_0 | H | 0, s_0 \rangle &= \epsilon_0 \\ \langle 0, s_0 | H | 1, s_1 \rangle &= V_{01} \\ \langle 1, s_1 | H | 1, s_1 \rangle &= \epsilon_1 \\ \langle 1, s_1 | H | 2, s_0 \rangle &= V_{12}, \end{aligned} \quad (14)$$

where  $H = H_0 + V$  is the Hamiltonian including the defect, and 2 denotes the

neighboring unit cell. Following Singh and Madhukar, the diagonal element of the Green's function matrix which includes a defect is given by

$$G_{00} = \frac{1}{(E - \tilde{\epsilon}_0) - \frac{4V^2}{(E - \tilde{\epsilon}_1) - \frac{3V_{12}^2}{E - \epsilon_0 - VT_0}}}, \quad (15)$$

where  $T_0$  is given by

$$T_0 = \frac{1}{V} \left[ (E - \epsilon_0) - \frac{3V^2}{E - \epsilon_1 - \frac{4V^2}{E - \epsilon_0 - \frac{1}{G_{00}}}} \right] \quad (16)$$

For an ideal defect at site 0, we have  $V_{12} = V$ , and  $\tilde{\epsilon}_1 = \epsilon_1$ . Therefore, Eq(16) becomes

$$\tilde{G}_{00} = \frac{G_{00}}{1 - (\tilde{\epsilon}_0 - \epsilon_0) G_{00}} \quad (17)$$

In the "ideal vacancy" model,  $\tilde{\epsilon} \rightarrow \infty$ ,  $G_{00}$ , thus, is zero. The deep level vacancy can then be determined. But using this model, the vacancy deep levels are determined by the relation

$$(E - \tilde{\epsilon}_1) - \left[ (E - \epsilon_1) + \Delta \right] \frac{\tilde{V}_{12}^2}{V^2} = 0, \quad (18)$$

where  $\Delta = 4V_{01}^2 G_{00}$ . The effects of lattice relaxation are included in  $V_{01}$  and  $V_{12}$ , so that Eq(18) gives these effects on vacancy deep levels.

**Table1: Effects of lattice relaxation on substitutional deep levels.**

System	$d_H(\text{\AA})$	$d_I(\text{\AA})$	$\Delta x = d_I - d_H$	% of relaxation	deep levels <sup>a</sup>	
					(no relax)	(relaxed)
MCT: Cd <sub>Te</sub> <sup>b</sup>	2.8	2.97	0.17	6.1	C.B. <sup>c</sup>	C.B.
MCT: Mg <sub>Te</sub>	2.8	2.96	0.16	5.7	0.3E <sub>g</sub> <sup>d</sup>	0.5E <sub>g</sub>
MCT: Zn <sub>Te</sub>	2.8	2.98	0.18	6.4	0.5E <sub>g</sub>	0.9E <sub>g</sub>
MCT: Hg <sub>Te</sub> <sup>b</sup>	2.8	2.97	0.17	6.1	C.B.	C.B.
MZT: Zn <sub>Te</sub> <sup>b</sup>	2.74	2.61	-0.13	4.7	0.98E <sub>g</sub>	0.7E <sub>g</sub>
MZT: Mg <sub>Te</sub>	2.74	2.60	-0.14	5.1	0.5E <sub>g</sub>	0.3E <sub>g</sub>
MZT: Cd <sub>Te</sub>	2.74	2.60	-0.14	5.1	C.B.	C.B.
MZT: Hg <sub>Te</sub> <sup>b</sup>	2.74	2.60	-0.14	5.1	C.B.	C.B.
MZS: Be <sub>Se</sub>	2.62	2.74	0.12	4.6	0.3E <sub>g</sub>	0.6E <sub>g</sub>
MZS: Tl <sub>Se</sub>	2.62	2.77	0.15	5.7	-0.1E <sub>g</sub>	0.4E <sub>g</sub>
MZS: In <sub>Se</sub>	2.62	2.77	0.15	5.7	-1.1E <sub>g</sub>	0.3E <sub>g</sub>
MZS: Hg <sub>Se</sub> <sup>b</sup>	2.62	2.73	0.11	4.2	C.B.	C.B.
MZS: Zn <sub>Se</sub> <sup>b</sup>	2.62	2.73	0.11	4.2	C.B.	C.B.

a. All deep levels in this table are anion site, p-like deep levels.

b. All these are antisite impurities.

c. C.B. means conduction band.

d. E<sub>g</sub> means energy band gap.

**Table2: Effects of lattice relaxation on interstitial deep levels**

System	$d_H(\text{\AA})$	$d_I(\text{\AA})$	$\Delta x = d_I - d_H$	% of relaxation	deep levels <sup>a</sup>	
					(no relax)	(relaxed)
MCT: Cd <sup>b</sup>	2.8	2.94	0.12	4.3	0.74E <sub>g</sub> <sup>d</sup>	0.77E <sub>g</sub>
MCT: Mg	2.8	3.10	0.24	8.6	0.98E <sub>g</sub>	C.B. <sup>c</sup>
MCT: Zn	2.8	2.81	0.01	0.3	0.1E <sub>g</sub>	0.1E <sub>g</sub>
MCT: Hg <sup>b</sup>	2.8	2.90	0.10	3.6	0.82E <sub>g</sub>	0.83E <sub>g</sub>
MCT: Au	2.8	2.90	0.10	3.6	0.9E <sub>g</sub>	0.91E <sub>g</sub>
MCT: Ag	2.8	2.91	0.11	3.9	0.87E <sub>g</sub>	0.88E <sub>g</sub>
MCT: Cu	2.8	2.91	0.11	3.9	0.2E <sub>g</sub>	0.22E <sub>g</sub>
MCT: Te <sup>b</sup>	2.8	2.95	0.15	5.4	C.B.	C.B.
MCT: N	2.8	2.56	-0.24	8.6	0.9E <sub>g</sub>	0.7E <sub>g</sub>
MCT: O	2.8	2.54	-0.26	9.3	0.8E <sub>g</sub>	0.6E <sub>g</sub>
MCT: Ar	2.8	2.59	-0.21	7.5	0.82E <sub>g</sub>	0.62E <sub>g</sub>
MCT: F	2.8	2.52	-0.28	10	0.44E <sub>g</sub>	0.24E <sub>g</sub>
MZT: Zr <sup>b</sup>	2.74	2.92	0.18	6.6	V.B. <sup>c</sup>	0.04E <sub>g</sub>
MZT: Mg	2.74	2.80	0.06	2.2	0.9E <sub>g</sub>	0.91E <sub>g</sub>
MZT: Cd	2.74	2.82	0.08	2.9	0.6E <sub>g</sub>	0.61E <sub>g</sub>
MZT: Hg <sup>b</sup>	2.74	2.81	0.07	2.5	0.68E <sub>g</sub>	0.69E <sub>g</sub>
MZT: Au	2.74	2.80	0.06	2.2	0.74E <sub>g</sub>	0.55E <sub>g</sub>
MZT: Ag	2.74	2.80	0.06	2.2	0.70E <sub>g</sub>	0.71E <sub>g</sub>
MZT: Cu	2.74	2.88	0.14	5.1	0.18E <sub>g</sub>	0.30E <sub>g</sub>
MZT: Te <sup>b</sup>	2.74	2.35	-0.41	15	C.B.	C.B.
MZT: N	2.74	3.10	0.36	13	C.B.	C.B.
MZT: O	2.74	3.14	0.40	14.6	0.8E <sub>g</sub>	C.B.
MZT: Ar	2.74	3.15	0.41	15	0.9E <sub>g</sub>	C.B.
MZT: F	2.74	3.18	0.44	16	0.3E <sub>g</sub>	0.5E <sub>g</sub>

**Table 2 : (continued)**

MZS: Hg <sup>b</sup>	2.62	2.71	0.09	3.4	0.98E <sub>g</sub>	C.B.
MZS: Zn <sup>b</sup>	2.62	2.78	0.16	6.1	0.04E <sub>g</sub>	0.14E <sub>g</sub>
MZS: Cd	2.62	2.72	0.10	3.8	0.86E <sub>g</sub>	0.88E <sub>g</sub>
MZS: Cu	2.62	2.75	0.13	5.0	0.24E <sub>g</sub>	0.34E <sub>g</sub>
MZS: Ag	2.62	2.71	0.09	3.4	C.B.	C.B.
MZS: Se <sup>b</sup>	2.62	2.58	-0.04	1.5	C.B.	C.B.
MZS: N	2.62	2.61	-0.01	0.0	C.B.	C.B.
MZS: O	2.62	2.37	-0.25	9.5	0.98E <sub>g</sub>	C.B.
MZS: F	2.62	2.51	-0.11	4.2	0.50E <sub>g</sub>	0.40E <sub>g</sub>

- a. All deep levels in this table are either anion site, p-like deep levels or cation site, s-like deep levels. All interstitials are on the preferred positions.
- b. All these are self-interstitials.
- c. C.B. means conduction band edge, and V.B. means valence band edge.
- d. E<sub>g</sub> means energy band gap.

**Table 3: Comparison of the predicted deep levels from the present theory with experimental data**

system	deep levels	
	experiment <sup>a</sup>	theory
Hg <sub>I</sub> <sup>b</sup> (donor)	$0.8E_g^c$	$0.83E_g$
Te <sub>I</sub> <sup>b</sup> (recom) <sup>d</sup>	$0.5E_g$	$E_c^e + 0.1\text{eV}^f$
Te <sub>Hg</sub> (recom)	$0.5E_g$	$E_c + 0.06\text{eV}$
Cu <sub>Te</sub> (donor)	$0.8E_g$	$E_c + 0.06\text{eV}$
Au <sub>Te</sub> (donor)	$0.8E_g$	$E_c + 0.04\text{eV}$
Au <sub>I</sub> <sup>b</sup> (donor)	$0.8E_g$	$0.91E_g$

- a. Data obtained from References e1 - e3.
- b. These are interstitial impurities.
- c.  $E_g$  means energy band gap.
- d. Recombination center.
- e.  $E_c$  means conduction band edge.
- f. The difference between data and theory result can be explained by the effects of charged-state splitting.
- g. The x values for the experimental data here are in the range  $0.2 < x < 0.3$ . for our calculations,  $x=0.22$ . As seen by Figs. 1 and 2, the change in the energy levels for  $0.2 < x < 0.3$  is very small and can be ignored for rough comparisons.



#### IV. Results for Shallow Levels in II-VI Materials

In the mid year report<sup>(a1)</sup>, we already gave a fairly complete discussion of the basic theory of shallow impurity levels in II-VI materials. In the very lowest approximation we obtain the simple hydrogenic model (with an appropriately scaled Bohr radius and Rydberg energy) but of course this is not a good approximation for our materials. To get better results, we must include the effects of the following.

1. Non-parabolic Bands
2. Screening
3. Site Dependence
4. Central Cell Corrections
5. Alloy Disorder
6. Lattice Coupling
7. Lattice Relaxation
8. Impurity Interactions
9. Band Coupling and Degeneracy

From previous work to first order<sup>(a1)</sup>, the Hamiltonian that corrects for non-parabolic behavior is

$$H^1 = ap_z^2 + bp_z \phi p_z + cp_+ \phi p_- + dp_- \phi p_+ \quad (19)$$

where  $\vec{p}$  is the momentum operator and  $\phi$  is the hydrogenic potential. The coefficients a, b, c, and d are given in the mid year report.

Using appropriate values for the parameters for MCT and MZT we can evaluate  $E_{\text{gap}}$ ,  $E_{\text{donor}}$ , ground state and the ground state donor wave function  $\psi_0$ . To first order

$$\Delta E = \langle \psi_0 | H^1 | \psi_0 \rangle. \quad (20)$$

Our results are given in Table IV. The results predict an approximate 10% downward shift in binding energy due to the effect of non-parabolicity. Of course, many other factors come into play as noted above. Perhaps the most interesting part of this is that we predict an increase in binding due to non-parabolicity.

# TABLE 4

	MCT	MZT
P	$1.290 \times 10^{19} \frac{\text{eV cm}}{\text{erg sec}}$	$1.238 \times 10^{19} \frac{\text{eV cm}}{\text{erg sec}}$
X	.19	.13
K	17.56	18.35
$\Delta$	1.05 eV	.9 eV
T	300 K	300 K
$E_g$	.16 eV	0.141 eV
$E_{\text{Ground}}^{\text{Donor}}$	- 0.014 eV	- 0.01443 eV
$\Delta E$	- 0.00146 eV	- 0.00211 eV
$\left  \frac{\Delta E}{E_{\text{Gap}}} \right $	.9%	1.5%
$\left  \frac{\Delta E}{E_{\text{Ground}}^{\text{Donor}}} \right $	- 10.4%	- 14.6%
T (same p, x, k, $\Delta$ )	77K	77K
$E_g$	.0841 eV	0.0800 eV
$E_{\text{Ground}}^{\text{Donor}}$	- 0.008842 eV	- 0.00828 eV
$\Delta E$	- .001268 eV	- 0.00116 eV
$\left  \frac{\Delta E}{E_{\text{Gap}}} \right $	1.5%	1.45%

Results for shallow levels in II-VI Materials

	MCT	MZT
$\frac{\Delta E}{ E_{\text{Donor}}^{\text{Ground}} }$	1.45%	- 14%
$E_g$ (same p, x, k, $\Delta$ )	.1 eV	.1 eV
$E_{\text{Donor}}^{\text{Ground}}$	- 0.010082 eV	- 0.009785 eV
$\Delta E$	- 0.001352 eV	- 0.0012464 eV
$ \Delta E / E_{\text{Gap}} $	1.4%	1.25%
$\Delta E /  E_{\text{Donor}}^{\text{Ground}} $	- 13.4%	- 12.7%

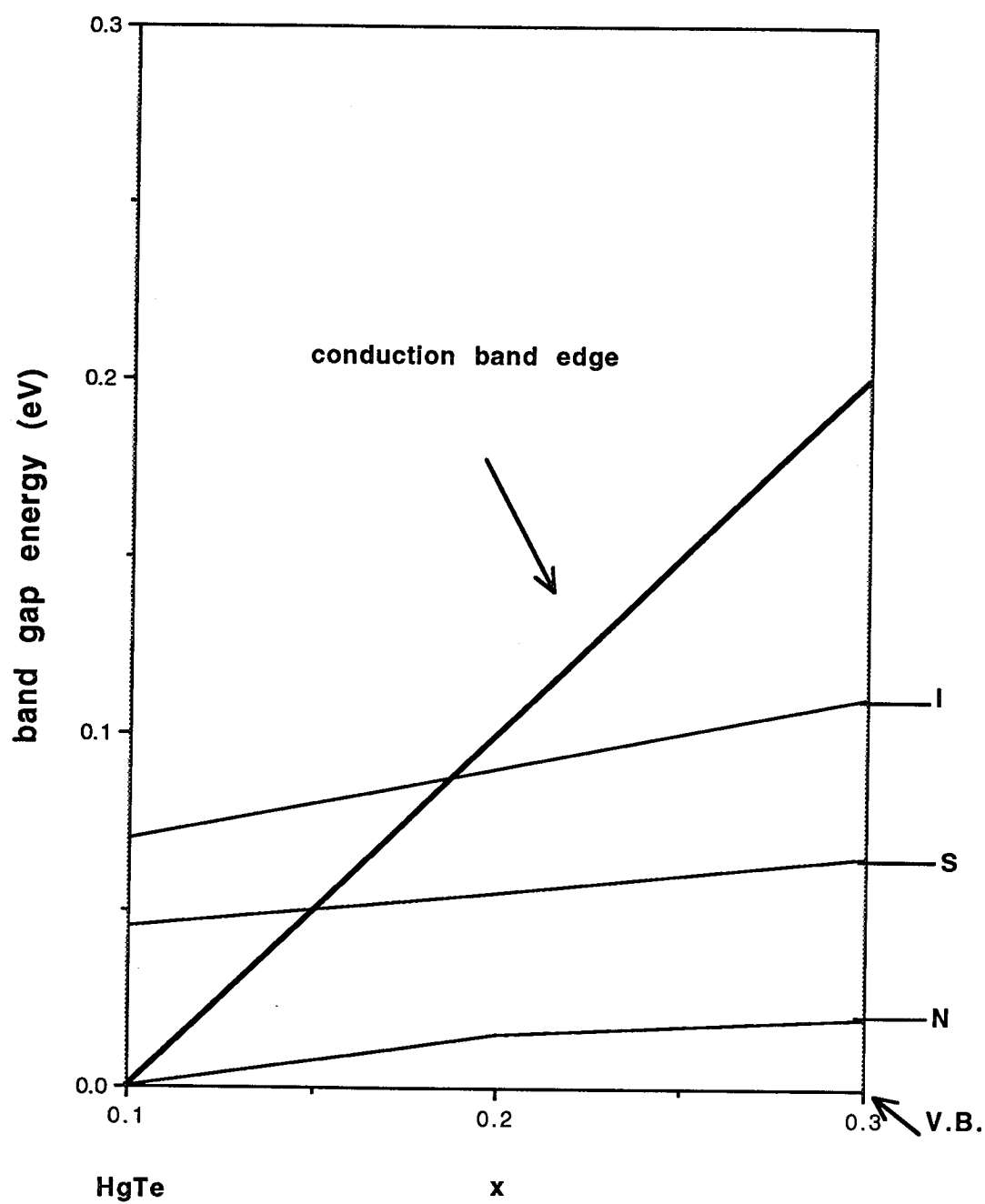


**Fig. 1** Substitutional Deep Levels in MCT as a Function of  $x$  (cation - site, s - like)

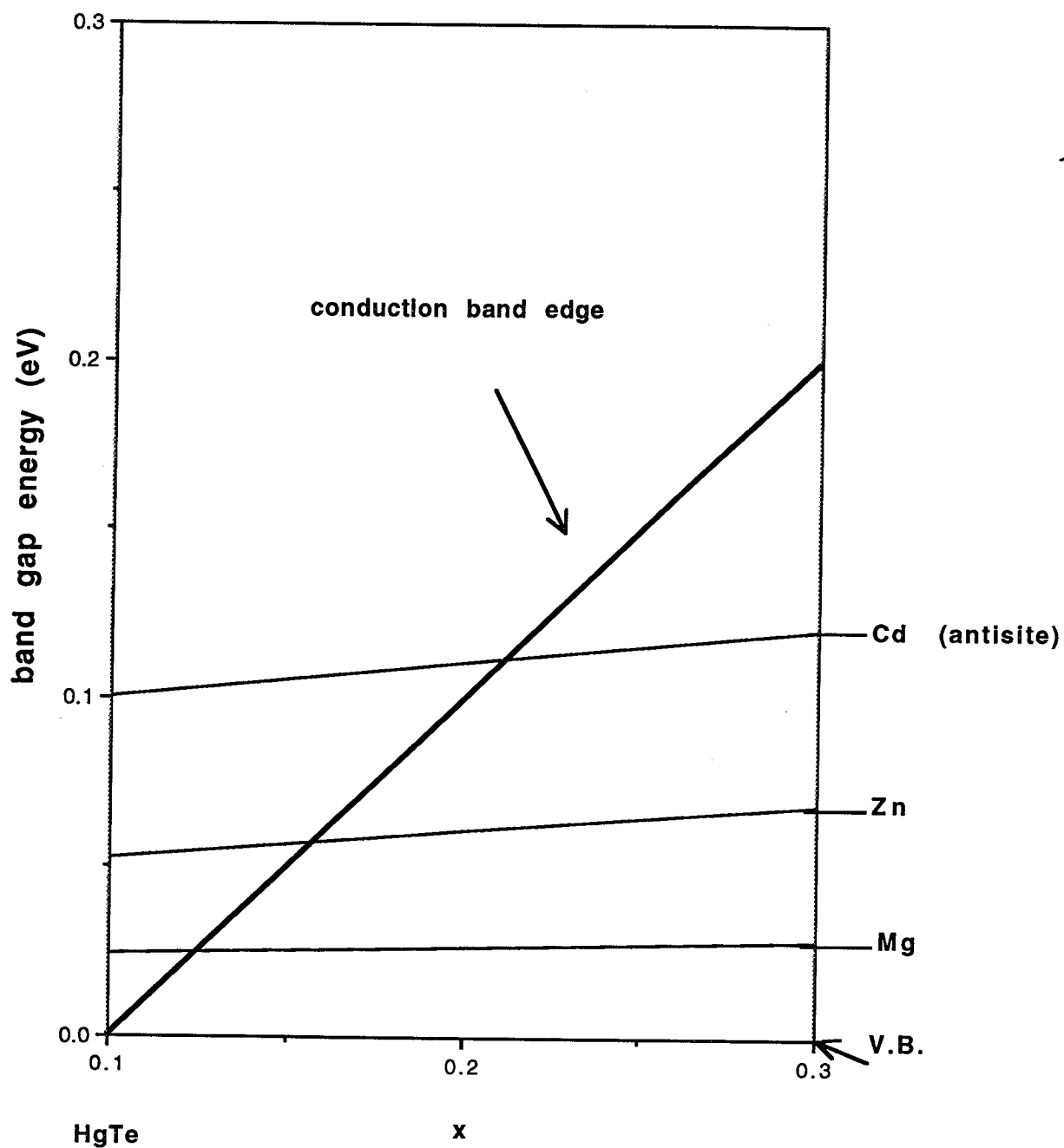


**Fig. 2 Substitutional Deep Levels in MCT as a Function of  $x$  (anion - site, p - like)**

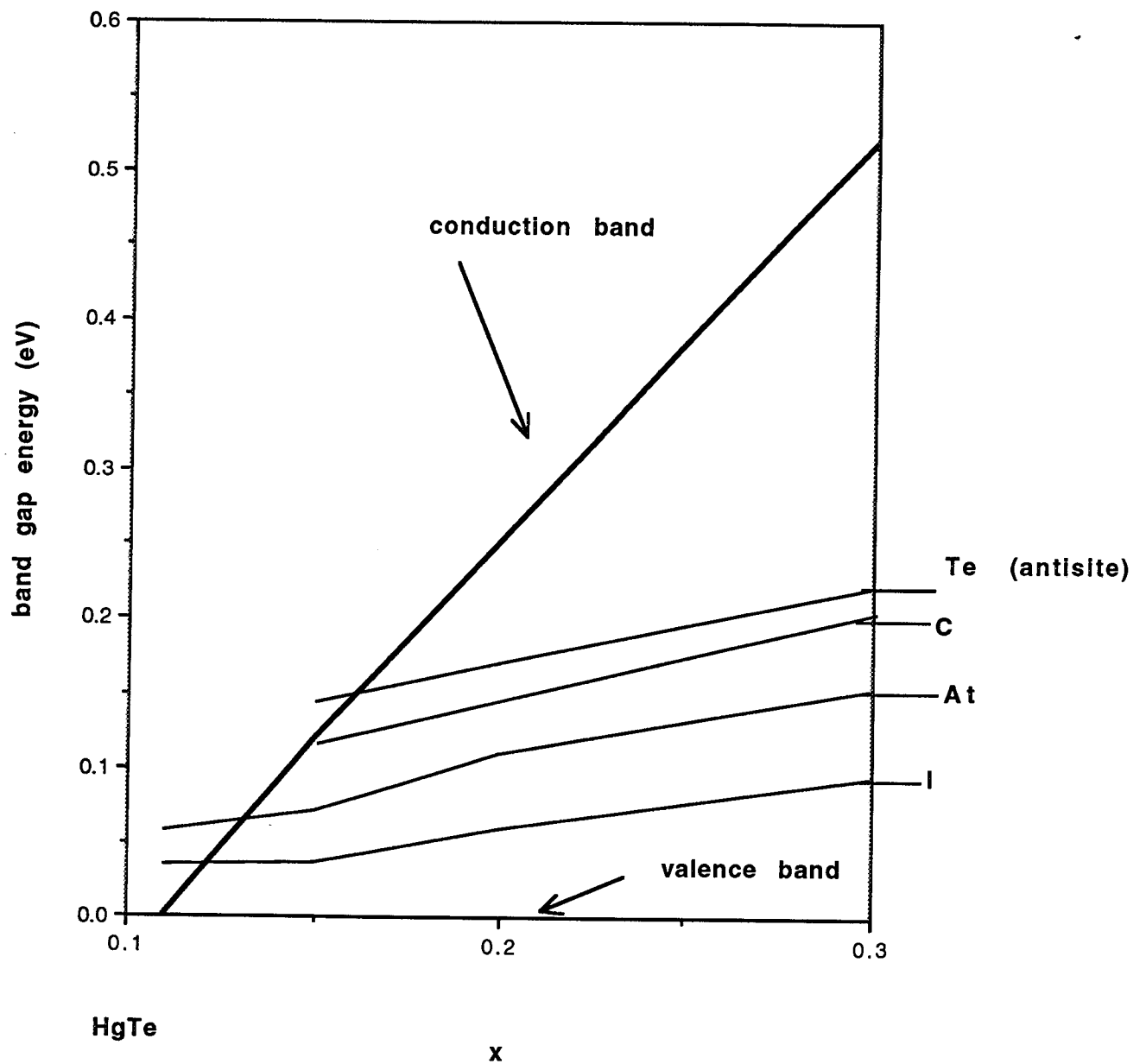


**Fig.3** Substitutional Deep Levels in MZT as a Function of  $x$  (cation - site, s - like)

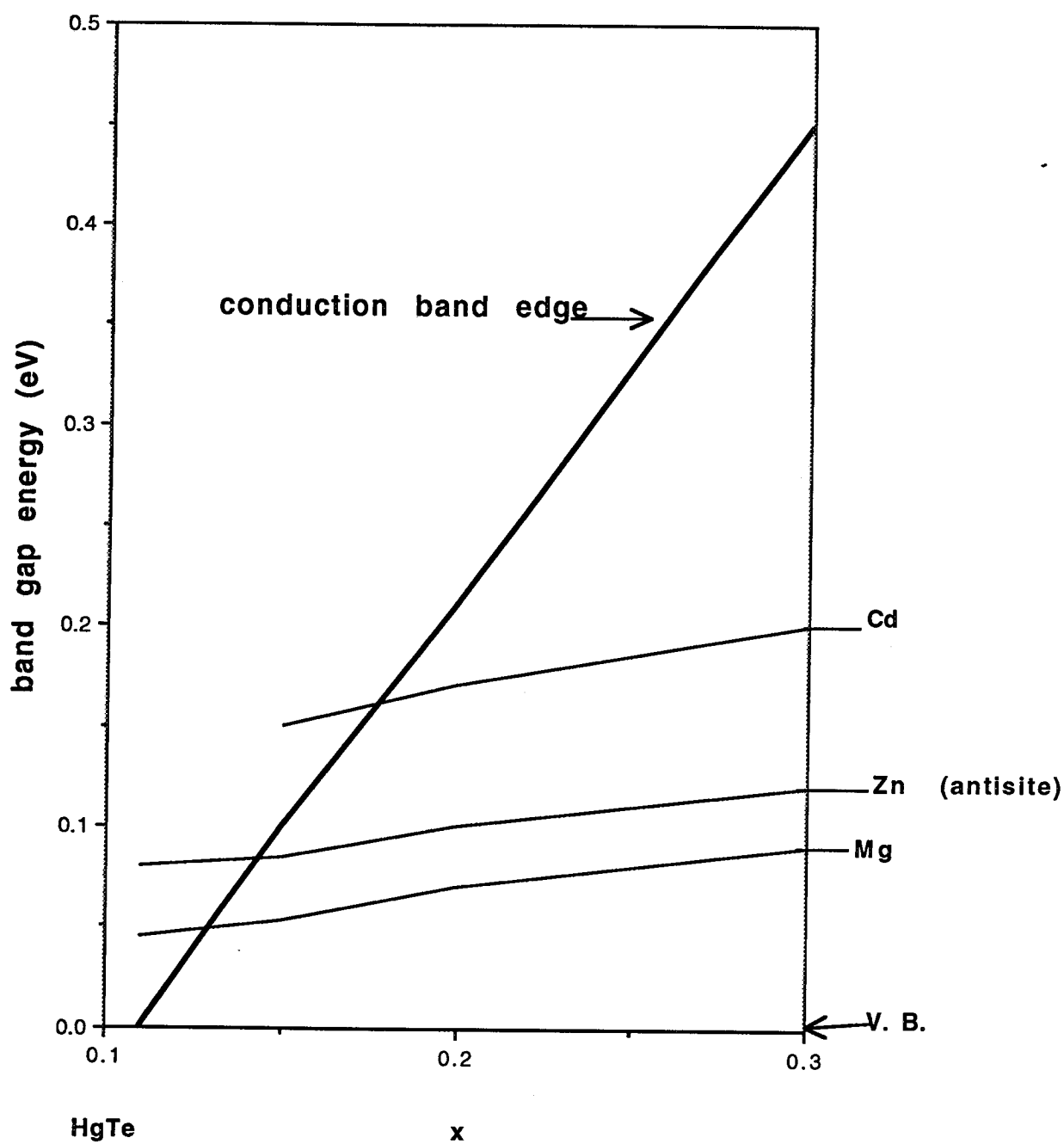


**Fig.4** Substitutional Deep Levels in MZT as a Function of  $x$  (anion - site, p - like)

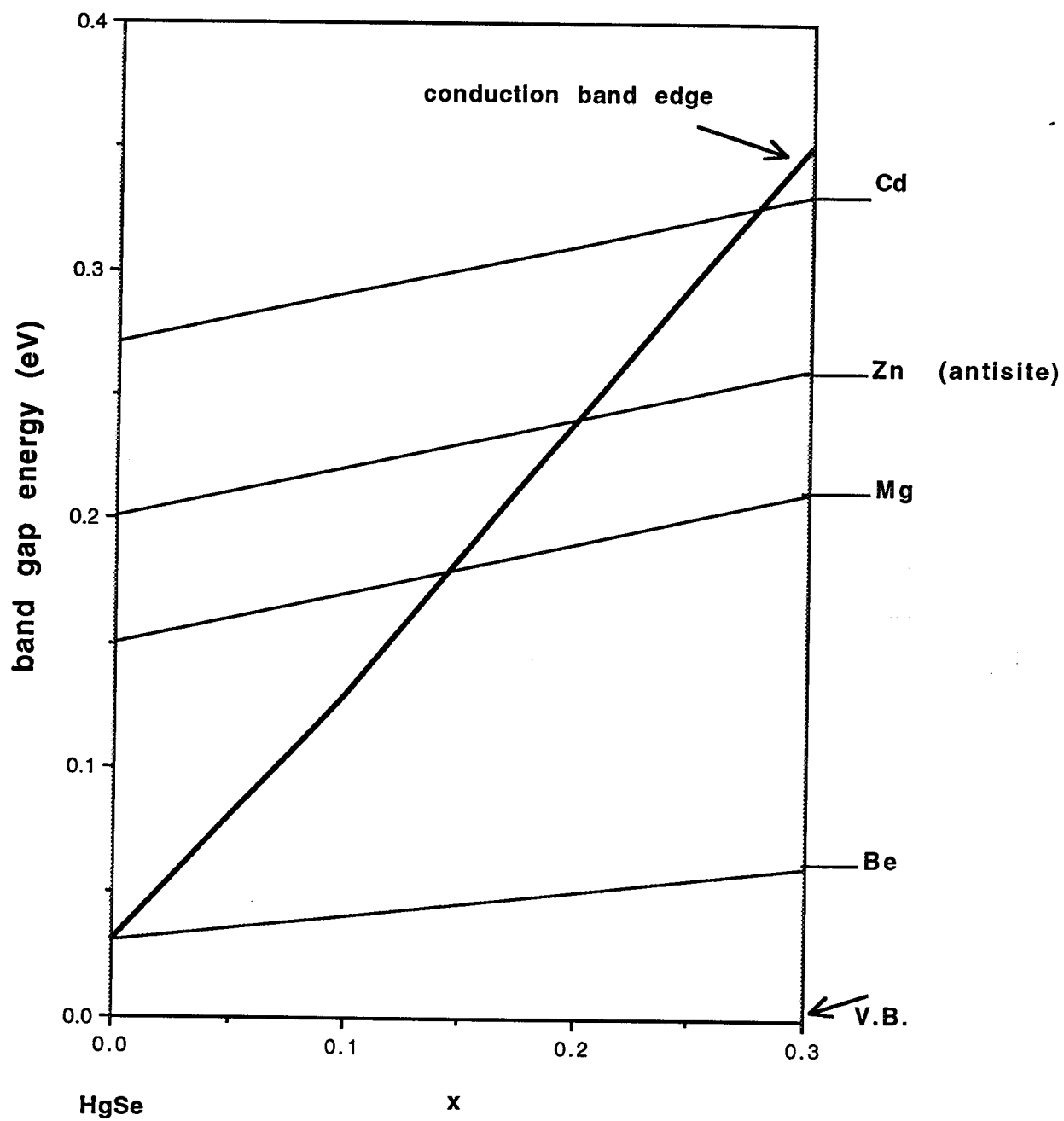


**Fig.5 Substitutional Deep Levels in MZS as a Function of  $x$  (anion - site, p - like)**



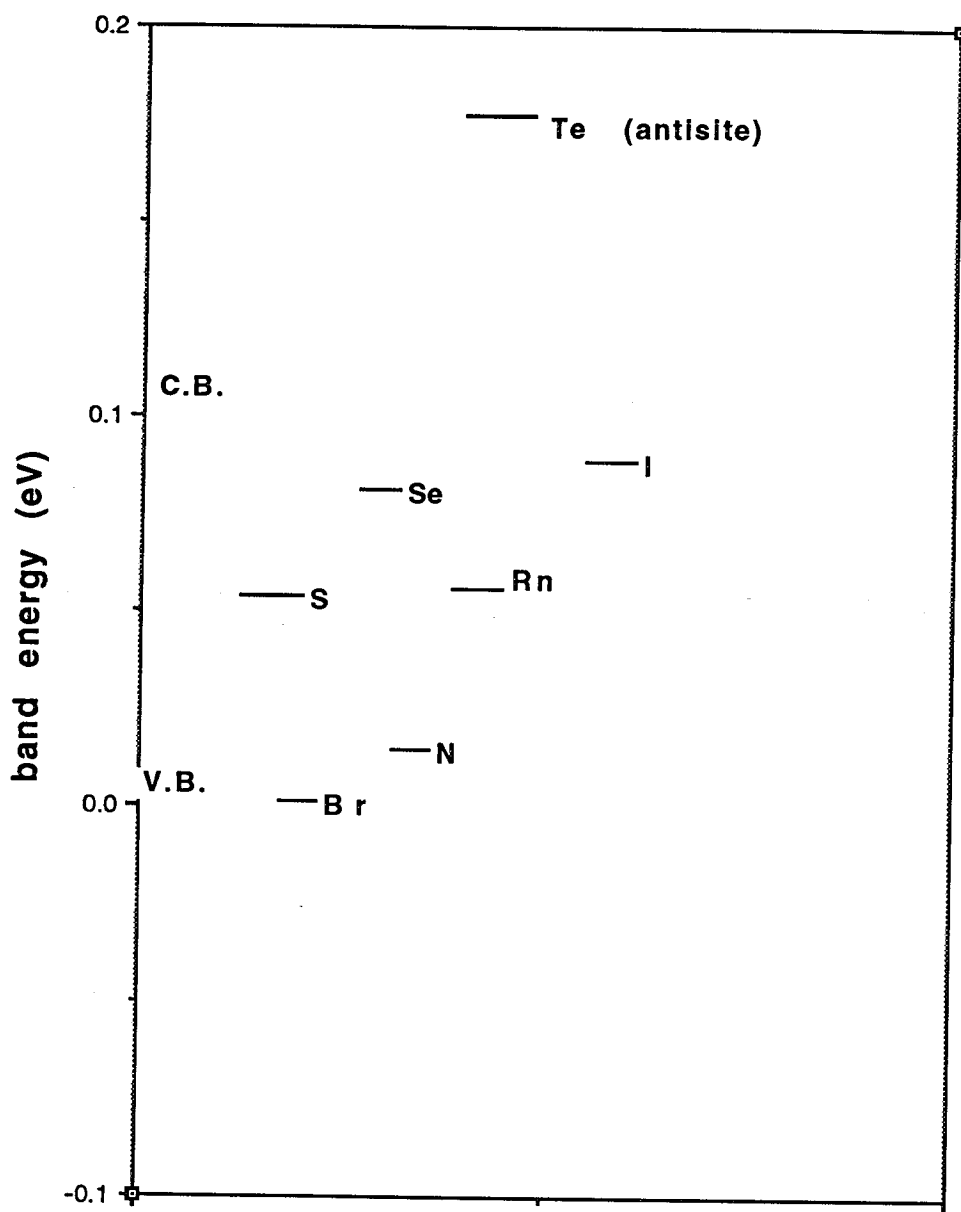


**Fig. 6 Substitutional Deep Levels in MCT for  $E_g = 0.1$  eV (cation - site, s - like)**

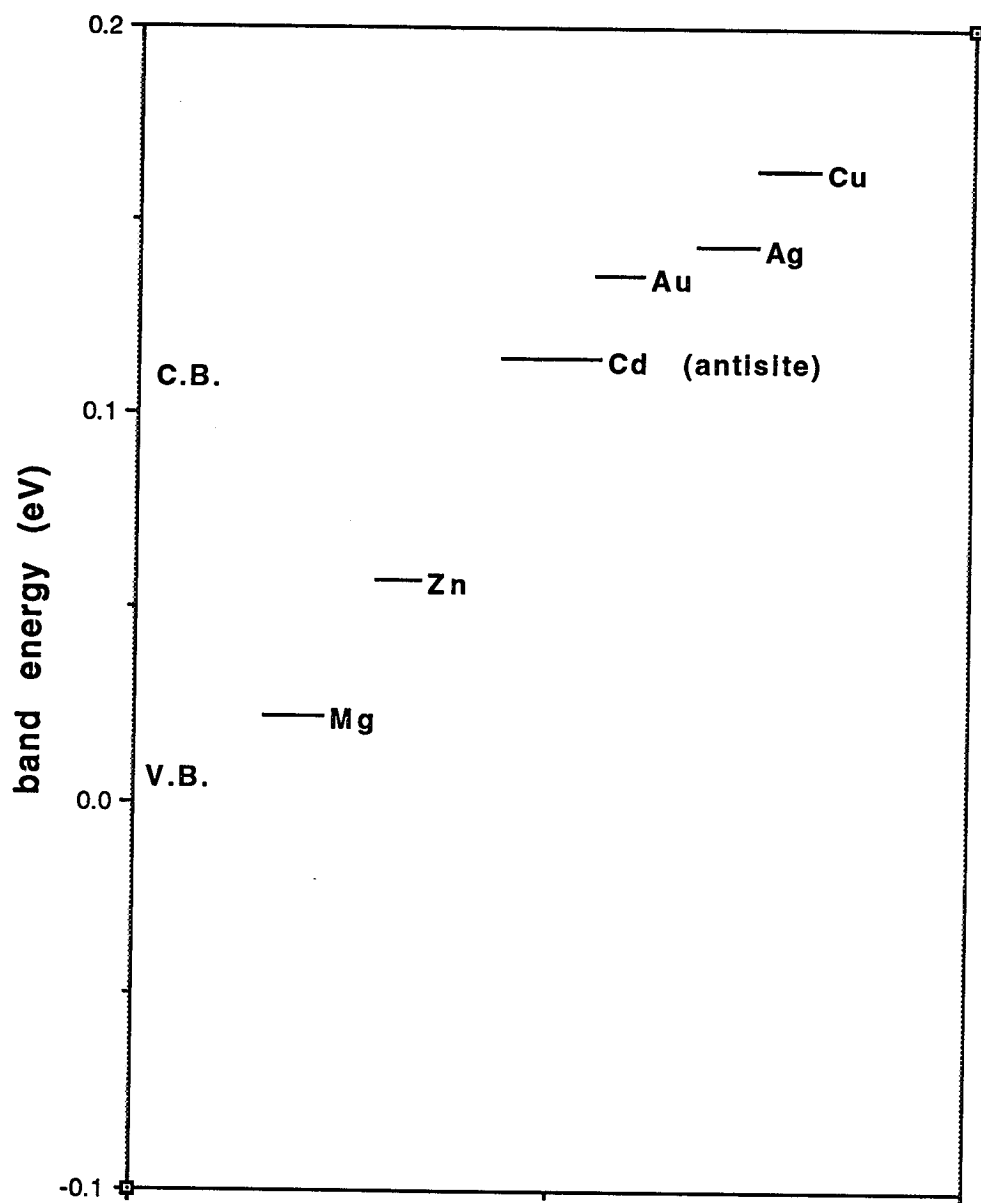


**Fig. 7** Substitutional Deep Levels in MCT for  $E_g = 0.1$  eV (anion - site, p - like)

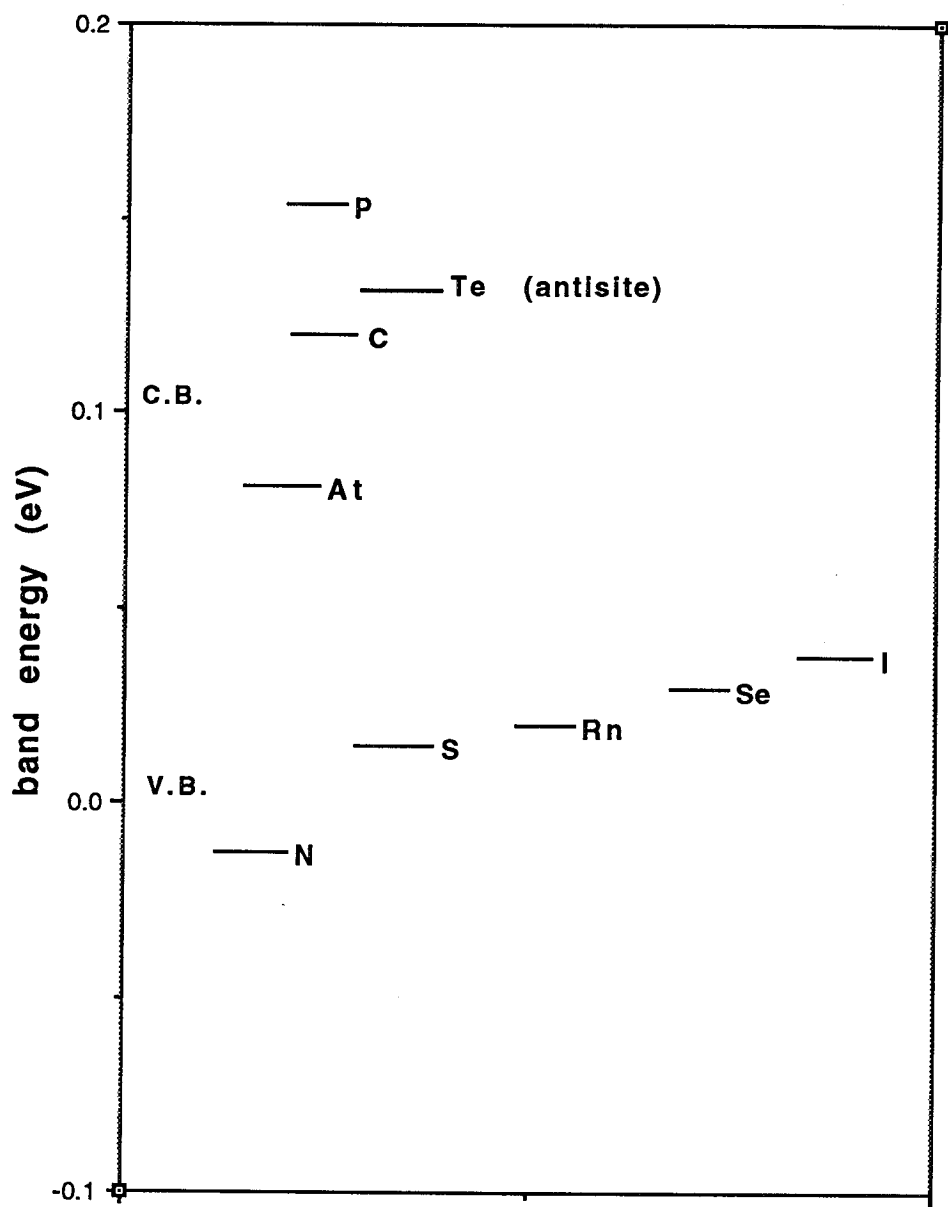


**Fig. 8 Substitutional Deep Levels in MZT for  
Eg = 0.1 eV (cation - site, s - like)**

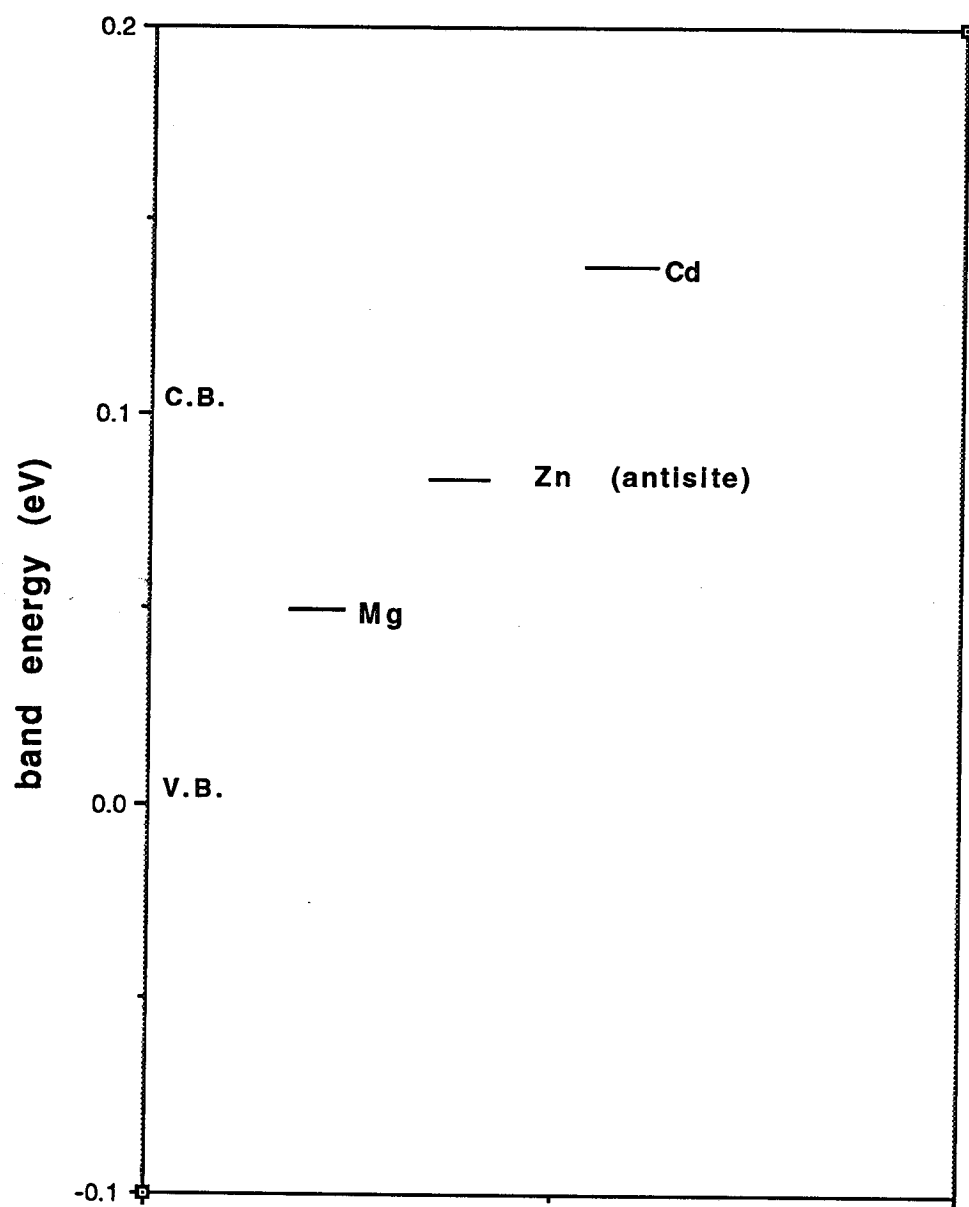


**Fig. 9** Substitutional Deep Levels in MZT for  $E_g = 0.1$  eV (anion - site, p - like)

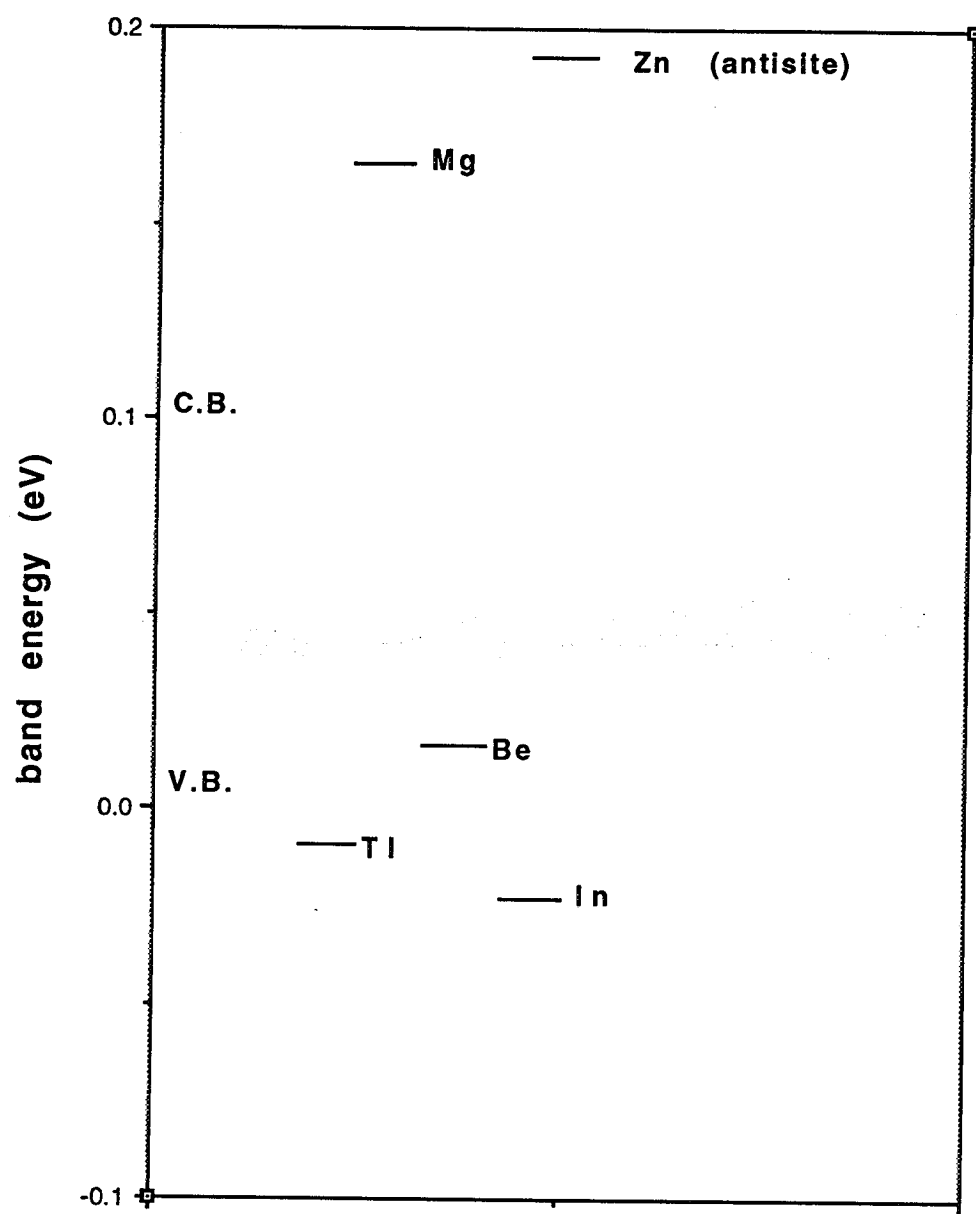


**Fig. 10** Substitutional Deep Levels in MZS  
for  $E_g = 0.1$  eV (anion - site, p - like)

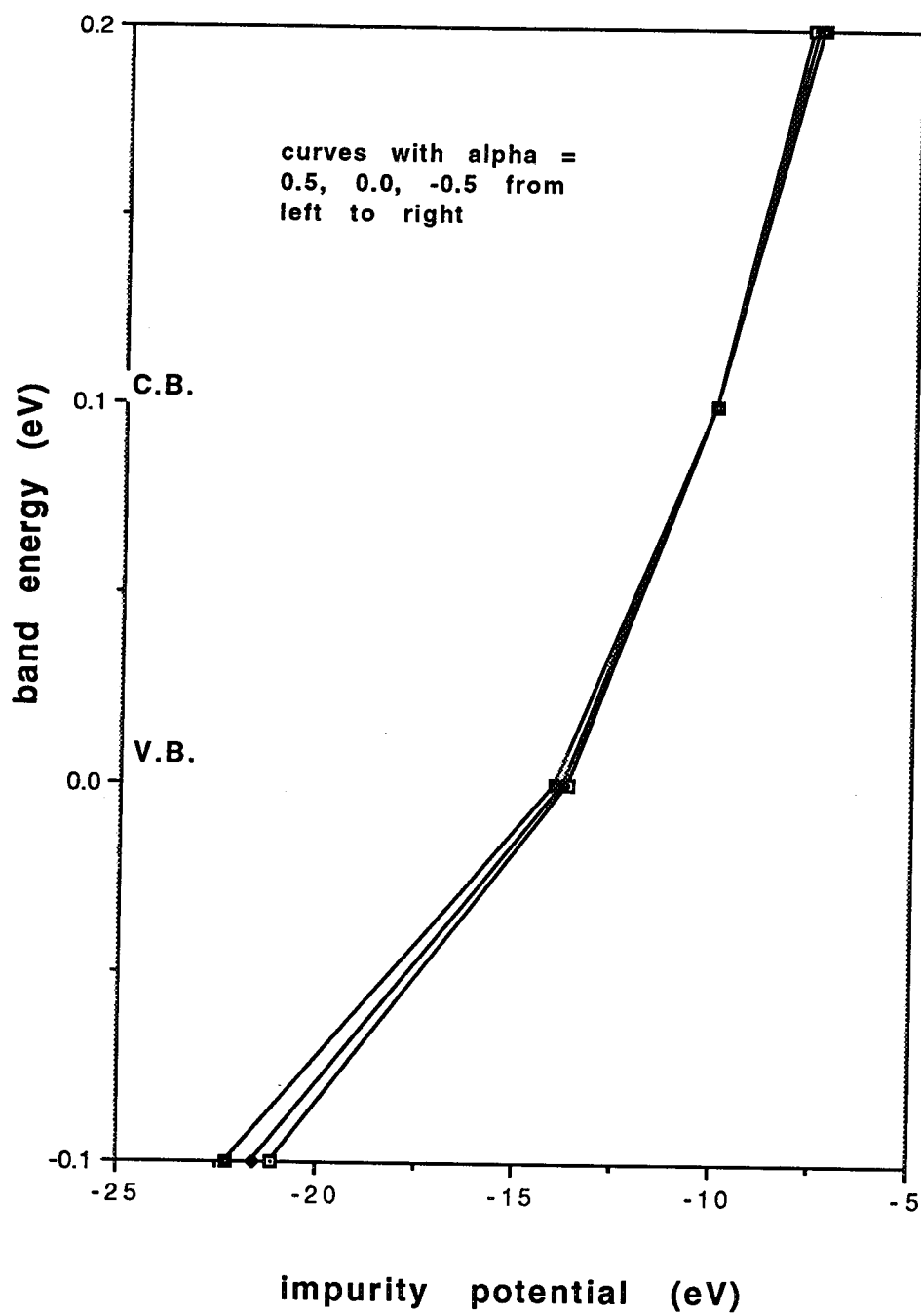


**Fig.11 Substitutional Deep Levels in MCT for  
 $E_g = 0.1$  eV with Lattice Relaxation  
(cation-site, s - like)**

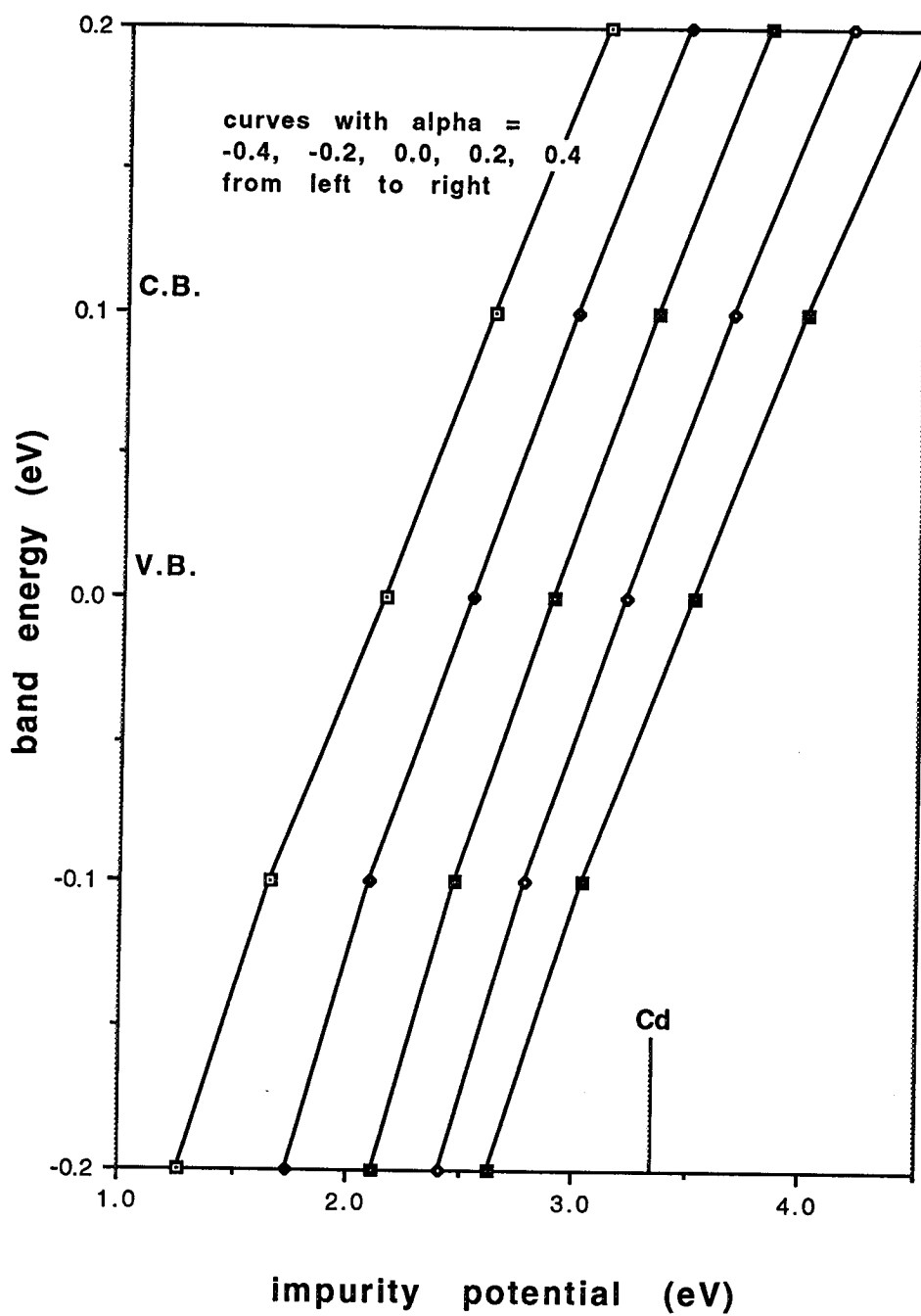


**Fig.12 Substitutional Deep Levels in MCT  
 for  $E_g = 0.1$  eV with Lattice Relaxation  
 (anion - site, p - like)**

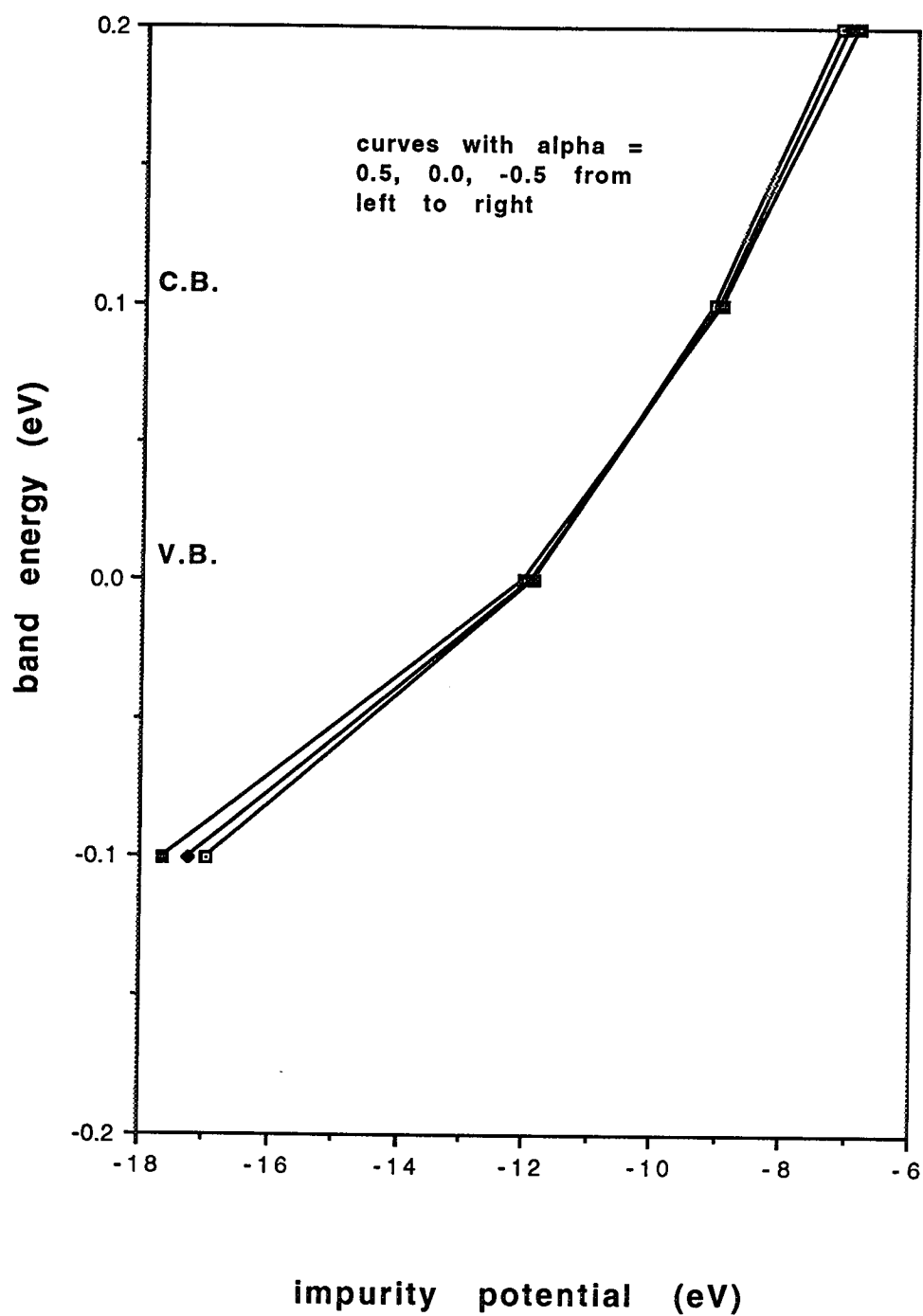


**Fig. 13** Substitutional Deep Levels in MZT for  $E_g = 0.1$  eV with Lattice Relaxation (cation - site, s - like)



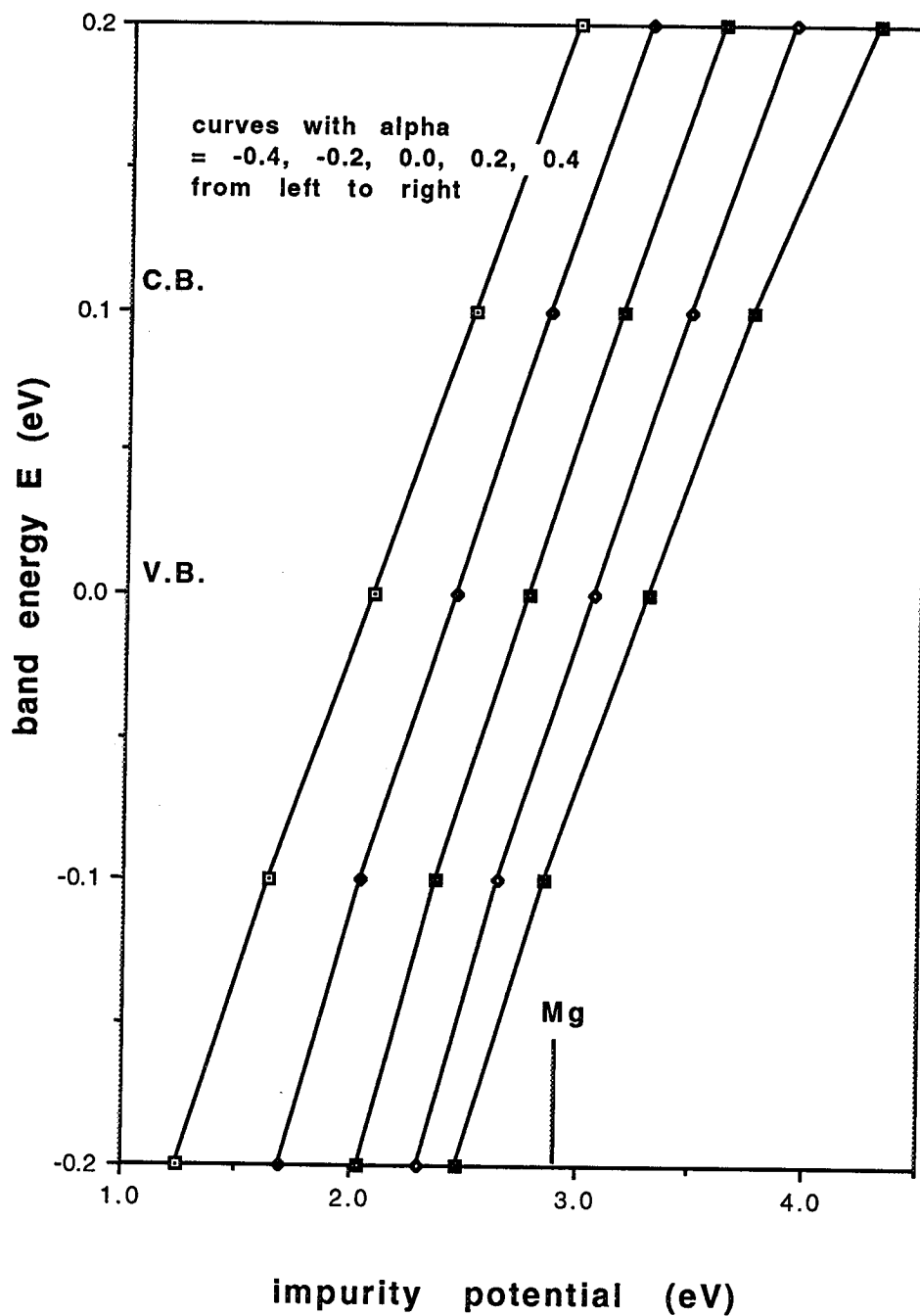


**Fig.14** Substitutional Deep Levels in MZT  
for  $E_g = 0.1$  eV With Lattice Relaxation  
(anion-site, p - like)

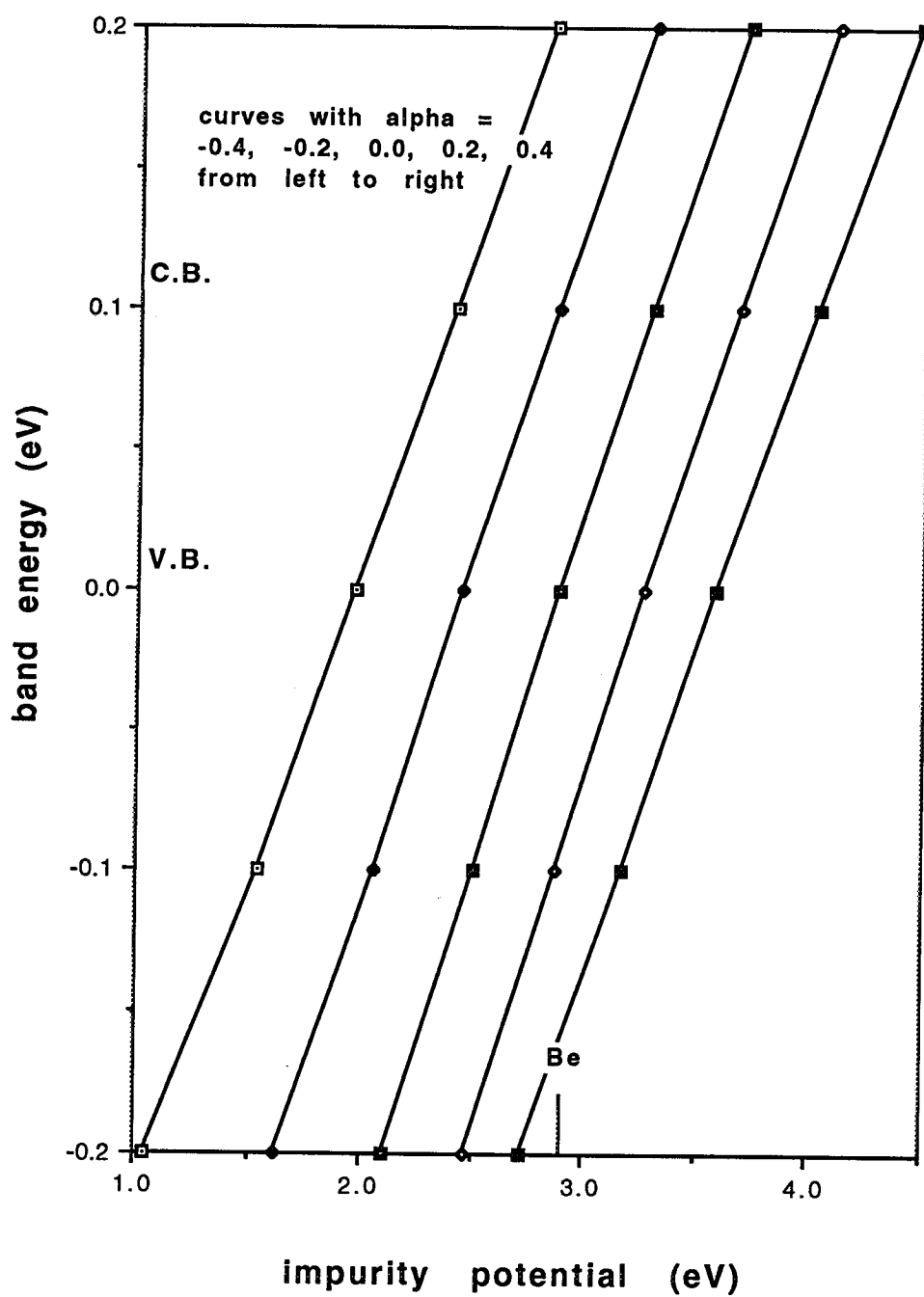


**Fig.15 Substitutional Deep Levels in MZS for  
 $E_g = 0.1$  eV with Lattice Relaxation  
 (anion-site, p - like)**

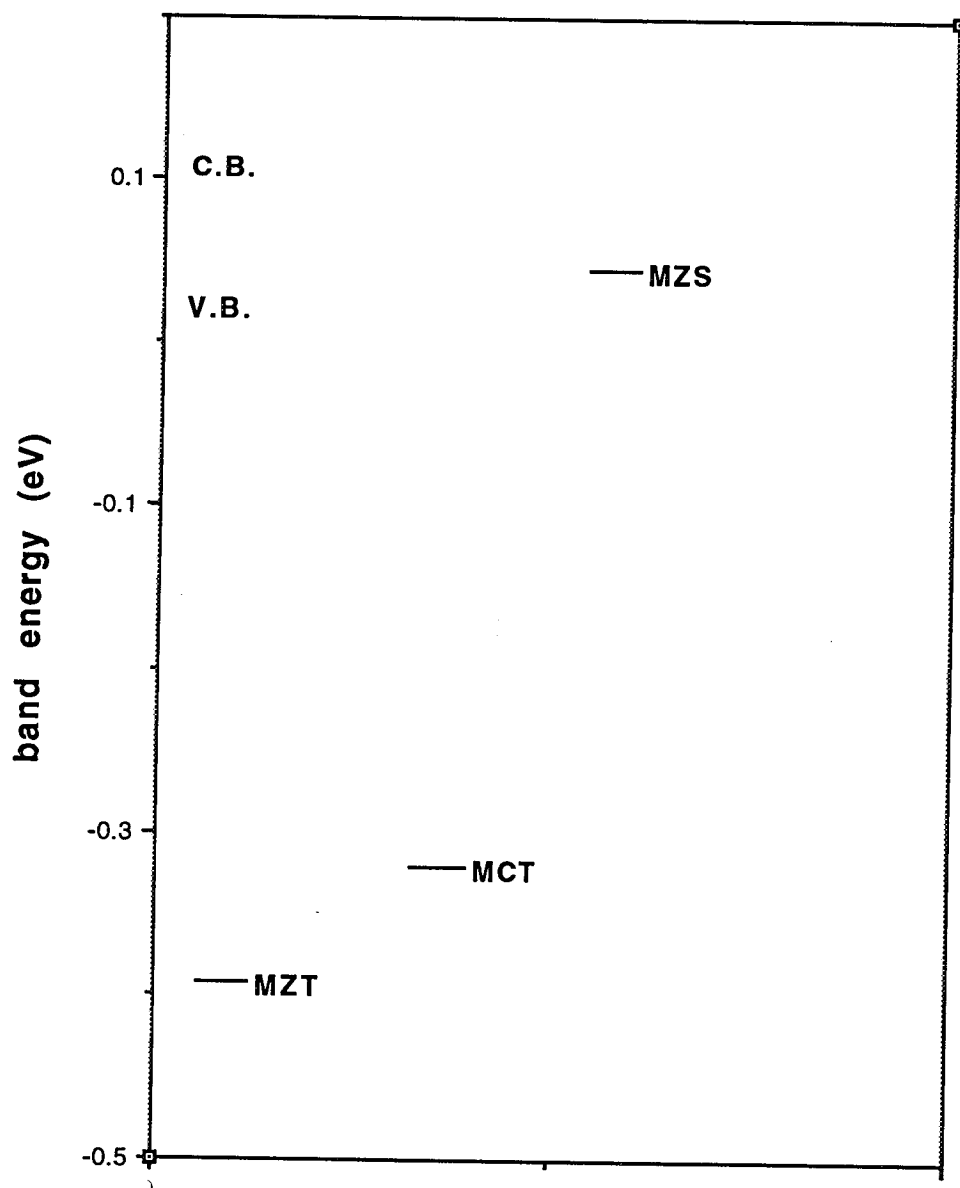


**Fig.16** Vacancy Deep Levels (cation - site,  
s - like)

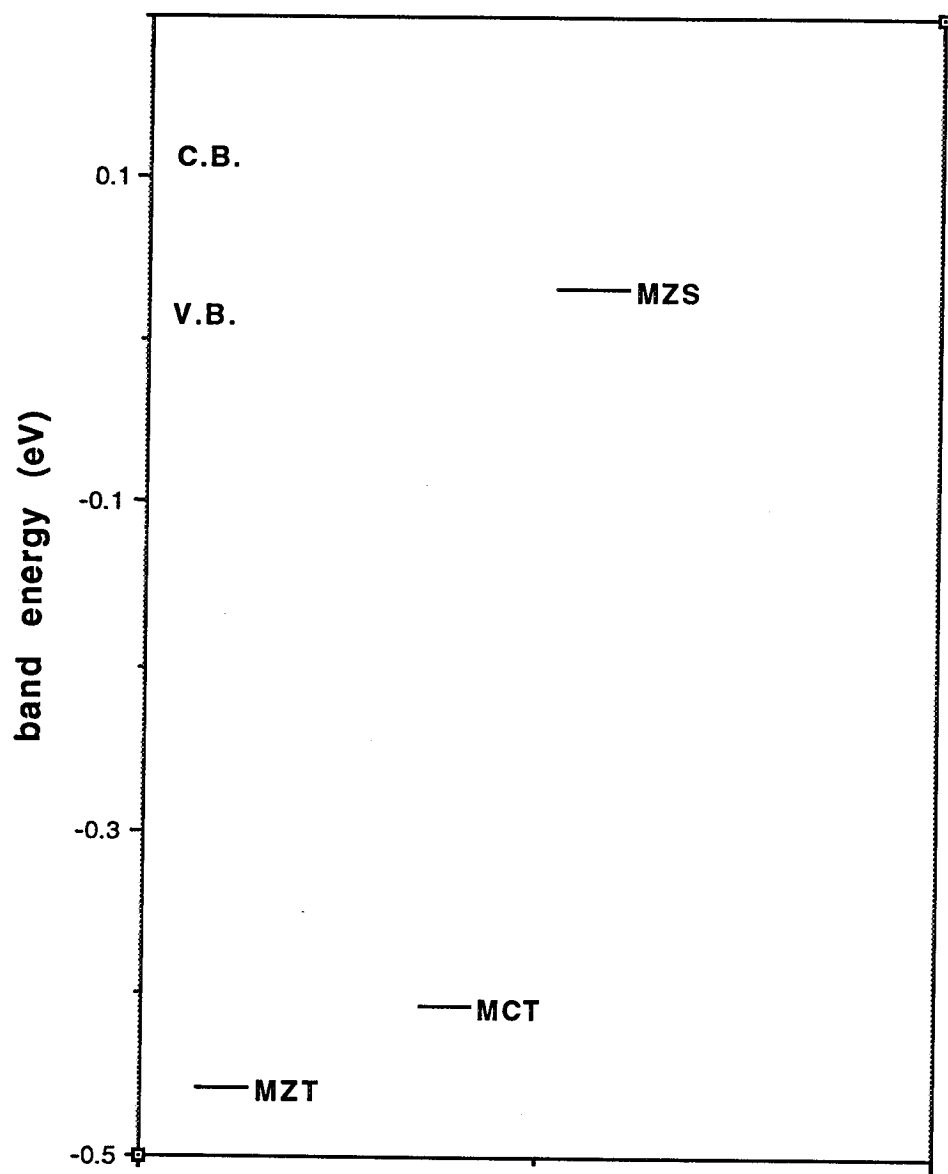


**Fig.17** Vacancy Deep Levels (anion - site,  
p - like)

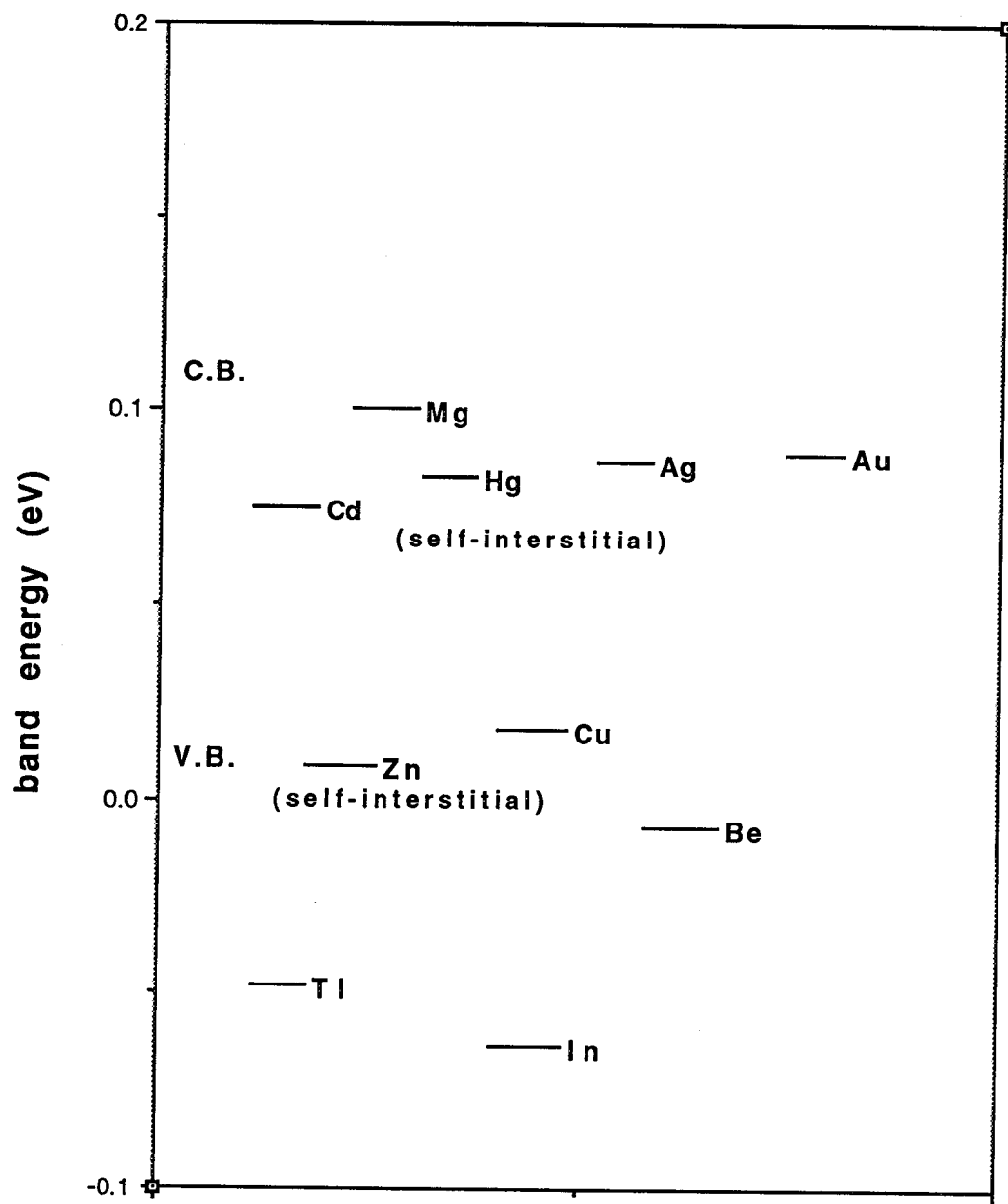


**Fig.18 Interstitial Deep Levels in MCT for  $E_g = 0.1$  eV (cation - site, s - like)**

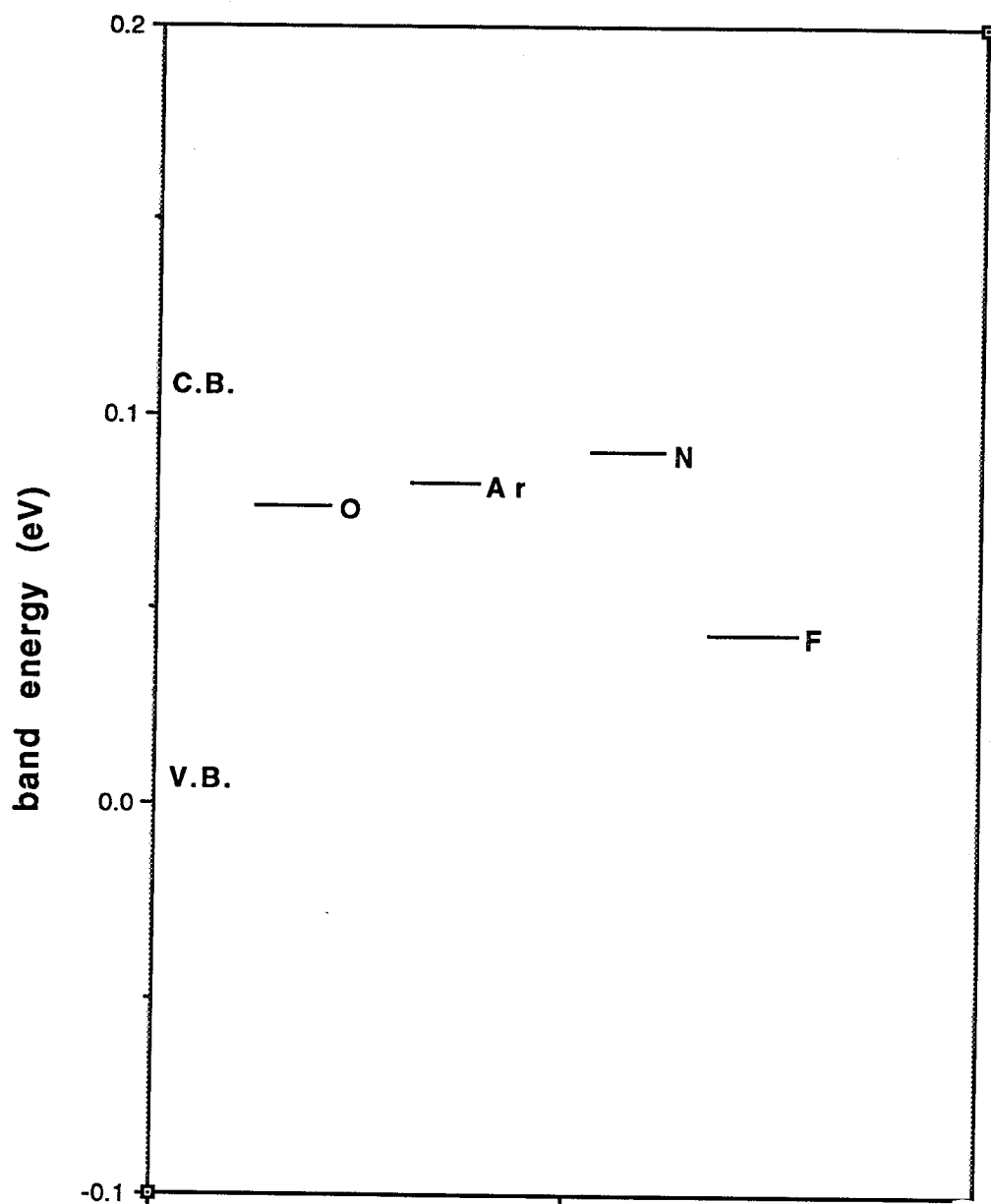


**Fig.19** Interstitial Deep Levels in MCT for  
 $E_g = 0.1$  eV (anion - site, p - like)

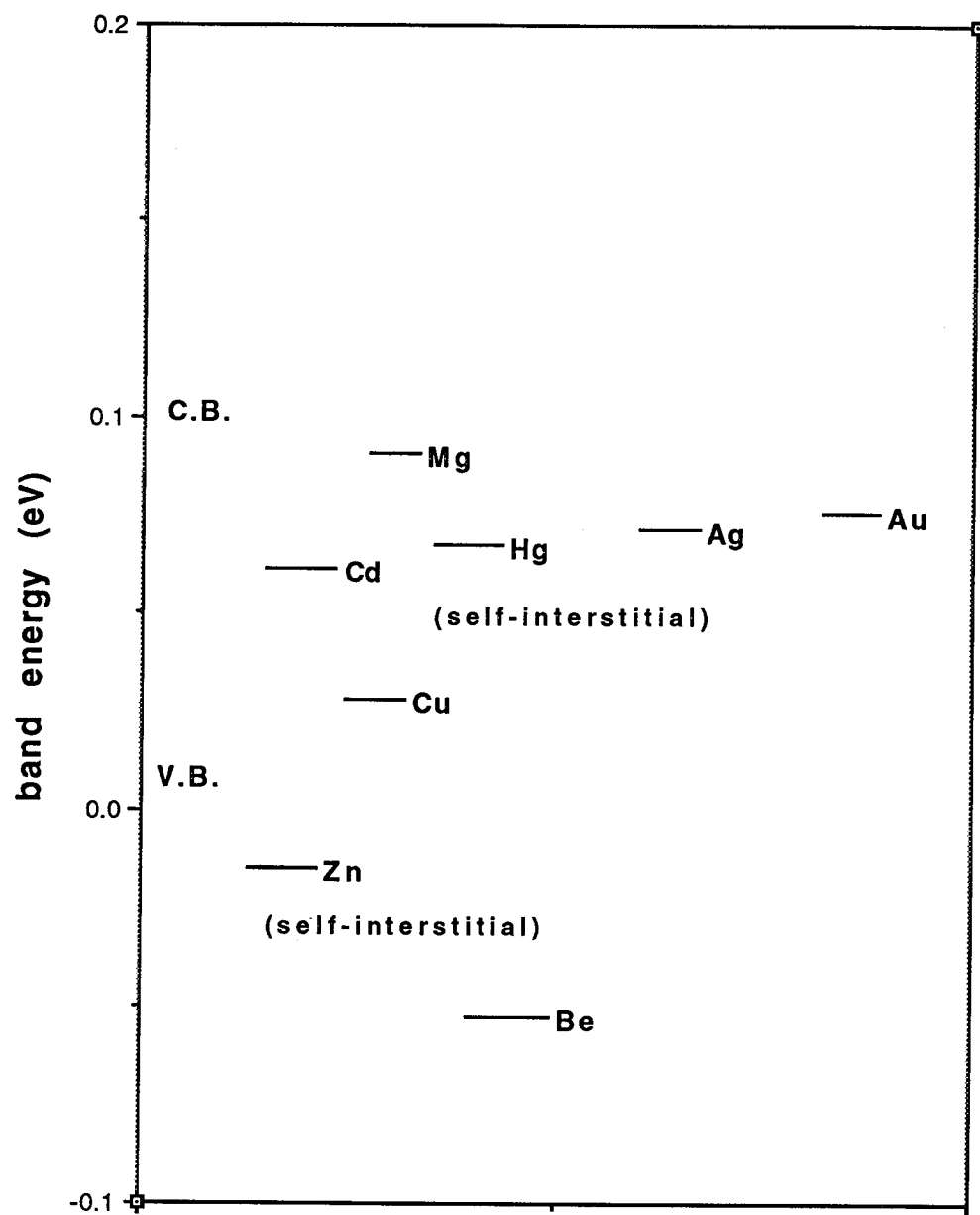


**Fig.20 Interstitial Deep Levels in MZT for  
E<sub>g</sub> = 0.1 eV (cation - site, s - like)**

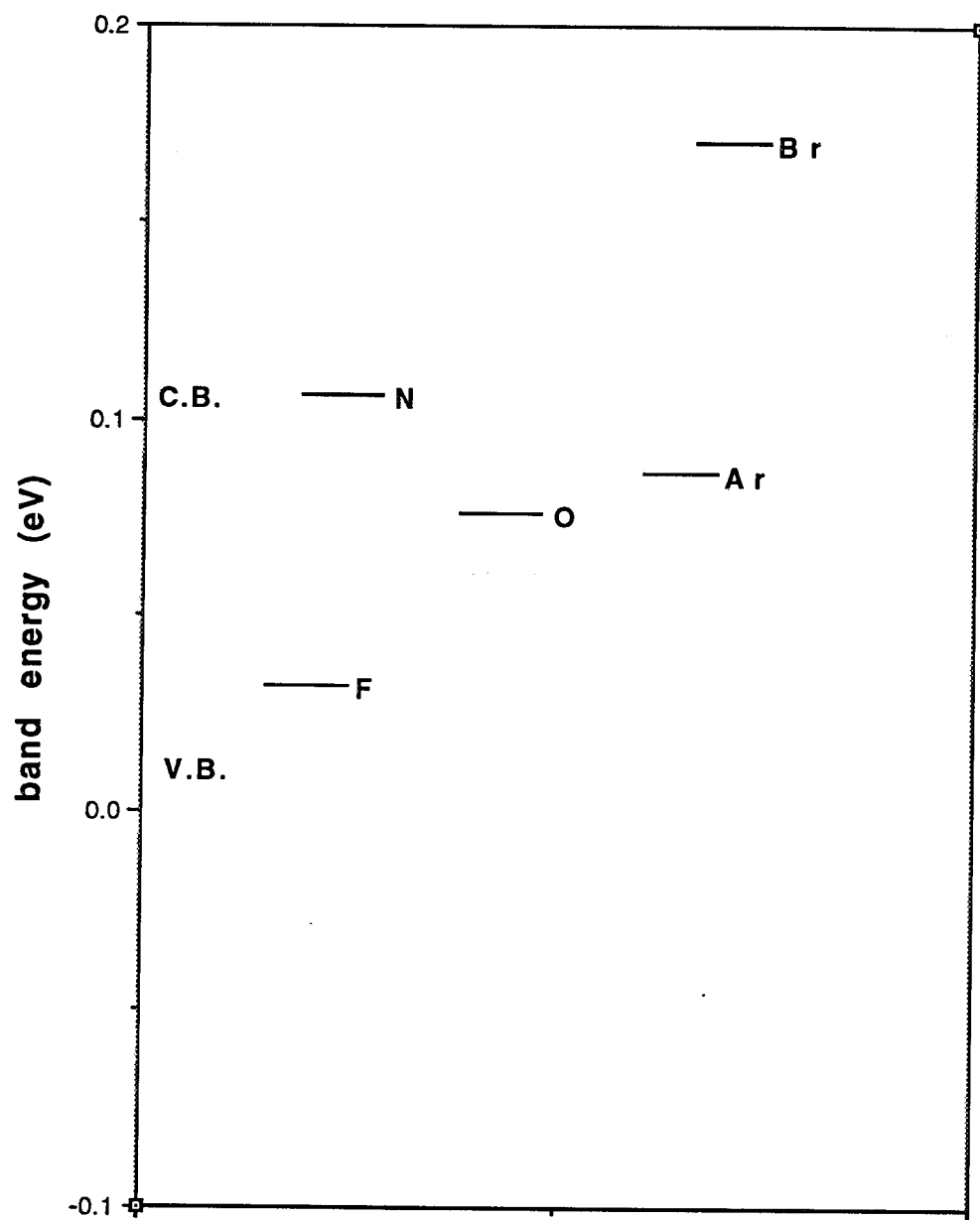
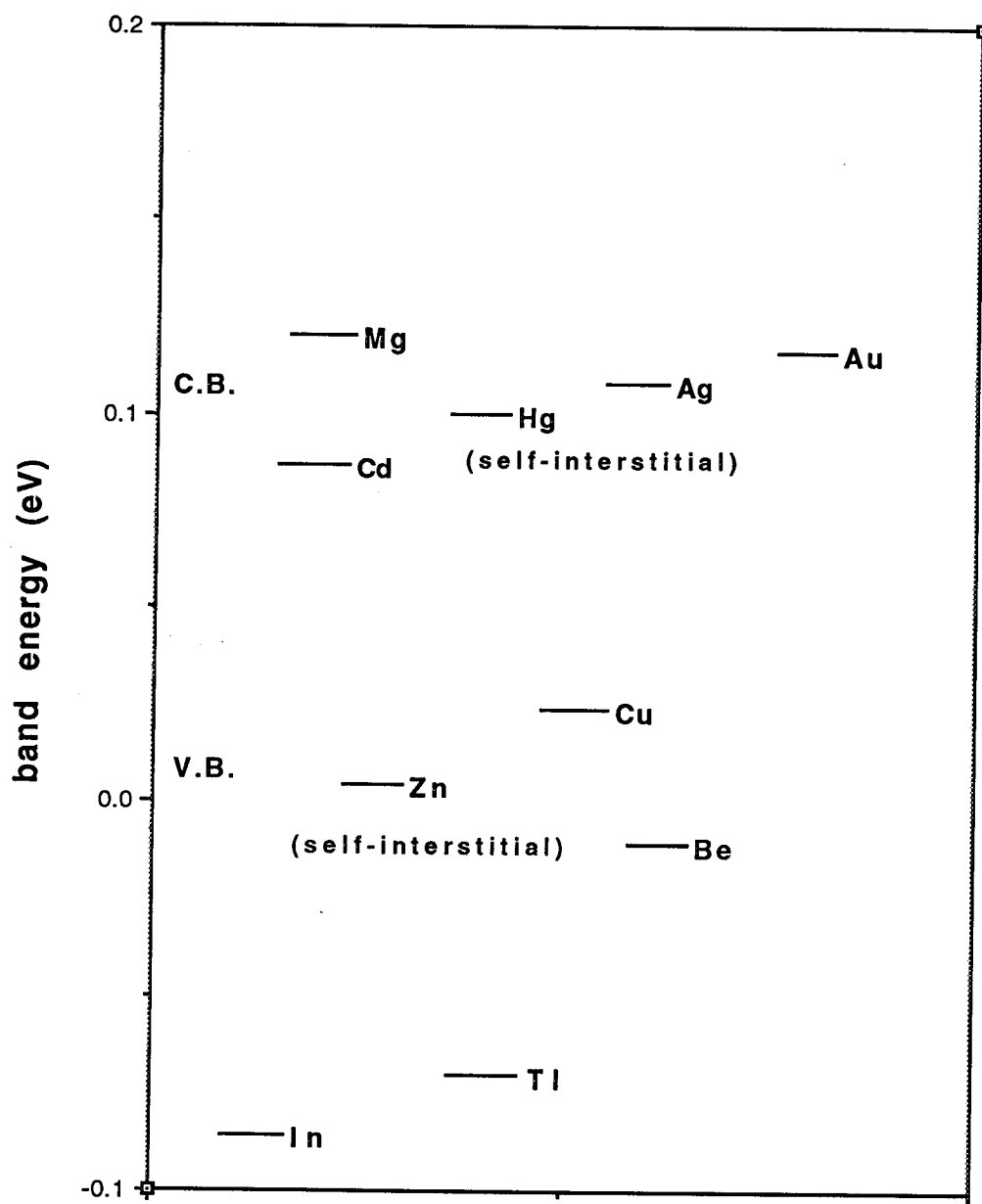


**Fig.21 Interstitial Deep Levels in MZT for  
Eg = 0.1 eV (anion - site, p - like)**





**Fir.22 Interstitial Deep Levels in MZS for  
E<sub>g</sub> = 0.1 eV (cation - site, s - like)**

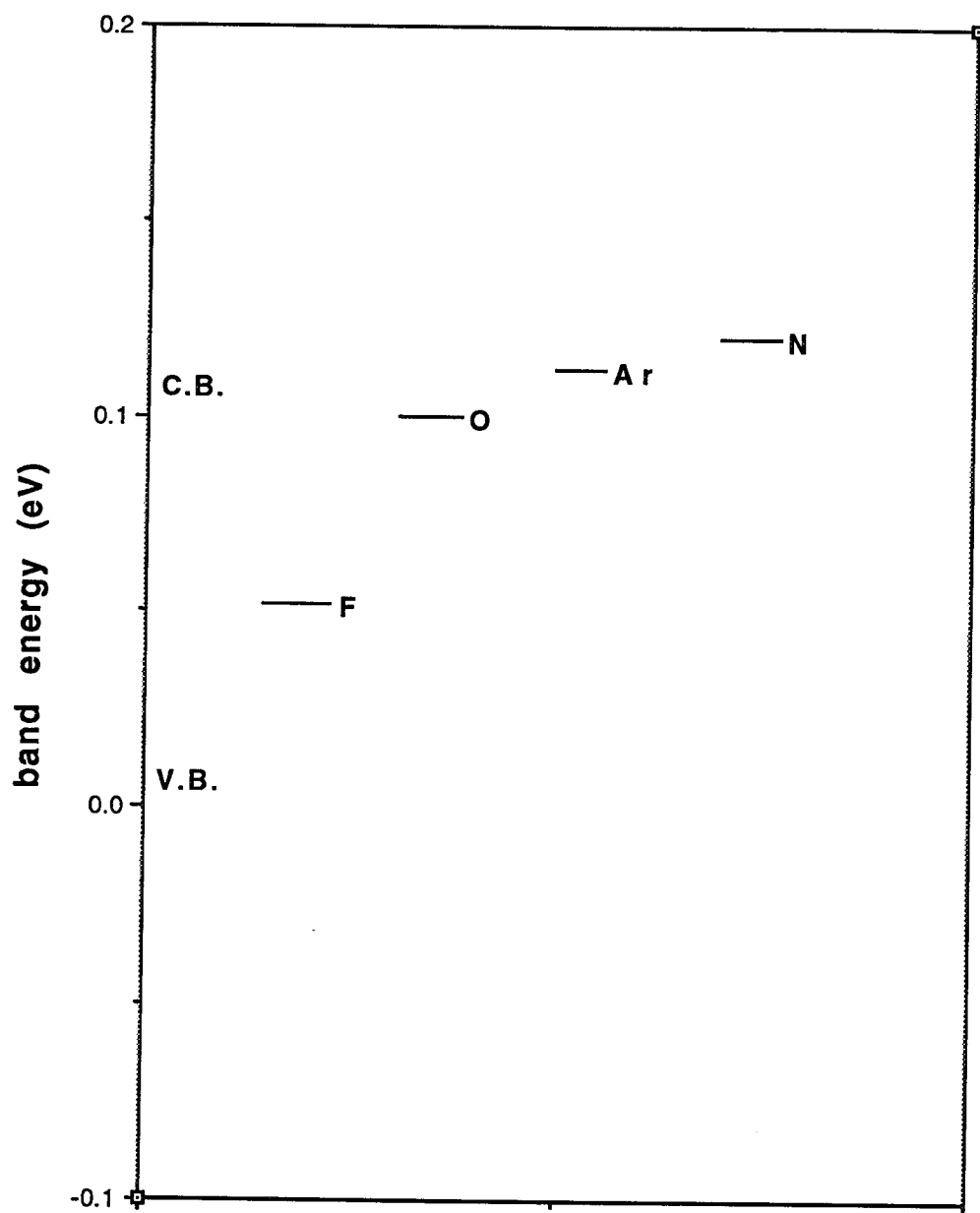
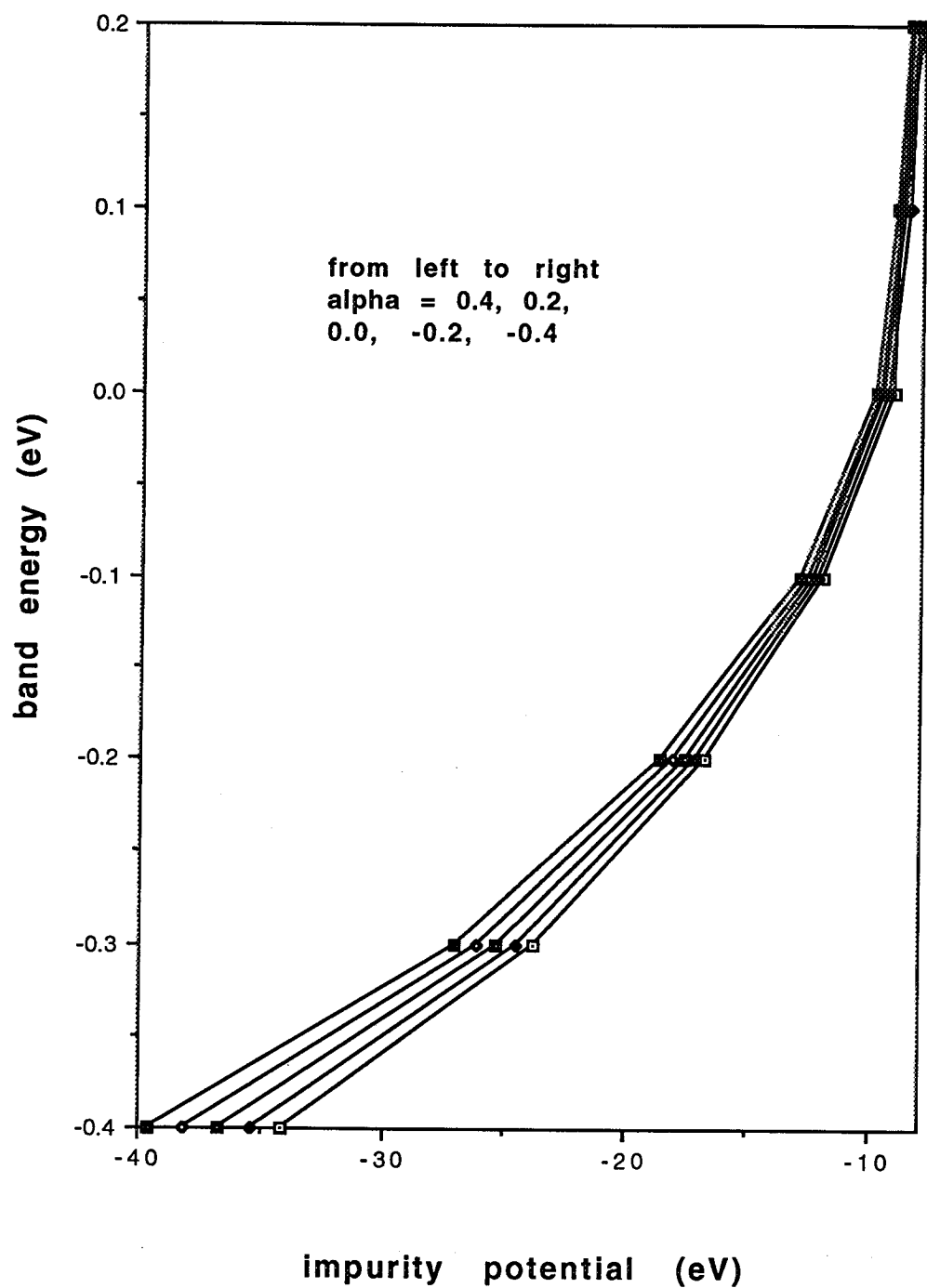
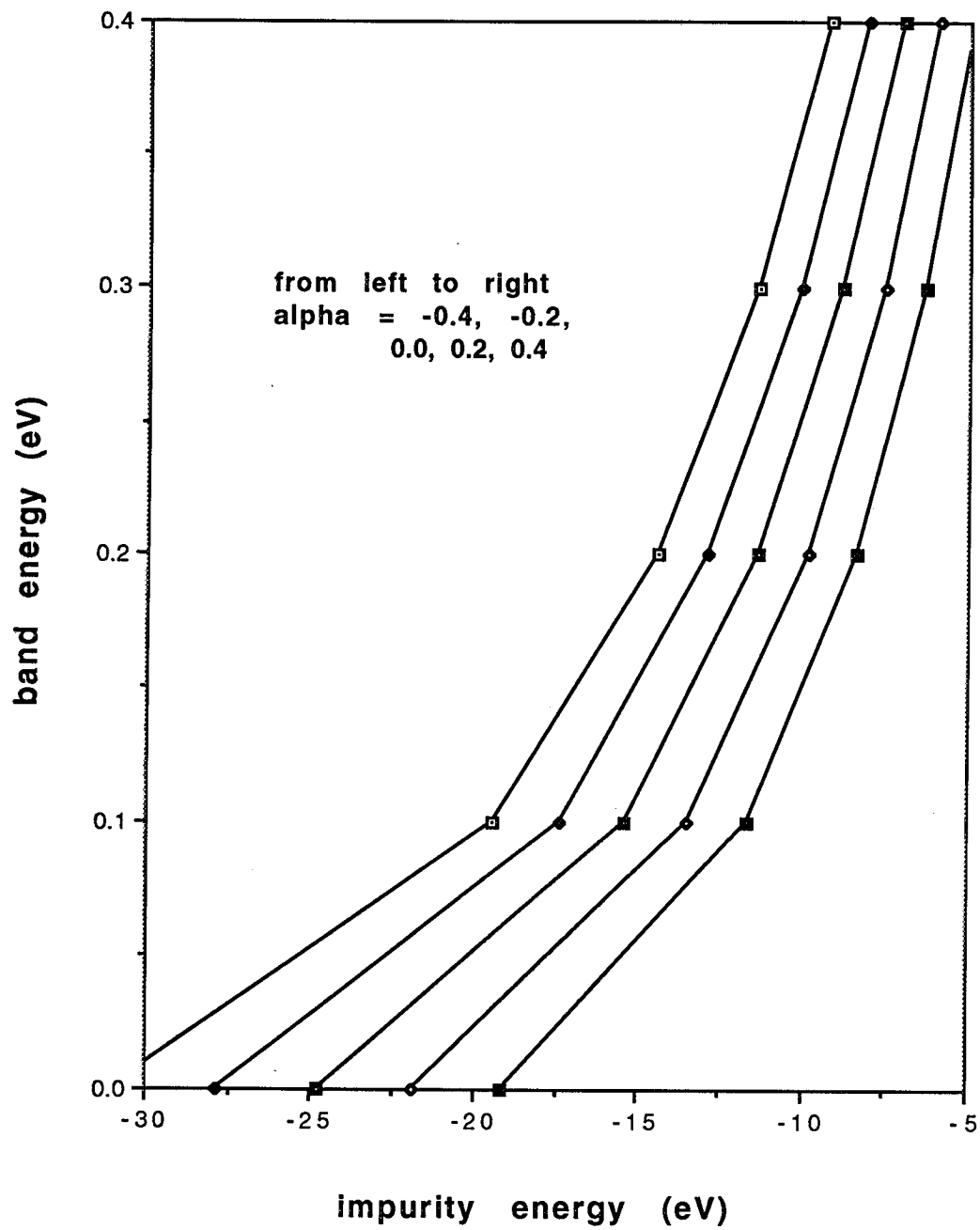


Fig.23 Interstitial Deep Levels in MZS for  
 $E_g = 0.1$  eV (anion - site, p - like)



**Fig.24** Interstitial Deep Levels in MCT for  
 $E_g = 0.1$  eV with Lattice Relaxation  
(cation - site, s - like)



**Fig. 25** Interstitial Deep Levels in MCT with Lattice relaxation (anion - site, p - like)

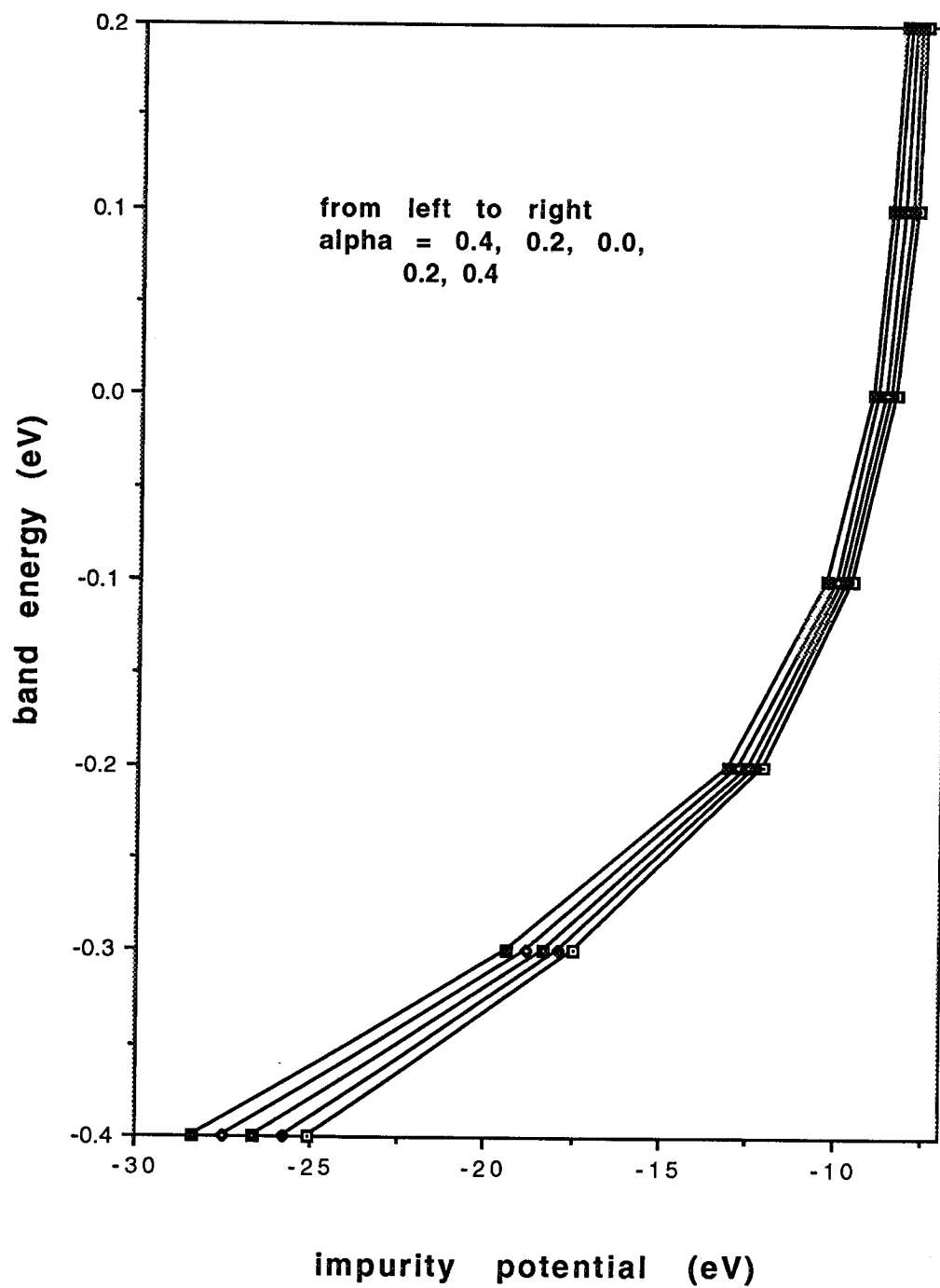


**Fig.26 Interstitial Deep Levels in MZT for  $E_g = 0.1$  eV with Lattice Relaxation (cation - site, s - like)**

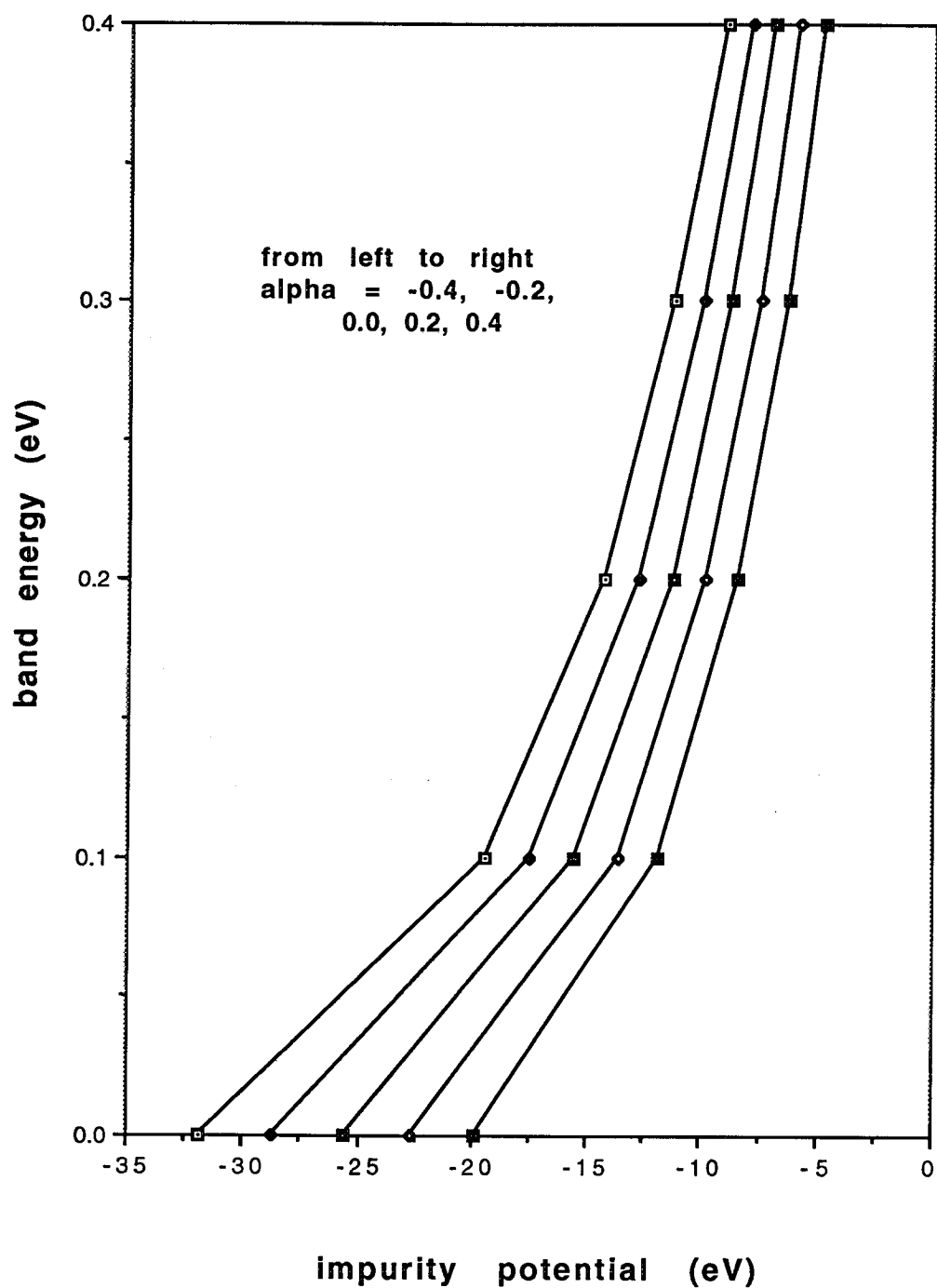


**Fig.27 Interstitial Deep Levels in MZT for  
 $E_g = 0.1$  eV with Lattice Relaxation  
 (anion - site, p - like)**

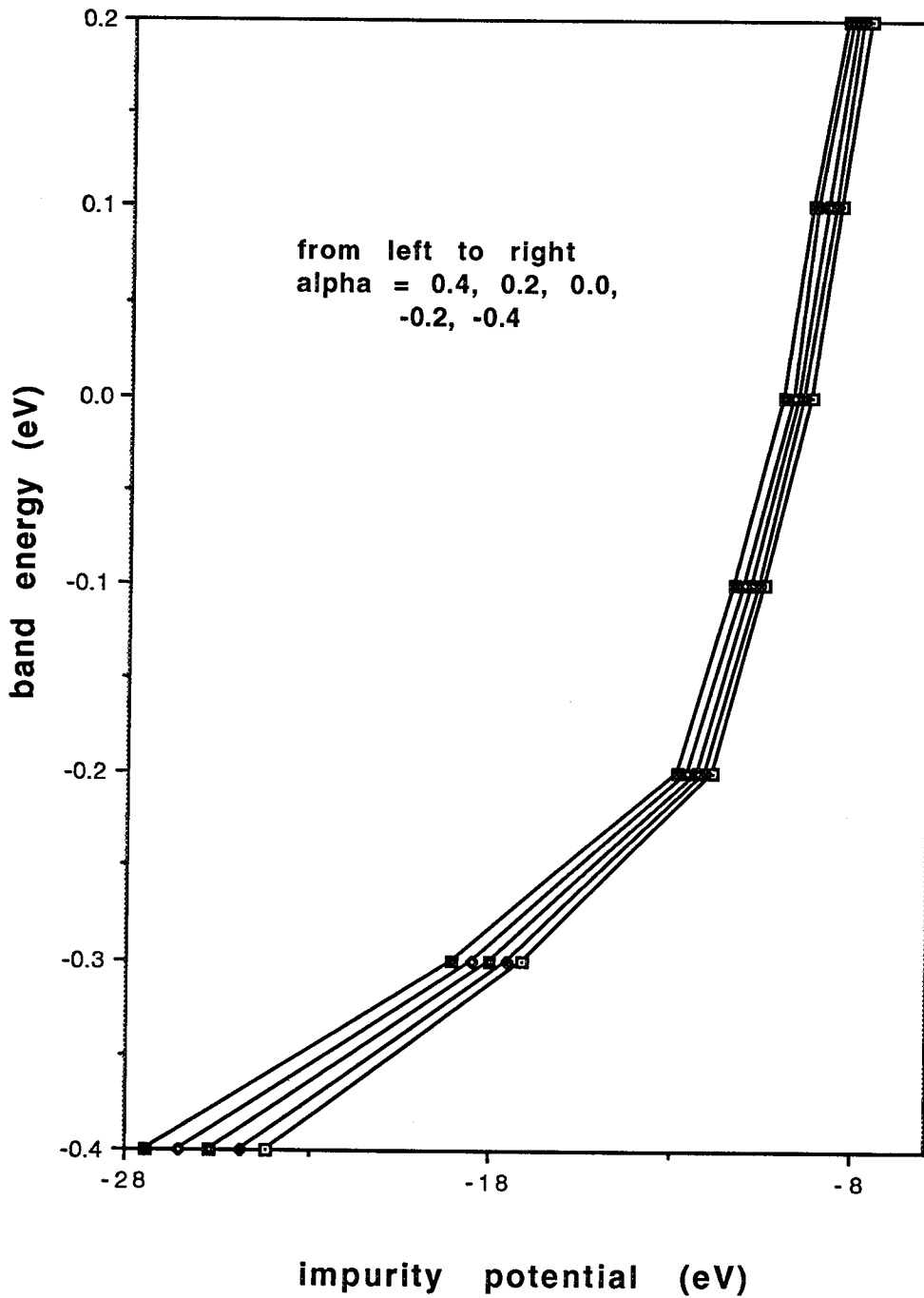


**Fig.28** Interstitial Deep Levels in MZS for  
 $E_g = 0.1$  eV with Lattice Relaxation  
(cation - site, s - like)

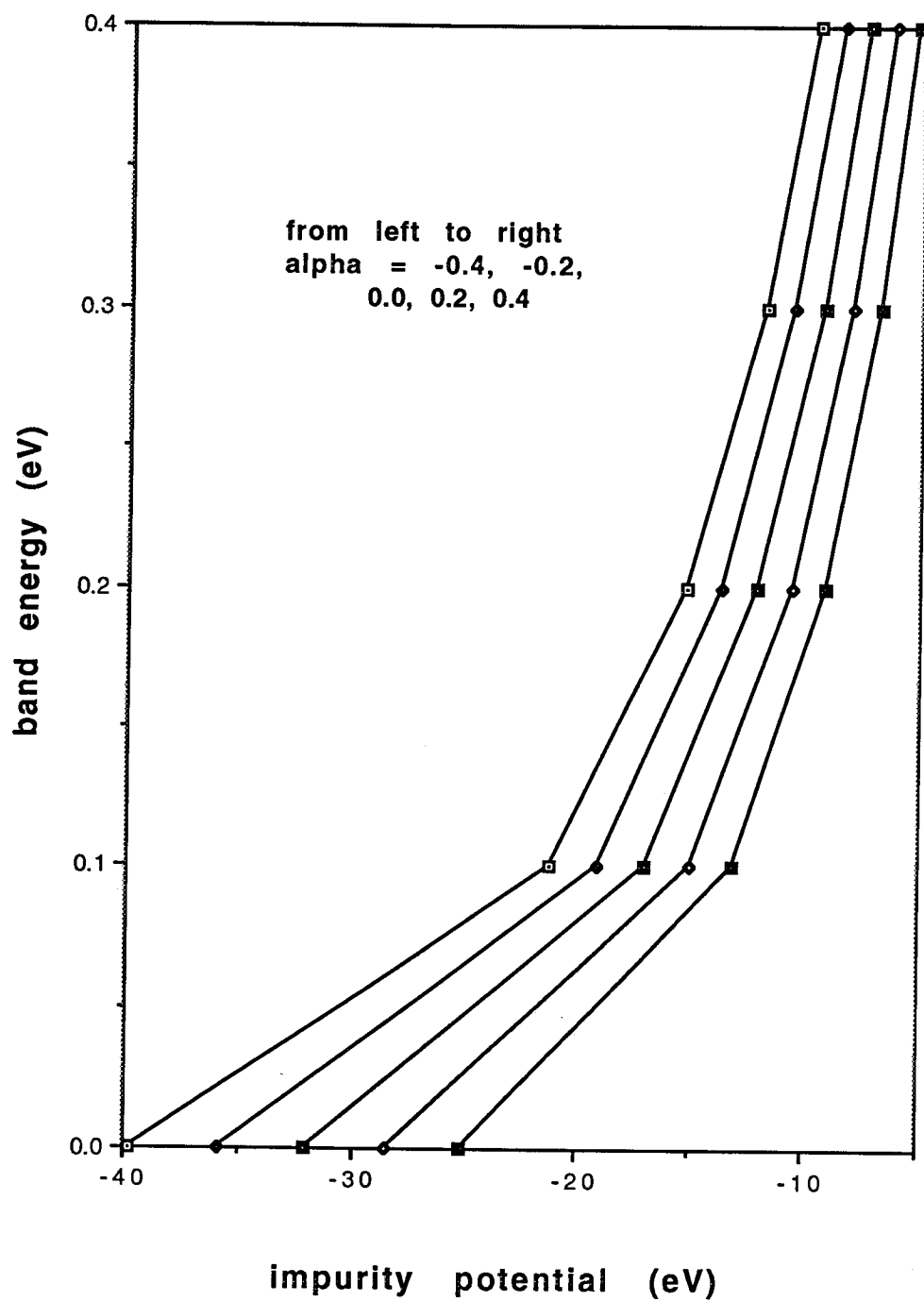


**Fig.29 Interstitial Deep Levels in MZS for  
 $E_g = 0.1$  eV with Lattice Relaxation  
 (anion - site, p - like)**



## V. Appendices

### A. References

- a1. J.D. Patterson, Semi-Annual Report: Electronic Characterization of Defects in Narrow Gap Semiconductors, NASA Grant No. NAG8-941, 25 June 1993. Also see References in this report.
- a2. W. Abdelhakiem, J.D. Patterson, S.L. Lehoczky, "A Comparison Between Electron Mobility in n-type  $\text{Hg}_{1-x}\text{Cd}_x\text{Te}$  and  $\text{Hg}_{1-x}\text{Zn}_x\text{Te}$ ," *Materials Letters* **11**, 47-51 (1991).
- a3. J.D. Patterson, W.A. Gobba, S.L. Lehoczky, "Electron Mobility in n-type  $\text{Hg}_{1-x}\text{Cd}_x\text{Te}$  and  $\text{Hg}_{1-x}\text{Zn}_x\text{Te}$  Alloys," *J. Mater. Research* **7**, 2211-2218 (1992).
- a4. W.A. Gobba, J.D. Patterson, and S.L. Lehoczky, "A Comparison Between Electron Mobilities in  $\text{Hg}_{1-x}\text{Cd}_x\text{Te}$  and  $\text{Hg}_{1-x}\text{Zn}_x\text{Te}$ ," *Infrared Phys.* **34**, 311-321 (1993).
- b 1. O. F. Sankey and J. D. Dow, "Theory of tetrahedral - site interstitial s - and p - bonded impurities in Si," *Phys. Rev. B* **27**, 7641 - 7653 (1983).
- b 2. P. Vogl, H. P. Hjalmarson, and J. D. Dow, "A semi - empirical tight - binding theory of the electronic structure of semiconductors," *J. Phys. Chem. Solids*, **V44**, 365 - 378 (1983).
- b 3. A. Kobayashi, O. F. Sankey, and J. D. Dow, "Chemical trends for defect energy levels in  $\text{Hg}_{1-x}\text{Cd}_x\text{Te}$ ," *Phys. Rev. B* **25**, 6367 - 6379 (1982).
- c 1. same as e2.
- c 2. A. Seyni, R. Granger, R. Triboulet, S. Rolland, and A. Lasbley, "Acceptor level in narrow gap  $\text{Hg}_{1-x}\text{Zn}_x\text{Te}$ ," *Phys. Stat. Sol. (a)* **V128**, K27 - K32 (1991).
- c 3. M. A. Berding, M van Schilfgaarde, and A. Sher, "Defect equilibrium in  $\text{HgTe}$ ," *J. Vac. Sci. Technol. B* **10**, 1471 - 1475 (1992).
- c 4. J. T. Schick and C. G. Morgan - Pond, "Point defects with lattice distortion in  $\text{CdTe}$  and  $\text{HgCdTe}$ ," *J. Vac. Sci. Technol. A* **8**, 1108 - 1111 (1990).
- c 5. S. Goettig and C. G. Morgan - Pond, "Deep interstitial levels in  $\text{Hg}_{1-x}\text{Cd}_x\text{Te}$ ," *J. Vac. Sci. Technol. A* **6**, 2670 - 2674 (1988).
- c 6. S. Geettig and C. G. Morgan - Pond, "Formation mechanisms of localized

- interstitial states in tetrahedrally bonded semiconductors," Phys. Rev. B42, 11743 - 11750 (1990).
- d 1. H. G. Grimmeiss, E. Janzen, and K. Larsson, "Multivalley spin splitting of 1s states for sulfur, selenium, and tellurium donors in silicon," Phys. Rev. B25, 2627 - 2632 (1982).
  - d 2. C. W. Myles, "Charge state splittings of deep levels in  $\text{Hg}_{1-x}\text{Cd}_x\text{Te}$ ," J. Vac. Sci. Technol. A6, 2675 - 2680 (1988).
  - d 3. M. Scheffler, J. Bernholc, N. O. Lipari, and S. T. Pantelides, "Electronic structure and identification of deep defects in GaP," Phys. Rev. B29, 3269 - 3282 (1984).
  - d 4. R. T. Collins and T. C. McGill, "Electronic properties of deep levels in p - type CdTe," J. Vac. Sci. Technol. A1, 1633 - 1636 (1983).
  - d 5. F. D. M. Haldane and P. W. Anderson, "Simple model of multiple charge states of transition - metal impurities in semiconductors," Phys. Rev. B13, 2553 - 2559 (1976).
  - d6. same as b1.
  - d 7. S. Lee, J. D. Dow, and O. F. Sankey, "Theory of charge - state splittings of deep levels," Phys. Rev. B31, 3910 - 3914 (1985).
  - d 8. J. Singh and A. Madhukar, "Method for calculating the electronic structure induced by short - ranged defects in semiconductors," Phys. Rev. B25, 7700 - 7712 (1982).
  - e 1. C. E. Jones, K. James, J. Merz, R. Braunstein, M. Burd, M. Eetemadi, S. Hutton, and J. Drumheller, "Status of point defects in  $\text{HgCdTe}$ ," J. Vac. Sci. Technol. A3, 131 - 137 (1985).
  - e 2. C. L. Litter, D. G. Seiler, and M. R. Loloee, "Magneto - optical investigation of impurity and defect levels in  $\text{HgCdTe}$  alloys," J. Vac. Sci. Technol. A8, 1133 - 1138 (1990).
  - e 3. A. Sher, M. A. Berding, M van Schilfgaarde, and An - Ban Chen, " $\text{HgCdTe}$  status review with emphasis on correlations, native defects, and diffusion," Semicond. Sci. technol. 6, c59 - c70 (1991).

**B. Publications and Reports Prepared for this Work**

- (a) Semi-Annual Report - June 25, 1993 (already submitted).
- (b) March 1994 American Physical Society Abstract of talk - included.
- (c) J. Patterson, Sandi Billings, and J. Mantovani, "Space Grown Crystals," Brevard Tech. J. 2 (8), 23-27 (1993). Paper included.
- (d) J.D. Patterson, "Narrow Gap Semiconductors," Overview submitted to Condensed Matter News on invitation.

# SEMI-ANNUAL REPORT

## TITLE OF GRANT:

Electronic Characterization of Defects in Narrow Gap Semiconductors

## TYPE OF REPORT:

Brief Summary of Project

## NAME OF PRINCIPAL INVESTIGATOR:

James D. Patterson

## PERIOD COVERED BY THE REPORT:

November 25, 1992 to June 25, 1993

(MID YEAR REPORT)

## NAME AND ADDRESS OF GRANTEE INSTITUTION:

Florida Institute of Technology  
150 West University Boulevard  
Melbourne, FL 32901

## GRANT NUMBER:

NAG8-941

George C. Marshall Space Flight Center  
Marshall Space Flight Center, AL 35812  
(Technical Officer: Sandor L. Lehoczky, ES75)

Abstract Submitted

for the        March        Meeting of the

American Physical Society

21 - 25 March 1994

Meeting Date

Suggested Title of  
session in which  
paper should be placed

Deep Defects in Semiconductors

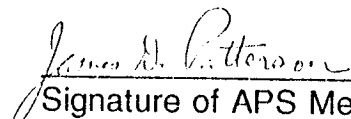
Deep Defects in Narrow Gap Semiconductors. W. LI , J. D. PATTERSON, FL Inst. of Tech. -- We use Green's function techniques to study deep substitutional (including antisite), interstitial and ideal vacancy defects in  $\text{Hg}_{1-x}\text{Cd}_x\text{Te}$ ,  $\text{Hg}_{1-x}\text{Zn}_x\text{Te}$  and  $\text{Hg}_{1-x}\text{Zn}_x\text{Se}$  as a function of  $x$ . For substitutional and interstitial impurities the effects of relaxation are included and its role in determining the location of the level is carefully considered. Of particular interest is which substitutional and interstitial atoms yield energy levels in the gap - that is can serve to trap carriers. We illustrate our results with tables and graphs. We also discuss important parameters involved in the calculation.

\* Supported by NASA Grant NAG8-941

☐ Prefer Poster Session

☒ Prefer Standard Session

☐ No preference

  
Signature of APS Member'

James D. Patterson  
Same name typewritten

Florida Institute of Technology  
Melbourne, FL 32901

# BREVARD TECHNICAL JOURNAL

## AUGUST 1993, VOLUME 2 NUMBER 8

*News & Features About the Business and the Science of Technology in Brevard*

### STAFF:

**Publisher**  
Will Standley

**Acting Senior Editor:**  
Will Standley

**Editor's Assistant:**  
Rose Lyons

### EDITORIAL COUNCIL:

David Block, Ph.D., P.E.  
Director, Florida Solar Energy Center

Lowell C. Gray, PE, CQA, CQE, CRE  
President, Quality Coaches, Inc.

Timothy Lane, MD, Ph.D.  
Wuesthoff Staff, Brevard Medical Society

Dennis R. Pape, Ph.D.  
President, Photonic Systems, Inc.

Bert Purga, Ph.D.  
Vice President, Academic Affairs, BCC

Bob Sullivan, Ph.D.  
Dean, College of Engineering, Florida Tech

Dan Wegerif, Ph.D.  
Principal, Merritt Systems, Inc.

James S. Whitehead, Esq.

### COVER ART:

NASA map shows first all-sky image at gamma-ray energies.  
(See Space News on page 20.)

BREVARD TECHNICAL JOURNAL is published monthly by BREVARD TECHNICAL JOURNAL, Inc., P.O. Box 560989, Rockledge, FL 32956. Telephone: (407) 690-0818. FAX: (407) 631-6866. Modem: (407) 631-3630. E-mail Internet address: 75076.1771@compuserve.com. E-mail Compuserve address: 75076.1771. Copyright ©1993 by BREVARD TECHNICAL JOURNAL. All rights reserved. No part of this issue may be reproduced by any means without the written permission of the publisher.

### FEATURE ARTICLES:

- 23 Space Grown Crystals  
*by Jim Patterson, Sandi Billings, & Jim Mantovani*
- 29 Company Profile: Software Productivity Solutions, Inc.  
*by Larry Lamoray*
- 35 Tests and Risks  
*by John P. Snyder*
- 39 Always Wanted An Airplane? Build One--EAA Can Help  
*by John J. Geil*

### MONTHLY FEATURES:

- 5 Business News
- 6 Stocks
- 9 Contract Awards
- 11 Patent Awards
- 13 Computer News
- 13 Stan Veit's Computer Notes
- 15 Education News
- 17 News & Events
- 19 Space News
- 21 Medical News
- 30 Calendar of Events
- 43 Amateur Radio
- 43 Science & Technology on TV
- 43 At Press Time
- 45 Upcoming Space Shuttle Flights
- 46 Computer Clubs
- 46 On-Line Systems
- 52 BTJ Buyer's Guide & Directory
- 54 Where to Contact
- 54 Classified Ads
- 55 Industrial/Commercial Real Estate Guide
- 59 Index to Advertisers

**Brevard Technical Journal Is...The Journal Of Brevard's Leading Industry**

# Space Grown Crystals

Jim Patterson, Sandi Billings, and  
Jim Mantovani

The exploitation of space began with the launch of Sputnik in 1957, which started the race to the moon and the race for dollars. In the name of national pride, taxpayer support was rallied not just for exploring the unknown, but also because of the promise that scientific returns will make money through the development of new products and, in the process, will raise the standard of living. Of course, space has been used for military purposes and for various benign remote sensing purposes, but the idea of manufacturing something in space is particularly attractive, promising a return on the dollar. After more than 5 years of promises, we may have found a space-based industry that will deliver.

The growing of crystals in space meets many of the criteria for space manufac-

ture. The product --- nearly defect-free crystals --- is extremely valuable, compact, and light, and made much better than on Earth. The growth of certain kinds of crystals seems to benefit from the microgravity environment of space.<sup>(1,2)</sup> The profitability of manufacturing crystals in space, however, remains an open question.

In this article we first review what crystals are and how they are grown, and then we discuss the concept of microgravity and why it might be an attractive environment for growing crystals. Before discussing the Space Station and the Space Shuttle, we will review some earlier techniques for growing crystals in microgravity. Finally, we will discuss some recent and proposed techniques for growing crystals in space.

Most people think they know what a crystal is --- after all, it's as clear as crys-

tal, isn't it? Actually, crystal glass isn't crystalline at all; it is a special kind of amorphous or random structure. A crystalline structure has a regular array of atoms, as regular as the arrangement of black and white squares on a checkerboard. This perhaps can give us a clue as to why it is difficult to grow perfect crystals on Earth under the influence of gravity.

## Crystal Defects

No crystal is perfect. Some defects may be desirable, such as the donors and acceptors introduced into semiconductors to change their electrical conductivity. Even when desirable, the number and types of

Table 1

### SOME CRYSTALS GROWN IN SPACE

CRYSTAL	USE
CdZnTe	Material Substrate for HgCdTe
HgCdTe	Infrared detection
HgZnTe	Infrared detection
GaAs (doped)	High Speed IC's and Lasers
InSb	Various electronic devices
PbSnTe	Broadband and Infrared detection
Protein	Research

The basic reason for growing all crystals in space is to produce large; defect free, homogeneous crystals.

#### About the authors:

Dr. Jim Patterson is the head of the Department of Physics and Space Sciences at Florida Tech. He joined the university in 1984 from the South Dakota School of Mines, and he loves to go back to his gold mine there whenever possible. Jim's specialty is theoretical solid state physics, and he currently is working under a NASA grant, studying narrow gap semiconductor materials for infrared detectors.

Sandi Billings became a science writer after earning her bachelor's degree in space science at Florida Tech. Currently, as the director of Teaching & Research Labs at Brevard Community College, Sandi manages the laboratories being developed in Palm Bay for chemical analysis, microbiology, and remote sensing/Geographic Information Systems.

Dr. Jim Mantovani, assistant professor of Physics and Space Sciences, does much of his research using a scanning tunneling microscope that he built at Florida Tech. Prior to joining the university, Jim spent three years at the Oak Ridge National Laboratory. He obtained a Ph.D. in Physics from Clemson University in 1985.

defects must be controlled, or the crystal won't behave as desired. The kinds of defects that occur are point, line, and plane defects.

Point defects come in many varieties: vacancies, self and foreign interstitials, substitutional impurities, and even antisite defects. Several point defects are illustrated in Figure 1. Antisite defects only arise in compound materials with at least two kinds of atoms. A typical com-

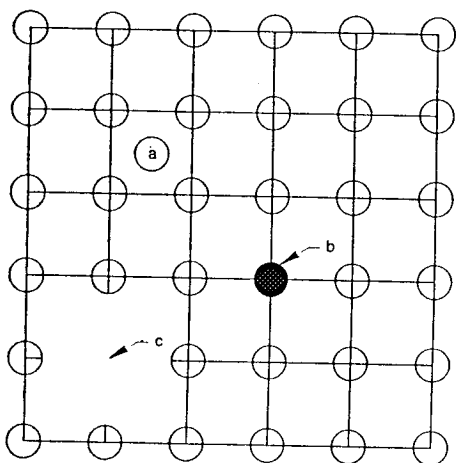


Figure 1. Point defects: (a) interstitial atom—self or foreign, (b) substitutional impurity, (c) vacancy—absence of atom.

pound crystal of interest is shown in Figure 2. An antisite defect occurs if an *A* atom is found on a *B* site or vice versa. Several of the crystals we will discuss are compound.

Line defects come in two types: edge and screw dislocations, which are shown in Figure 3. An edge dislocation is simply a missing half-plane of atoms. A screw dislocation, occurring when one part of a crystal is pushed up relative to other parts, can be visualized as cutting the pages of a book halfway across at the middle. Then the lower part of page 1 can be "taped" to the upper part of page 2 and similarly for the following pages. This would form a "spiral staircase." Except for the "taping," the idea is shown in Figure 3b.

Most crystals are really just collections of many small, individual crystals called grains. Grains come together at grain boundaries, which are examples of plane defects. For many purposes it is desirable not to have grains, but rather a large single crystal.

#### Crystal Growth<sup>(3,4)</sup>

One of the ways of growing crystals on Earth is the Bridgman technique, which

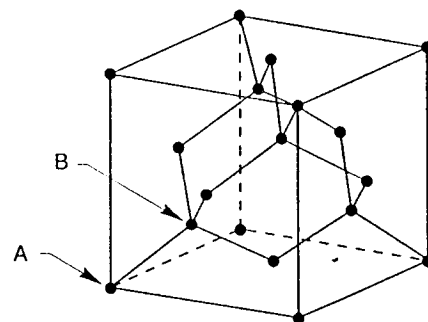


Figure 2. ZnS structure. *A* atoms (e.g., Zn) are located at sites to (0, 0, 0). *B* atoms (e.g., S) are located at sites equivalent to (*a*/*4*, *a*/*4*, *a*/*4*), where *a* is the length of the side of the unit cell shown.

also works in microgravity. In a common Bridgman process, shown in Figure 4, the material is melted in a stationary vertical column which tapers to a point at the bottom where there is an unmelted "seed" crystal. As the furnace moves up, the crystal resolidifies from the seed. The steps in the crystallization process are diffusion of molecules to the surface of the crystal (the solid melt interface); diffusion of molecules over the surface; binding of the molecules at the surface; and diffusion

### MIL-SPEC COMMERCIAL CONTRACT Assembly & Prep

QUALITY COMPONENT is a small business located in a modern, environmentally-controlled facility featuring full ESD protection, secure stocking and staging of customer materials, and rapid turnaround.

#### PC/Cable Assembly

MIL-STD-2000, WS 6536, NSA & NASA spec's

#### Tinning/Tape and Reel

Hot solder dip coating for components, connectors, & cables

#### Component Testing

Certified solderability and solvent resistance testing

Solder/SPC Training

Specification Consultants

Quality Assurance - ESD Protection

ISO 9002 Registration In Progress

For a free evaluation & estimate, call  
631-0799



QUALITY  
COMPONENT SERVICES INC.  
"Your Solder Service Center"

406 Richard Rd., #2, Rockledge, FL 32955

MIL-STD-2000  
CERTIFIED

## DESIGN DRAFTING ILLUSTRATION RENDERING

LET US HELP YOU CAPTURE  
AND VISUALIZE YOUR IDEAS  
WITH OUR 3-D COMPUTER  
DESIGN SYSTEM. OUTPUT  
INCLUDES: CONCEPT DRAWINGS,  
DETAIL DRAWINGS, AND  
PHOTO-RENDERINGS.

Vector

Cad  
Services

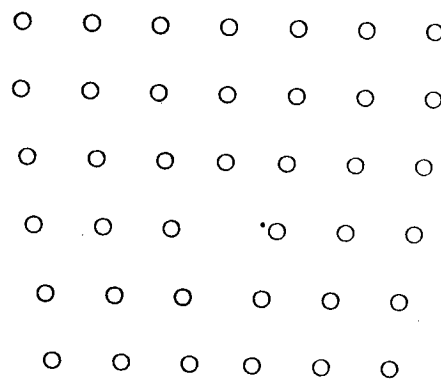
3245 N. Courtenay Pkwy. #34  
Merritt Isl, FL 32953  
407-453-2971



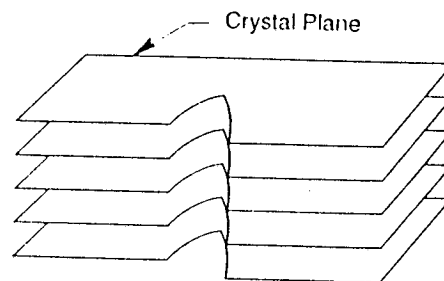
heat away from the surface of crystallization. When not too far from equilibrium conditions, screw dislocations can be an important aid to growth, because they have a higher probability of sticking to the step caused by the screw. Very large departures from equilibrium can cause similar growth to be unstable; it is then replaced by dendritic growth, forming thin crystals.

In addition to the Bridgman technique, the commonly used melt growth techniques are floating zone, growth from solution, and growth from vapor. The floating zone method, which has some similarities to the Bridgman technique, uses a rod of material (not single crystalline) and a single crystal rod of the same material. The rods are joined end to end and heated in a melt is formed. This melt is moved along the raw materials, and the crystal is grown from the seed. In microgravity there is no distortion of the molten zone, but convection can still be a problem. In terrestrial crystal growth the sample is heated and vaporized. It then flows to the cooler and is deposited on the substrate. Growth from solution is important primarily in protein crystal growth.

In gravity causes convection, buoyancy, hydrostatic pressure. Convection, especially turbulent convection, can introduce many kinds of defects to be introduced into the crystal. Without convection, crystal growth can occur under diffusion-controlled conditions, leading to improved chemical homogeneity and structural perfection. It is also possible to grow much larger single crystals than could be grown under the stress caused by gravity. The desired goal is to grow large single crystals which are nearly perfect. Once



(a)



(b)

Figure 3. Dislocations: (a) edge and (b) screw

this has been accomplished, controlled amounts of defects can be introduced as desired. In the absence of convection and other stresses introduced by gravity, nearly perfect single crystals are much more likely to form.

In microgravity, some effects that are totally masked by gravity-driven causes show up nicely, such as Marangoni convection. In a melt, the surface tension may vary with temperature, and in the absence of gravity this can be enough to cause convection--Marangoni convection, which may cause striations in crystals grown in space.

### Microgravity

First we should talk about what microgravity is and what it is not. It is not the absence of gravity, or even a region where gravity is very small. Unless one goes very far from massive bodies, this is impossible. Even at a Shuttle orbit of 300 km above the Earth, the force of gravity is 91% the value experienced on the Earth. Microgravity is accomplished by having almost all the effects of gravity canceled out by free fall.

Newton himself understood the principle, illustrated in Figure 5. If one mounts a cannon on a large mountain on an otherwise flat Earth and fires the cannon ball horizontally, it will land some distance from the base of the mountain. Adding more powder will cause the ball to go further. Finally a point will be reached when the ball falls exactly the same amount that the Earth curves. The ball will then be in free fall, and in orbit. The effects of gravity for objects inside the ball will be very small. In an orbiting satellite there will be exactly one surface where the

effects of gravity are negligible and at other places inside one has "microgravity."

There are many ways to produce microgravity; all you have to do is arrange to be in free fall.<sup>(2)</sup> Drop towers and drop tubes offer two ways of accomplishing this. The first commercial use of microgravity was probably the drop tower used in 1785 in England to make spherical lead balls. Marshall Space Flight Center has both a drop tower and a drop tube 100 meters high - this alone allows one to have free fall, or microgravity, for about 5 seconds. In a drop tower the entire experimental package is dropped. For crystal growth experiments, this means the furnace as well as the instrumentation and the specimen are all placed in a special canister and dropped. In a drop tube, there is an enclosure in which, for example, only the molten sample would be dropped. Special aerodynamic design, vacuum, or other means is used to reduce air drag and hence obtain real free fall. For slightly longer times (20 seconds or so), the KC 135 aircraft can be put into a parabolic path to produce microgravity. Extending this idea, rockets have been used to produce microgravity for periods of about 400 seconds.

For long-duration experiments, the experimental package needs to be in orbit. Such research began with SKYLAB in 1973 and has continued with the Space Shuttle and the Space Lab in 1983. We now look forward to Space Station Freedom and to spending very long times in space. This is important for crystal growth, because some crystals grow so slowly that the process is about as exciting as grass growing. And the longer that we have to grow crystals in space, the larger we can grow them.

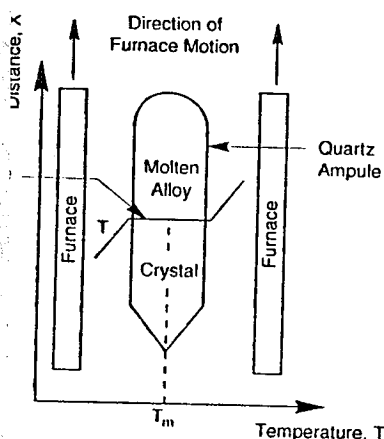


Figure 4. Crystal growth by the Bridgman technique.  $T_m$  is the melting temperature of the crystal.

## Crystals and Crystal Growth Furnaces for Space

Many crystals are being considered for growth in space. Among the more interesting of them are the narrow gap semiconductor alloys, Mercury Cadmium Telluride (MCT), Mercury Zinc Telluride (MZT), and Mercury Zinc Selenide (MZS)<sup>(6)</sup>. At Florida Tech in Melbourne, FL, authors Jim Patterson and Jim Mantovani are studying these materials under NASA research contracts. One use of these semiconductor crystals of interest to NASA is making infrared detectors<sup>(6,7,8)</sup>.

Because of its stability with respect to mercury, MZT appears to be a strong competitor to MCT. It is very hard to produce homogeneous bulk crystals of MZT on Earth due to convection and composition segregation driven by gravity. We also need to point out that these compound systems have phase diagrams which must be considered in predicting the nature of the crystal formed.<sup>(9)</sup> For MCT we see in Figure 6 that the fraction of CdTe which solidifies depends on the temperature.

Scientists and engineers are presently

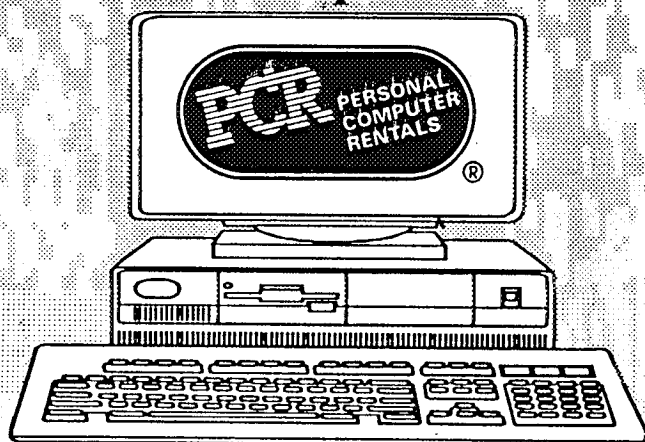
hard at work producing crystal growth furnaces for use in microgravity. A typical one, used by Dr. S.L. Lehoczky of Marshall Space Flight Center,<sup>(9)</sup> is shown in Figure 7. It has three major elements: (1) an avionics subsystem (the electronics to control its operation); (2) the environmental control system, obviously used to produce the proper environment in either fluid or vacuum; and (3) the furnace, which consists of several parts. Typically the furnace is set up to have several heating zones which produce a temperature gradient. It is found that it is better to move the furnace itself rather than the crystal, so as not to introduce instabilities into the growing process. Even so, movements in the Shuttle can produce g-jitter.

Besides MCT, MZT, and MZS, there are several other crystals being considered for growth in microgravity, as listed in Table I. These include InSb, GaAs, and protein crystals. However, the whole subject of crystal-growing is far more complicated than many would imagine.<sup>(9,10)</sup> Despite much initial excitement, the viability for commercial growth of crystals in space is an open question, which a number of Brevard industries and universities will continue to explore.

## REFERENCES

1. Materials Sciences in Space, Edited by B. Feuerbacher, H. Hamacher, and R.J. Nauman. Springer-Verlag, Berlin, 1986. (See especially articles by R.J. Nauman, "Historical Development," pp. 10-30; D.T.J. Hurle, "Crystal Growth," pp. 379-400; and P.R. Sahn and J.C. Sturm, "Solidification," p.p. 149-167.)
2. Opportunities for Academic Research in a Low-Gravity Environment, Edited by G.A. Hazelrigg and J.M. Reynolds, American Institute of Aeronautics and Astronautics, Inc. 1986. (See especially "Facilities and Programs for Research in a Low-Gravity Environment" by Richard E. Halpern, pp. 1-35.)
3. Parker, R. L. "Crystal Growth Mechanisms: Energetics, Kinetics, and Transport," Solid State Physics 25, pp. 151-299 (1970). Edited by H. Ehrenreich, F. Seitz, and D. Turnbull, Academic Press, New York.
4. K.F. Kelton, "Crystal Nucleation in Liquids and Glasses," Solid State Physics 45, 75-177 (1991), Edited by H.

## Need to Rent a Computer?



**Daily. Weekly. Monthly**

.IBM .HP Lasers  
.Macintosh .Display Monitors  
.Compatibles .LCD Panels & More..

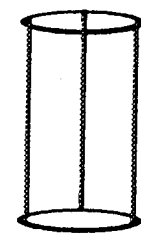
**Call the professionals in PC Rentals  
...We Deliver Service!**

**800-333-3326**

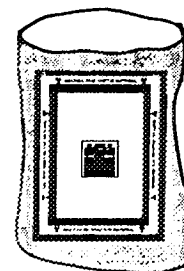


## ProTech Corporation

- ✓ Collapsible Safety Drum - Replaces the old 55 Gal. drum and weighs just 10 lbs.
- ✓ Tear resistant clear and opaque plastic bags made from Safety Grade plastic. Up to 6 color printing.
- ✓ Waterproof nylon bags.
- ✓ Easy/Fast personnel barriers (Insta-Barriers) stanchions & accessories.
- ✓ No hardware or tools required.
- ✓ Top quality products that work together.
- ✓ Custom design products made from steel/plastic/PVC/cloth/nylon.



COLLAPSIBLE DRUMS



DISPOSABLE TRASH AND SPECIALTY BAGS

*Quality products/safety tested!*

**(407) 722-3303**

renreich and D. Turnbull. Academic Press, New York.

Materials Processing in the Reduced Gravity Environment of Space, Edited by J. E. Rindome. Elsevier, New York, 1982. (See especially the article by S.L. Hoczky and F.R. Szofran, "Directional Solidification and Characterization of  $Hg_{1-x}Cd_xTe$  Alloys," pp. 409-420.)

Patterson, Jim, and Billings, Sandra. "Infrared: Light in the Dark," Brevard Technical Journal 1(9), pp. 33-34, 43 (1992).

Bulcerak, Raymond. "Mercury Cadmium Telluride Material Requirements for Infrared Systems," J. Vac. Sci. Technol. B 10(4), pp. 1352-1358 (1992).

Amieson, John A. "Infrared technology: advances 1975-84, challenges 1985-90," Optical Engineering 25(5), pp. 688-692 (1986).

Miller, W. A. The Science of Crystallization--Microscopic Interfacial Phenomena, Cambridge University Press, Cambridge, 1991.

Miller, W. A. The Science of Crystallization--Macroscopic Phenomena and Deformation, Cambridge University Press, Cambridge, 1991.

END

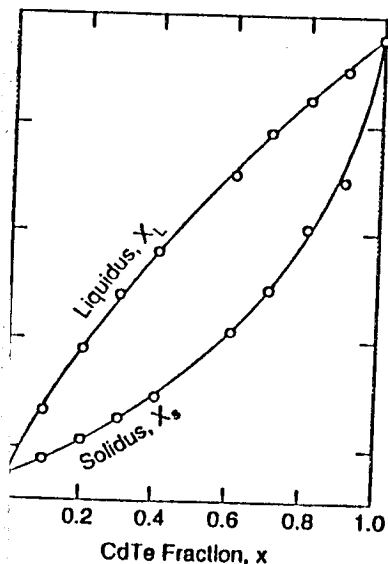
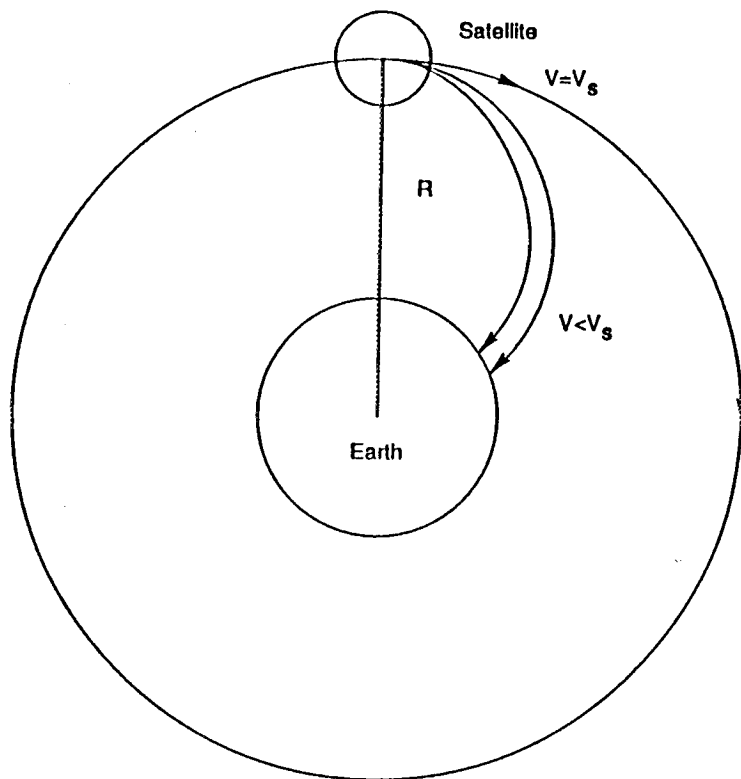


Figure 6.  $Hg_{1-x}Cd_xTe$  phase diagram.



$$G \frac{M_s M_E}{R^2} = \frac{M_s V^2}{R} \Rightarrow V_s = \sqrt{\frac{GM_E}{R}}$$

Figure 5. Microgravity in Free Fall

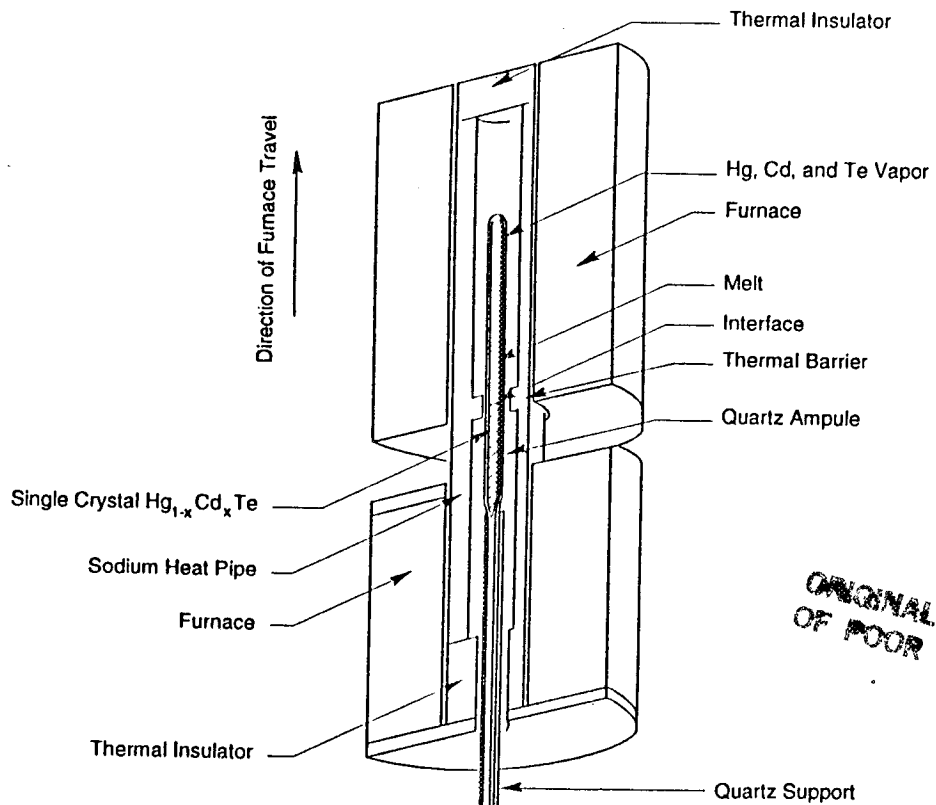


Figure 7. Schematic of Bridgman crystal growth furnace for mercury cadmium telluride.

# NARROW GAP SEMICONDUCTORS

by  
J.D. Patterson

Florida Institute of Technology  
Melbourne, FL 32901-6988  
U.S.A.

## *Introduction*

Not all semiconductors are alike. Narrow gap semiconductors (NGS)<sup>(1-7)</sup> are often defined as having an energy gap, as measured from the top of the valence band to the bottom of the conduction band, of less than or about 0.5 eV. This is to be contrasted with the energy gap in Si at room temperature of about 1.1 eV. NGS can be regarded as being intermediate between covalently bonded solids and metals. Because of the narrow gap between them, there is a strong interaction between the conduction and valence bands and the energy dispersion relation becomes non-parabolic ( $E$  not proportional to  $k^2$ ). Also, since the effective mass of carriers depends on their kinetic energy at the Fermi surface, the mobility may depend on the carrier concentration. NGS are sensitive to external influences such as temperature, external magnetic fields, and strain, features which make them strong candidates for sensors of many kinds. Besides their principal use as infrared detectors and emitters, NGS have application or potential application in magnetoresistive, Hall effect, and thermoelectric devices, and in semiconductor strain gauges. IR detectors, of course, have a large variety of uses including military (night vision and detecting the plume of ballistic missiles) and peaceful (remote sensing and security systems).

As has been observed<sup>(8)</sup>, narrow gap semiconductors have been in use for a long time. Their first recorded use was as eye liners for the ladies of early Egypt. For this, crushed Galena (PbS, lead sulphide) was used. A still later use of Galena was as a crystal in early crystal detector radios. PbS is a member of the IV-VI lead salt family which also includes PbSe and PbTe. They have been used as infrared (IR) detectors, but their main use nowadays is for lasers. By using several compounds (e.g. PbSnTe, PbSe and PbEuSeTe), the wavelengths from 3 to 30 nanometers can be covered.

More recently discussed materials, such as the III-V family of semiconductors, have found a good deal of application (see Table I). A particularly important member of this group is InSb a NGS first discussed in detail by Welker<sup>(9)</sup> in 1952. Later E.O. Kane<sup>(10)</sup> gave a fairly simple discussion of its band structure. InSb is still an important material for use in IR detectors.

The materials that we are particularly concerned with in this review are the II-VI compound semiconductors which include mercury cadmium telluride (MCT) and mercury zinc telluride (MZT) (see Table II). Lawson<sup>(11)</sup> was the first to do detailed work with the MCT alloys. He showed how one could continuously vary the energy gap by varying the ratio of the concentration of Cd to Hg. He thus developed materials which operate as IR detectors in the 10 micrometer range of wavelength and at 77K. Several other NGS (e.g. Bi<sub>2</sub>Te<sub>3</sub>, Te, and Mg<sub>2</sub>Sn) are mentioned in the paper by R.S. Allgaier in the collection edited by Seiler and Littler<sup>(2)</sup>.

### **General Remarks**

In this paper we will focus our attention on the II-VI compound narrow gap semiconductors<sup>(12-14)</sup>. Figs. 1-3 show the zinc blende crystal structure of the materials, their first Brillouin zone, and an example of their calculated band structure. ZnTe and CdTe are both direct band gap semiconductors. Fig. (4a) shows the energy gap of MCT vs.  $x$ , the fraction of Cd, at room temperature (upper curve) and at 77K (lower curve). One reason MCT is so important is that its energy gap  $E_g$  can be tuned by varying  $x$  as we have just shown. In practice, the calculation of the dependence of  $E_g$  on composition and temperature is very difficult and so one often resorts to obtaining  $E_g(x,T)$  through curve fitting. A good empirical approximation for the energy gap in  $Hg_{1-x}Cd_xTe$  is<sup>(15)</sup>

$$E_g(x,T) = -0.302 + 1.93x + (5.35)(10^{-4})(1-2x)T - 0.81x^2 + 0.832x^3 \quad (\text{eV})$$

for  $0 < x < 1$  and  $4.2 < T < 300\text{K}$ . (1)

Fig. (4b) shows the energy gap for several materials (at room temperature) and the corresponding inverse cutoff wavelength ( $\lambda_c$ ) given by

$$\lambda_c^{-1} = E_g / 1.24 \quad , \quad (2)$$

for  $\lambda_c$  in micrometers and  $E_g$  in eV. Photons of energy less than  $E_g$  are not absorbed and  $\lambda_c$  is the corresponding wavelength above which no absorption occurs.

Fig. 5 sketches the energy vs.  $k$  dependence for the conduction band, heavy and light hole bands, and the split off bands as determined by the model of Kane<sup>(10)</sup> originally for InSb. For further details see the appendix.

The II-VI semiconductors, that we are particularly concerned with here, are important for several reasons, as indicated in a summary of the properties of the most important member of this group (MCT) given in Table 3. Some useful properties of elements

involved in compound MCT semiconductors are given in Table 4. We go on to discuss two particularly important compound semiconductors MCT and MZT.

### ***MCT and MZT***

We will discuss in some detail two properties which are subjects of current research, namely electron mobility and deep defects.

#### Mobility

High mobility materials make good IR detectors, among other things, hence the theory of mobility is of practical importance. The theory for compound II-VI semiconductors is more complicated than the theory of simple semiconductors. These complications arise due to the non-parabolic nature of the energy band and the highly ionic character of the material which makes polar interactions of the electrons with the longitudinal phonons play an important role at "high" temperature (high being room temperature for many of these materials). In this interaction, the phonon energy is comparable to the electron energy. The scattering is inelastic, the relaxation time approximation is inappropriate, and a variational principle has to be used to solve the non-iterated Boltzmann equation. Another complication is due to narrowness of the band gap which implies a non-negligible number of thermally excited electrons, so screening has to be taken into consideration.

The collisions considered in our calculation involve: ionized impurities, holes, compositional disorder, acoustic phonons and optical phonons. At low (typically about 50K) temperature for n-type materials, the scattering is mainly due to ionized impurities. This scattering process decreases with increasing temperature, since the charged impurity atoms do not scatter high-energy electrons very effectively. The theory for hole scattering is somewhat similar to that for ionized impurities. At high (typically room) temperature, the scattering is mainly due to longitudinal optic phonons.

Since the two atoms in the unit cell are different, the longitudinal optic mode of the lattice vibrations polarizes the crystal and an electric field is produced. The Frohlich perturbation potential is used to describe the interaction of the electrons with the polarization field. For the acoustic phonons one uses the deformation potential which arises from changes in the energy gap as a result of changes in the spacing of the atoms. In a compound semiconductor, like HgCdTe, electrons suffer an additional scattering due to the random locations of Hg and Cd atoms. This is termed compositional disorder scattering. With known band structure and interactions, the Boltzmann transport equation can be solved for the electron energy distribution function  $f$ , from which the mobility can be obtained. If  $f$  is known, we can calculate the conductivity by first calculating the electron current density  $J_x$ ,

$$J_x = \int e V_x f D(E) dE, \quad (3)$$

where  $D(E)$  is the density of states per unit volume and  $V_x$  is the velocity of the charge carriers in the direction of the impressed electric field and current flow. Hence the electron mobility can be calculated from

$$\mu = \left| J_x / ne \right| \quad (4)$$

where  $n$  is the number of electrons per unit volume and  $e$  is their charge.

Typical results, obtained by this procedure, are shown in Fig. 6<sup>(16)</sup>.

### Defects

Defects control the properties of semiconductors. The effects of both shallow and deep defects (see Table 5) are considered here. Present understanding of shallow defects (which supply carriers) in semiconductors originated with the classic work of Kohn and Luttinger<sup>(17)</sup>. The study of deep defects has evolved more slowly but goes back to the fundamental paper of Slater and Koster<sup>(17)</sup>. Deep defects are important for both fundamental and industrial research because of their important role in recombination of charge carriers (electrons and holes). The study of defects in narrow gap semiconductors represents a much less clear story than in semiconductors like Si and GaAs. Here, both shallow defects (caused by long range potentials) and deep defects (from short range potentials) are far from being completely understood. All defects we study are point defects. Until one can identify and characterize all appropriate defects, it is impossible to make clear statements about the quality of a crystal. A full characterization of the crystal perfection involves not only a theoretical study of all common defects but also experimental verification of models for them. The simplest model of a shallow defect in NGS assumes the defect is fully ionized but there is not a lot one can do with such a model since most of the physics has been approximated away. Deep defects may produce energy levels near the center or near the band edge<sup>(17)</sup>. Neglect of the long range component (Coulomb tail) for deep defects near the band edge is not a good approximation, since it is precisely here that small Coulomb tail effects can be important. The Green's Function model, however, gives an accurate estimate of energy trends for deep defects with energies well in the gap. The model uses the customary Green's function<sup>(17)</sup>,

$$G^{(0)}(E) = (E - H_0)^{-1} \quad (5)$$

where  $H_0$  is the Hamiltonian of the perfect crystal, and one can show directly from Schrodinger's equations that the defect energies  $E$  are determined by

$$\det (I - G^o(E) V) = 0 \quad (6)$$

where  $V$  is the defect potential. The Green's Function can be constructed once band structure calculations are available. With a judicious choice of  $V$ , this technique has been found to produce very good results<sup>(17)</sup>, particularly as regards to chemical trends:

There are several kinds of defects as shown in Fig. 7 and Table 6. We study substitutional (including antisite, e.g. a Te on a Hg site in MCT), interstitial and ideal vacancy defects (see Fig. 7 and Table 7). Vacancies and self interstitials are the most common native defects. The ideal vacancy model assumes that a vacancy is formed by removing an atom from the crystal, but leaving all other atoms in the same position. This is not a very good model and results for this case will not be presented here. For substitutional and interstitial impurities, the effects of relaxation of the atoms neighboring the substitutional or interstitial impurity are included. Future improvements should include charge state interactions (where the impurity is not neutral) and dealing with non ideal vacancies in which relaxation is included.

In considering interstitials, one should note that tetrahedral symmetry for interstitials is different from tetrahedral symmetry for substitutional defects because nearest neighbors are closer for interstitials than for substitutional impurities. For deep defects some results, obtained by us, for the substitutional and interstitial cases are shown in Fig. 8a-8d. In all cases we have chosen  $x$  so the bandgap is exactly 0.1 eV. For MCT this works out to be  $x = 0.22$  at  $T \cong 0K$  and for MZT this is  $x = 0.15$  at  $T \cong 0K$ . Cation sites are mercury, cadmium or zinc sites. Anion sites are tellurium sites. By group theory the important levels in tetrahedral symmetry are predominantly s or p like (technically  $A_1$  or  $T_2$ ). For the figures, the calculation has been done for each of the atoms indicated and after relaxation of neighboring atomic positions, the defect energy level comes out as indicated.

### ***The Future***

An excellent discussion of future applications has appeared. See "New developments and trends in the physics and technology of narrow-gap semiconductors," by R.A. Stradling in the book edited by Seiler and Littler<sup>(2)</sup>. The future for NGS seems to be concerned with applications using new materials and structures<sup>(18)</sup>: multilayers, superlattices, multi-quantum wells, resonant tunneling devices, strained layers and magnetic semiconductors. The surface has barely been scratched as to utilization of these new ideas. One of the areas of greatest activity at present is in making IR devices from superlattice-like structures. One advantage of superlattices is that one can separate the ionized donors (which also scatter carriers) from the region where the carriers move. Superlattices also produce "mini bands" which allow us to tailor the effective energy gap. Another recent idea is strained layer superlattices. Here a



small lattice mismatch between layers can be used to create a strain which modifies the electronic properties in a desirable way. Another area of interest is in using superlattice type structures to create solar cells of improved efficiencies. Perhaps the easiest way to understand how this could occur is to consider layers of decreasing band gap. The first layer could remove lower energies in the solar spectrum, the next layer could be designed to remove higher energies and so forth until the whole spectrum is efficiently utilized. Experimental techniques of great present and future importance in order of decreasing expense include MBE (molecular beam epitaxy), MOCVD (metalo-organic chemical vapor deposition), and electrodeposition. The ability of these new techniques to grow materials of alternating layers of precise thickness of several nanometers has totally revolutionized the field of solid state physics. We are nearing the age of designer materials where one grows a material to specifications rather than hunts for a natural material of desired properties. At present, commercial application of these new areas has been slow, partly because exploitation of current technology, particularly in software, lags device production.

### ***Acknowledgements***

I wish to thank Dr. Weigang Li, Dr. Jim Mantovani, and Dr. Ryne Raffaele, of the materials physics group of Florida Tech, for helpful discussions. Dr. Li obtained the deep defect results shown in this paper. General discussions with Dr. Jay Burns have been most helpful. This work has been partially supported by NASA/Marshall Space flight Center Grant Number NAG8-941.

# APPENDIX

## Some Additional Band Structure Results

As in Kane's model applied to II-VI materials, for purposes of calculating the band structure it is customary to assume a virtual crystal approximation and ignore alloy disorder (which later can be put in as a perturbation to discuss certain effects). When one solves the secular equation of the Kane model, one finds the following equation for the conduction, light hole and split off band

$$E^3 + (\Delta - E_g) E^2 - (E_g \Delta + P^2 k^2) E - \frac{2}{3} \Delta P^2 k^2 = 0$$

where  $\Delta$  is the spin-orbit splitting<sup>(10)</sup>

(A1)

$E_g$  is the  $\Gamma_6 - \Gamma_8$  band gap

$P$  is the momentum matrix element<sup>(10)</sup>.

With the origin is chosen to be at the top of the valence band, if  $\Delta \gg E_g$  and  $Pk$ , and including heavy holes, one can show:

$$E = E_g + \frac{\hbar^2 k^2}{2m} + \frac{1}{2} \left( \sqrt{E_g^2 + 8 P^2 k^2 / 3} - E_g \right) \text{ Conduction Band} \quad (A2a)$$

$$E = -\frac{\hbar^2 k^2}{2m_{hh}} \text{ Heavy Holes} \quad (A2b)$$

$$E = -\frac{\hbar^2 k^2}{2m} - \frac{1}{2} \left( \sqrt{E_g^2 + 8 P^2 k^2 / 3} - E_g \right) \text{ Light Holes} \quad (A2c)$$

$$E = -\Delta - \frac{\hbar^2 k^2}{2m} - \frac{P^2 k^2}{(3 E_g + 3 \Delta)} \text{ Split-Off Band,} \quad (A2d)$$

where  $m$  is the mass of a free electron.

Knowing the  $E$  vs.  $k$  relation, the density of states per unit volume can be calculated from

$$D(E) = \frac{k^2}{\pi^2} \frac{dk}{dE}, \quad (A3)$$

which is useful for a variety of calculations, see e.g. Eqn (3).

Finally, in a further approximation, neglecting  $\frac{\hbar^2 k^2}{2m}$ , in (A2a) we can write a convenient simplification for the conduction band (where now  $E$  is referred to the bottom of the conduction band).

$$E \left( 1 + \frac{E}{E_g} \right) = \frac{\hbar^2 k^2}{2m_1}, \quad (A4)$$

where  $m_1 = \frac{3\hbar^2 E_g}{4P^2}.$

Since the momentum effective mass is given by

$$m_p = \hbar^2 k^2 \left( \frac{dE}{dk} \right)^{-1} \quad (A5)$$

we find with Eqns. (A4) and (A5),

$$\frac{m_p}{m_1} = 1 + \frac{2E}{E_g} \quad (A6)$$

which shows how  $m_p$  varies with energy. In many applications, only the electrons near the Fermi energy are important. From Eqn (A6) with  $E$  equal the Fermi energy, we see how  $m_p$  could vary if the Fermi energy varies due to change in electron concentration.

## REFERENCES

1. T.C. Harmon and Ivars Melngailis "Narrow Gap Semiconductors" in Applied Solid State Science, Edited by Raymond Wolfe, Academic Press, New York 1974, pp. 1-94.
2. David G. Seiler and C.L. Littler (Editors), "Narrow-Gap Semiconductors and Related Materials," Adam Hilger, Bristol (1990). 1989 International Conference on Narrow Gap Semiconductors and Related Materials (NIST, Gaithersburg).
3. E. Gornik, H. Heinrich, and L. Palmetshofer (Editors), "Physics of Narrow-Gap Semiconductors," Springer-Verlag, Berlin (1982).
4. J. Raniuszkiwicz, M. Gorska, E. Kaczmarek (Editors), "Physics of Narrow-Gap Semiconductors," Elsevier Scientific Publ. Co., Warsaw (1978).
5. W. Zawadzki, (Editor), "Narrow Gap Semiconductors Physics and Applications," Springer-Verlag (Berlin) (1980).
6. Peter B. Littlewood, "Structure and Bonding in Narrow Gap Semiconductors," Critical Reviews in Solid State Science 11, 229-285 (1982).
7. C. Haas, "Special Semiconducting Materials," in Crystalline Semiconducting Materials and Devices, Ed. by P.N. Butcher, N.H. March and M.P. Tosi, Plenum Press, New York, 1986 pp. 355-394.
8. W. Scanlon in Solid State Physics, ed by F. Seitz and D. Turnbull (New York, Academic Press) 9, 83 (1959).
9. H. Welker and H. Weiss, in Solid State Physics, ed by F. Seitz and D. Turnbull (New York, Academic Press) 3, 1 (1956).
10. E.O. Kane, "Band Structure of Indium Antimonide," J. Phys. Chem Solids 1, 249 (1987).
11. W.D. Lawson, S. Nielson, A.S. Young, Solid State Physics in Electronics and Communications (London, Academic Press) p. 830 (1960).
12. Donald Long and Joseph L. Schmitt, "Mercury-Cadmium Telluride and Closely Related Alloys," in Semiconductors and Semimetals vol. 5 Ed. by R.K. Willardson and A.C. Beer, Academic Press, New York, 1970, pp. 175ff.

13. David E. Seiler, "Physics and Chemistry of Mercury Cadmium Telluride and Novel IR Detector Materials," Am. Inst. Physics, New York, 1991. One of an annual series of workshops.
14. M. Jain (Editor); II-VI Semiconductor Compounds World Scientific, Singapore, (1993).
15. S.L. Lehoczky, C.J. Summers, F.R. Szofran, and B.G. Martin, "Electrical Characterization of  $\text{Ag}_{1-x}\text{Cd}_x\text{Te}$  Alloys," in Materials Processing in the Reduced Gravity Environment of Space, Guy E. Rindone (Editor) Elsevier Publ. Co. Amsterdam (1982) pp. 421-431.
16. J.D. Patterson, W.A. Gobba, S.L. Lehoczky, "Electron mobility in n-type  $\text{Hg}_{1-x}\text{Cd}_x\text{Te}$  and  $\text{Hg}_{1-x}\text{Zn}_x\text{Te}$  alloys," J. Mater. Res. 7, 2211-2218 (1992).
17. S.K. Pantelides, "The electronic structure of impurities and other point defects in semiconductors," Rev. Mod. Phys. 50, 797 (1978).
18. Edward T. Yu, James O. McCaldin, Thomas C. McGill, "Band Offsets in Semiconductor Heterojunctions," in Solid State Physics Edited by H. Ehrenreich and D. Turnbull 46, 1-146 (1992) Academic Press, Inc. Boston.

## FIGURE CAPTIONS

- FIGURE 1      The zinc-blende lattice for MCT, if the A sites are Te the B sites are either Hg or Cd. The unit cells have side  $a$ .
- FIGURE 2      The first Brillouin Zone of the fcc lattice with several points of high symmetry given the conventional labeling.
- FIGURE 3      Sketch of calculated band structure of CdTe and HgTe for higher energies.
- FIGURE 4      (a)    Energy gap versus  $x$  for  $T = 300$  (upper line) and  $T = 77$  (lower line).  
  
                  (b)    Cut off wave length vs.  $E_g$ . The positions of several NGS are listed.
- FIGURE 5      Schematic of Kane model band structure near  $k = 0$ . Results apply to MCT for  $x \geq 0.15$ .
- FIGURE 6      MCT (upper) and MZT (lower) electron mobility for the same energy gap.  $N_d = 5 \times 10^{14}/\text{cm}^3$ ,  $N_a = 2 \times 10^{14}/\text{cm}^3$ ,  $x(\text{MCT}) = 0.193$ ,  $x(\text{MZT}) = 0.1315$ .
- FIGURE 7      Schematic of different typical point defects. (a) Interstitial atom - self or foreign. (b) Substitutional impurity. (c) Vacancy - absence of atom.
- FIGURE 8      Deep levels in MCT and MZT  
  
                  (a)    Substitutional cations in MCT.  
  
                  (b)    Substitutional cations in MZT.  
  
                  (c)    Interstitials in MCT.  
  
                  (d)    Interstitials in MZT.

**FIGURE 1**

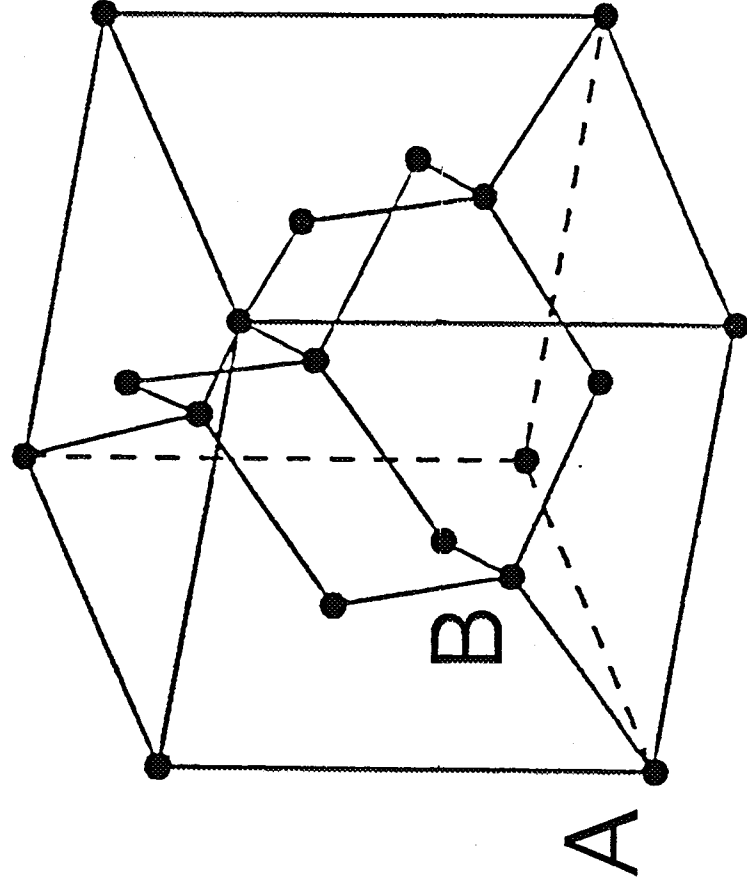
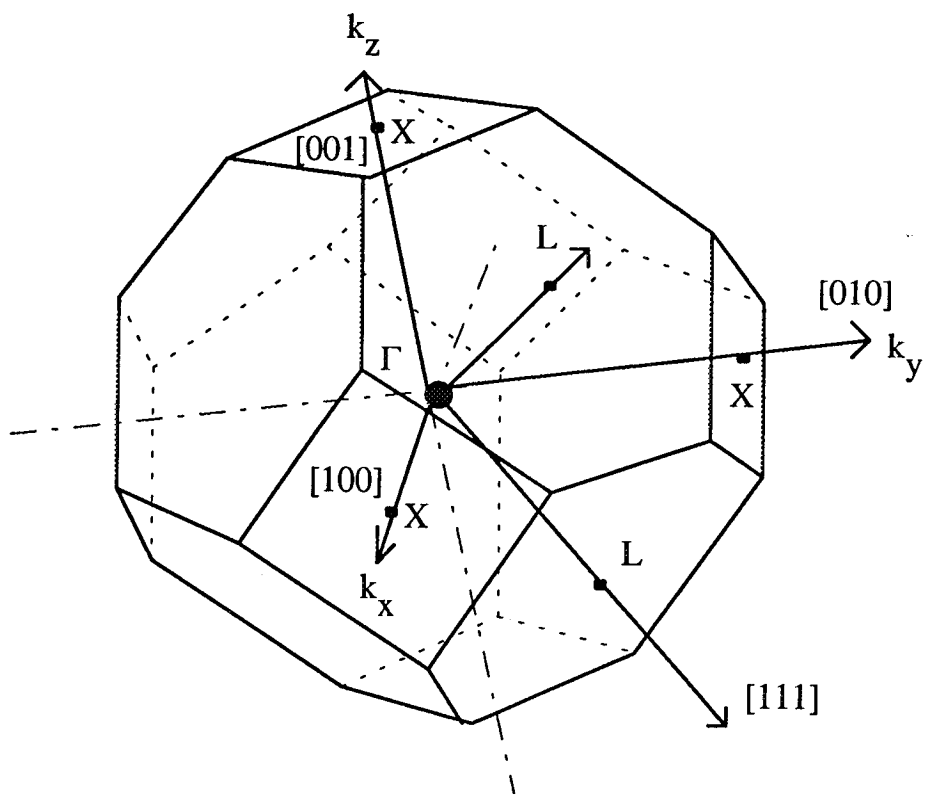


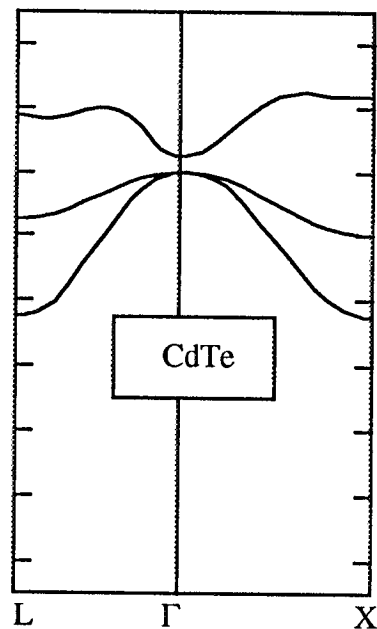
FIGURE 1



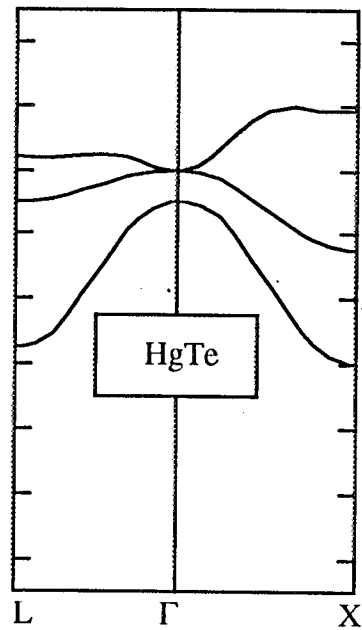
**FIGURE 2**



**FIGURE 3**



1.6 eV Energy Gap



0.0 eV Energy Gap

**FIGURE 4a**

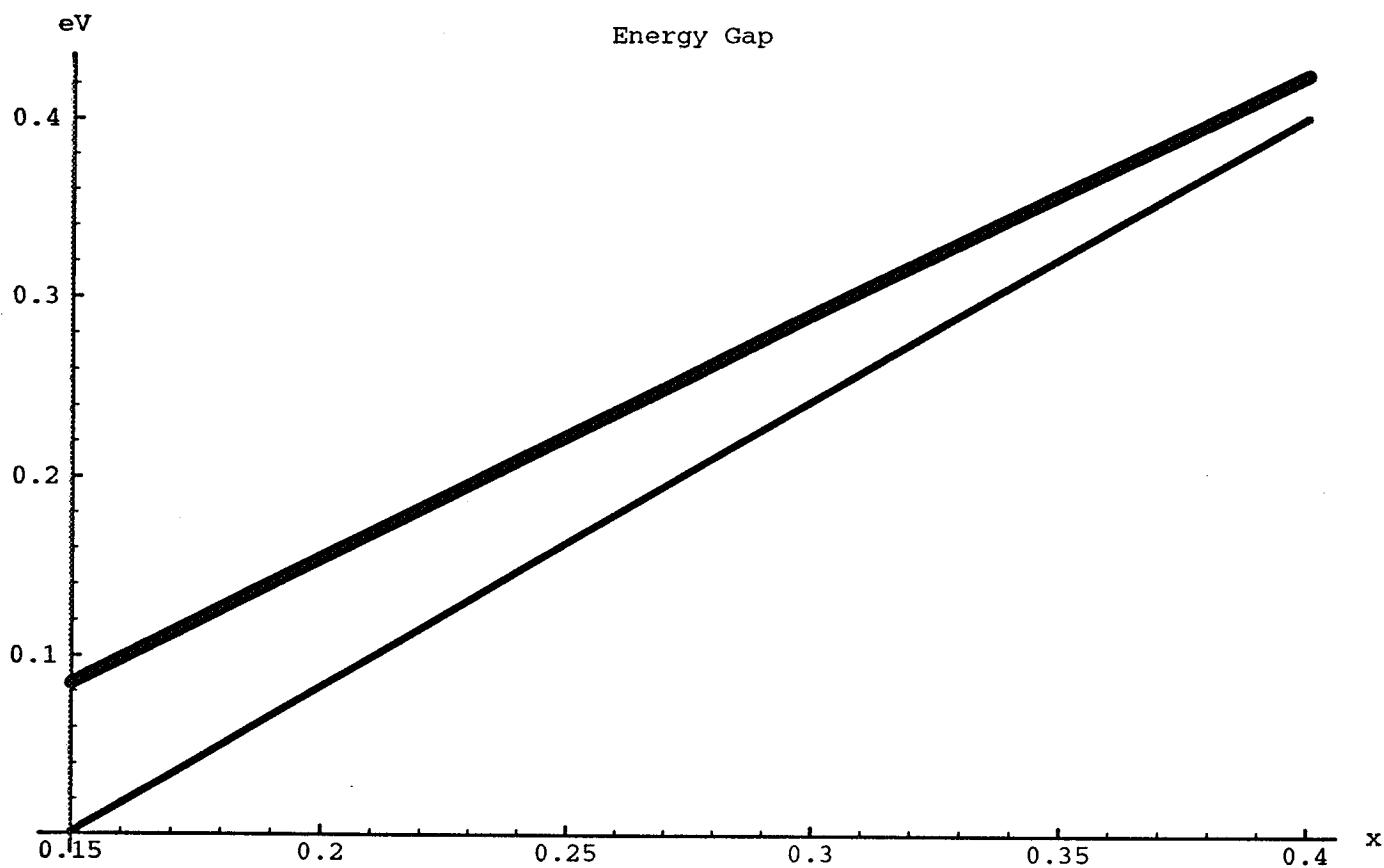
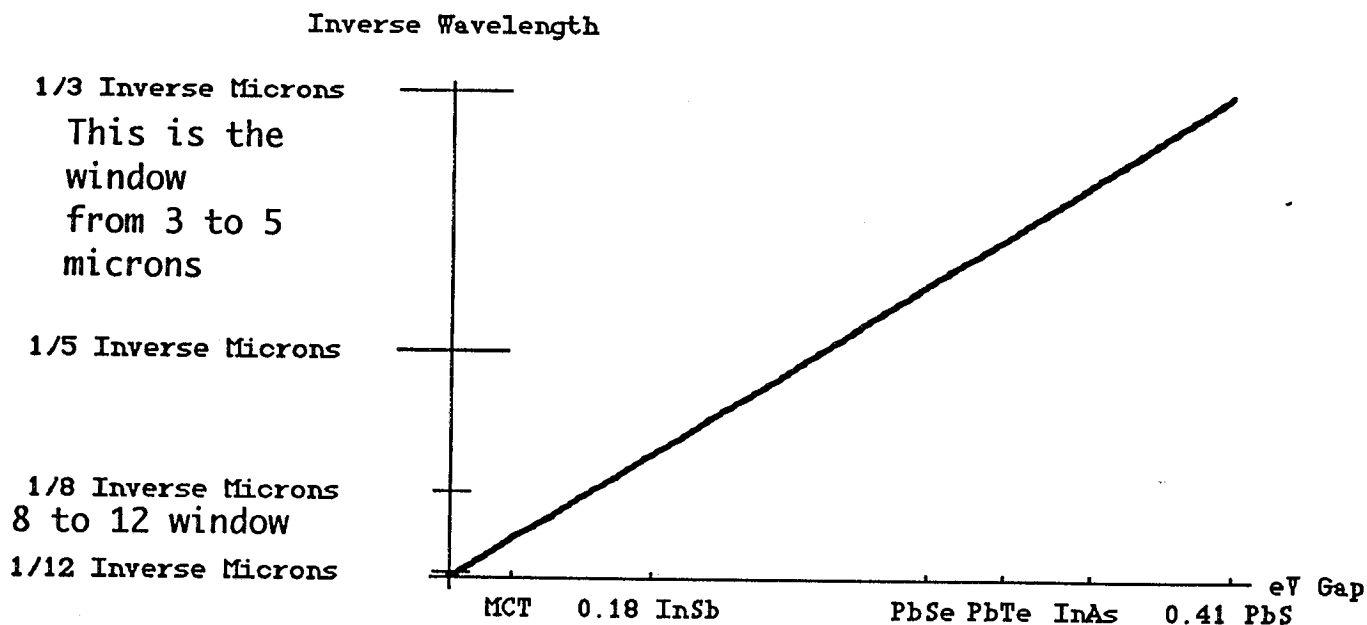


FIGURE 4a

**FIGURE 4b**





**FIGURE 5**

# Schematic of Kane Energy

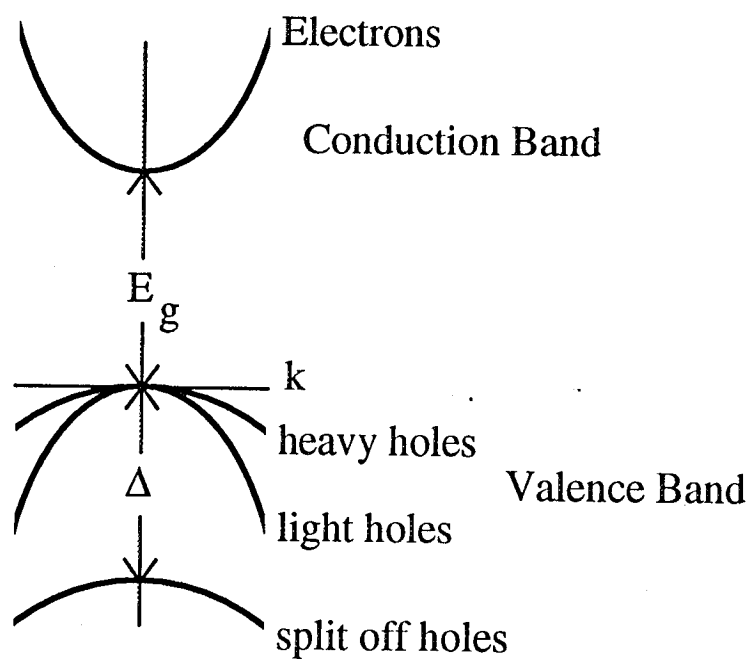


**FIGURE 6**

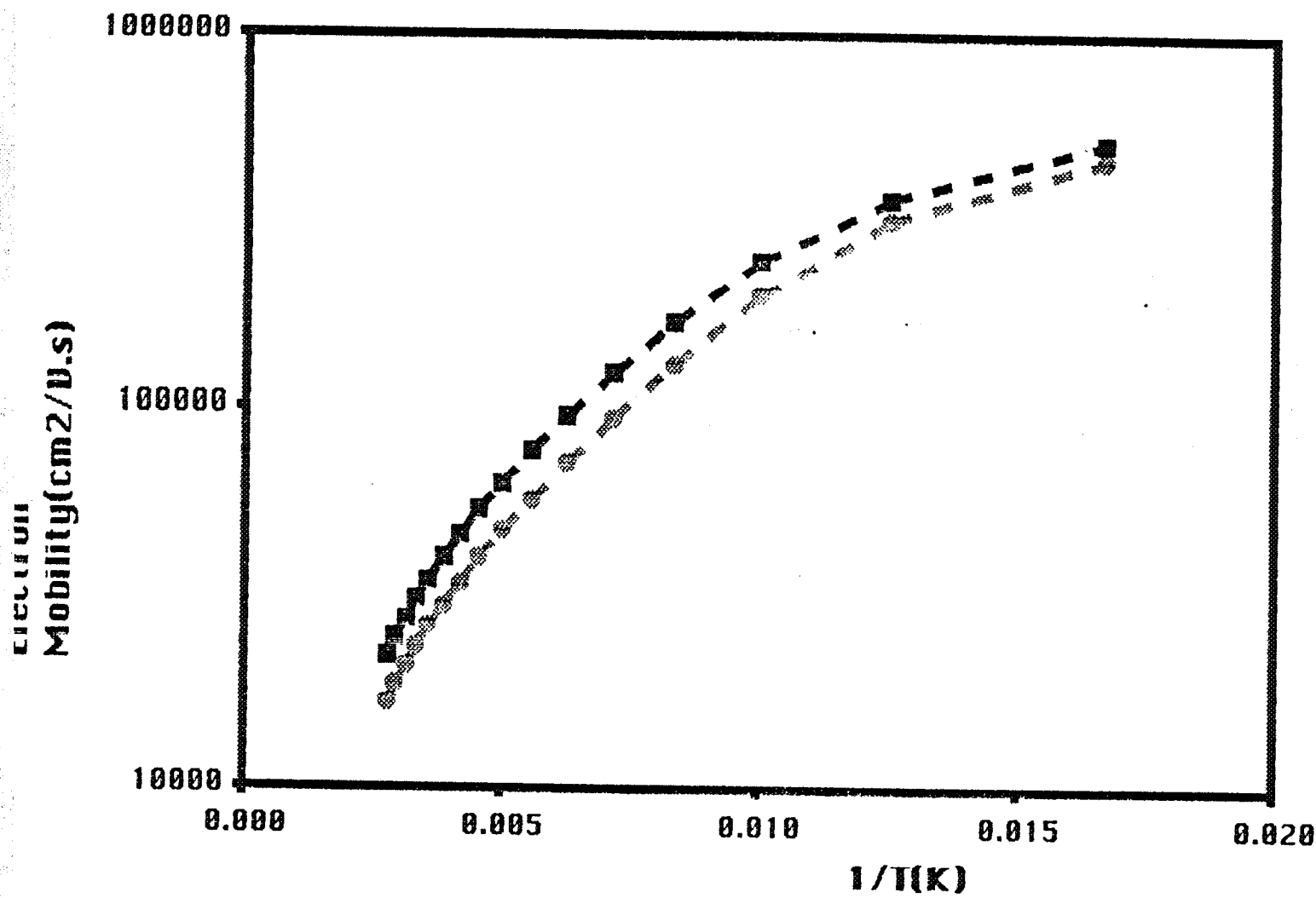
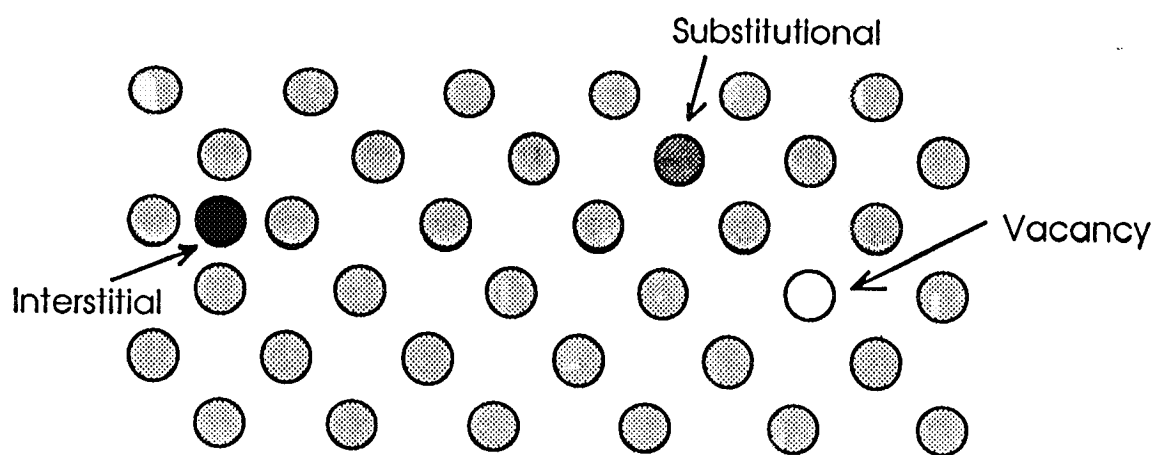


FIGURE 6

**FIGURE 7**



## POINT DEFECTS

FIGURE 7

**FIGURE 8a**

20

C-2

deep levels in MCT (cation site, s-like)

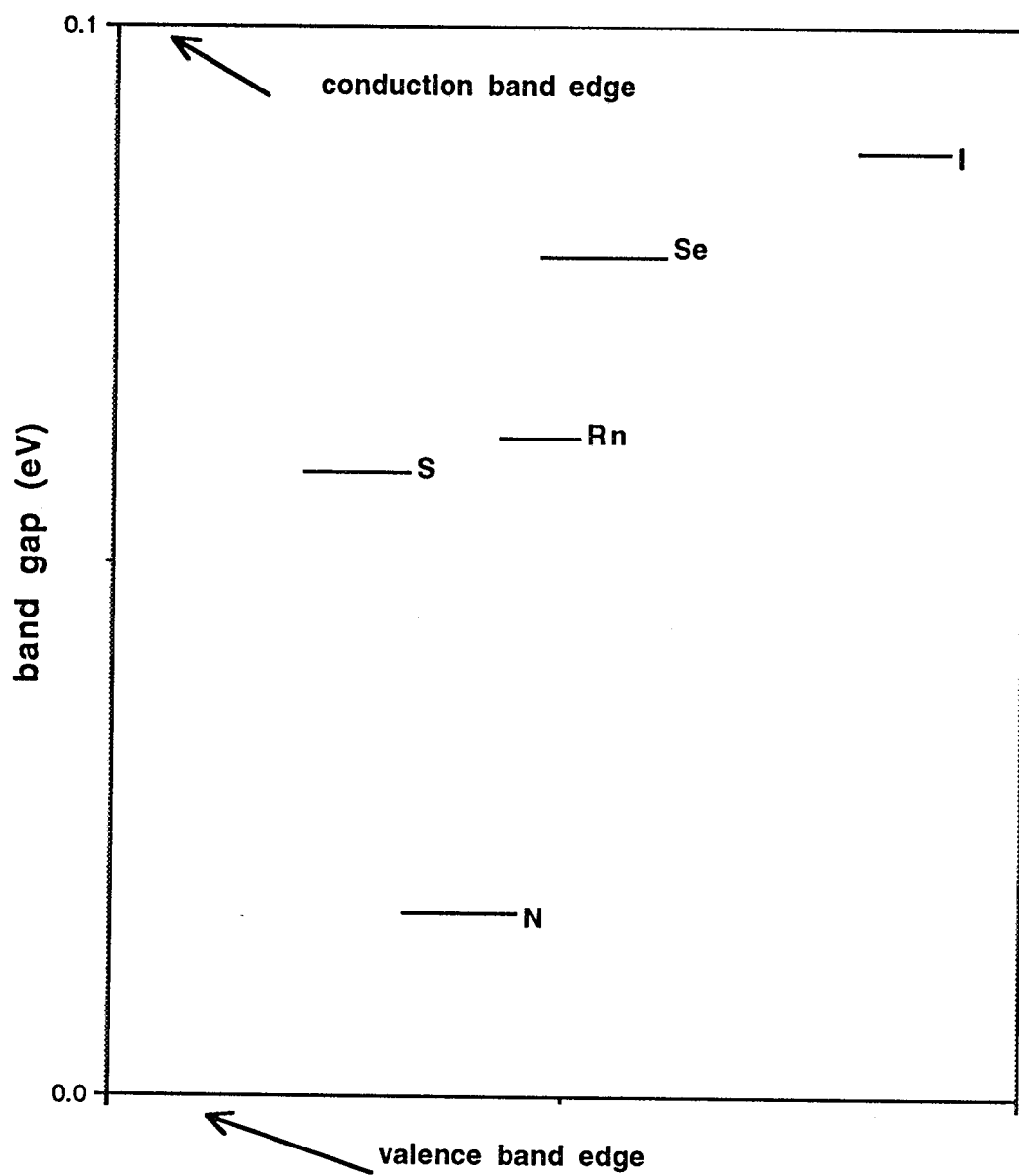




**FIGURE 8b**

deep levels in MZT (cation site, s-like)

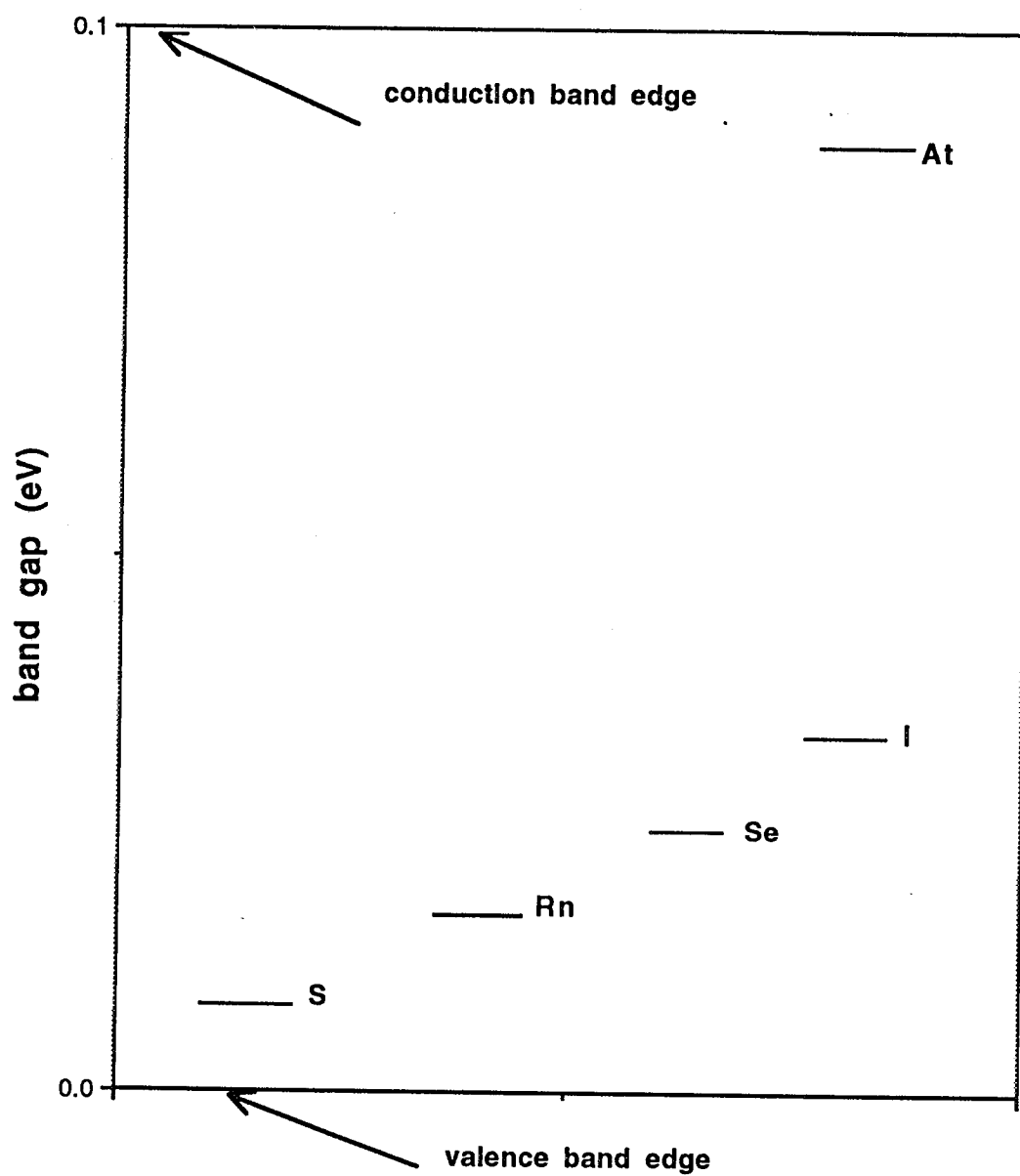


**FIGURE 8c**

deep levels induced by interstitials  
in MCT (cation site, s-like)

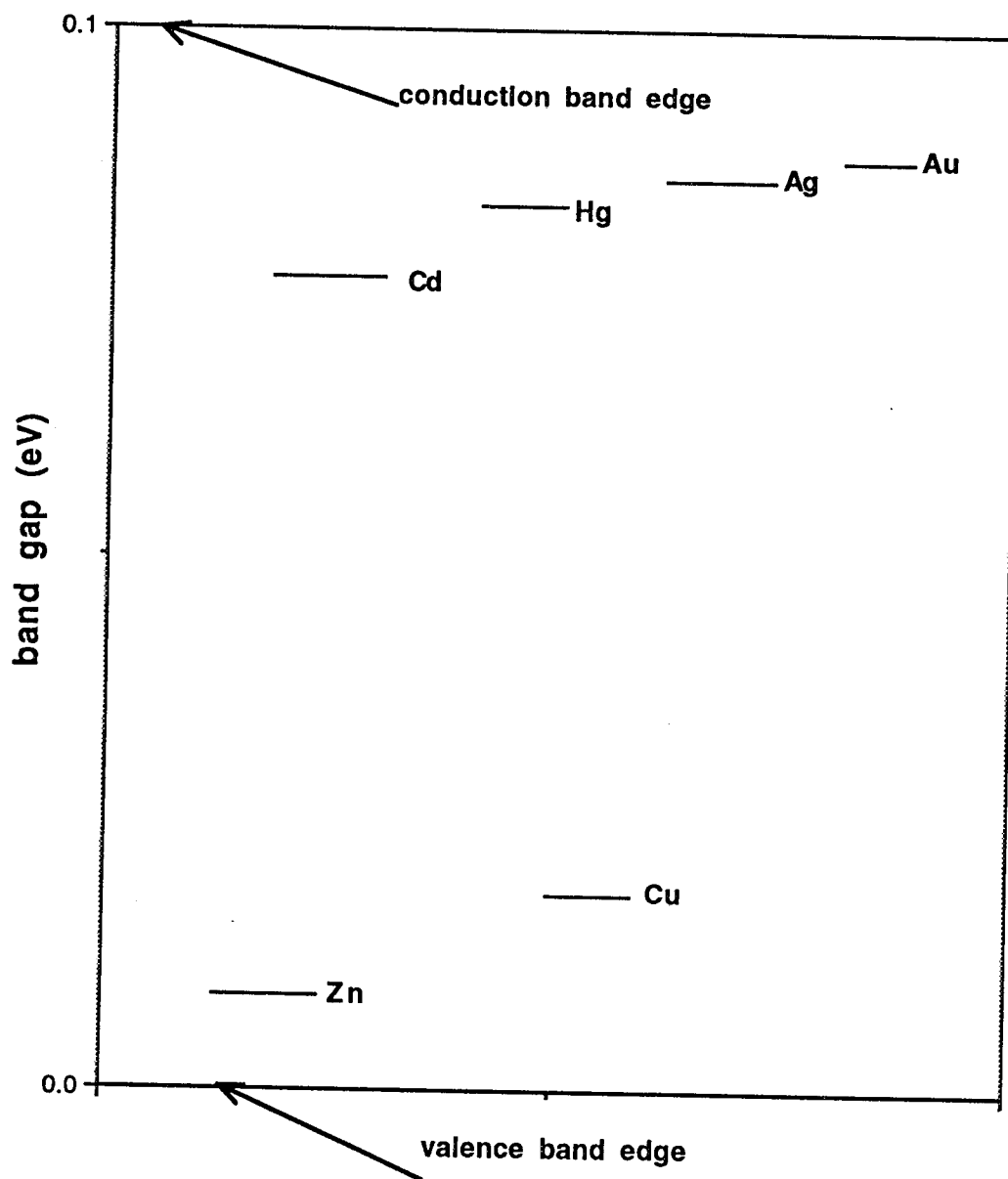


**FIGURE 8d**

deep levels induced by interstitials  
in MZT (cation site, s-like)

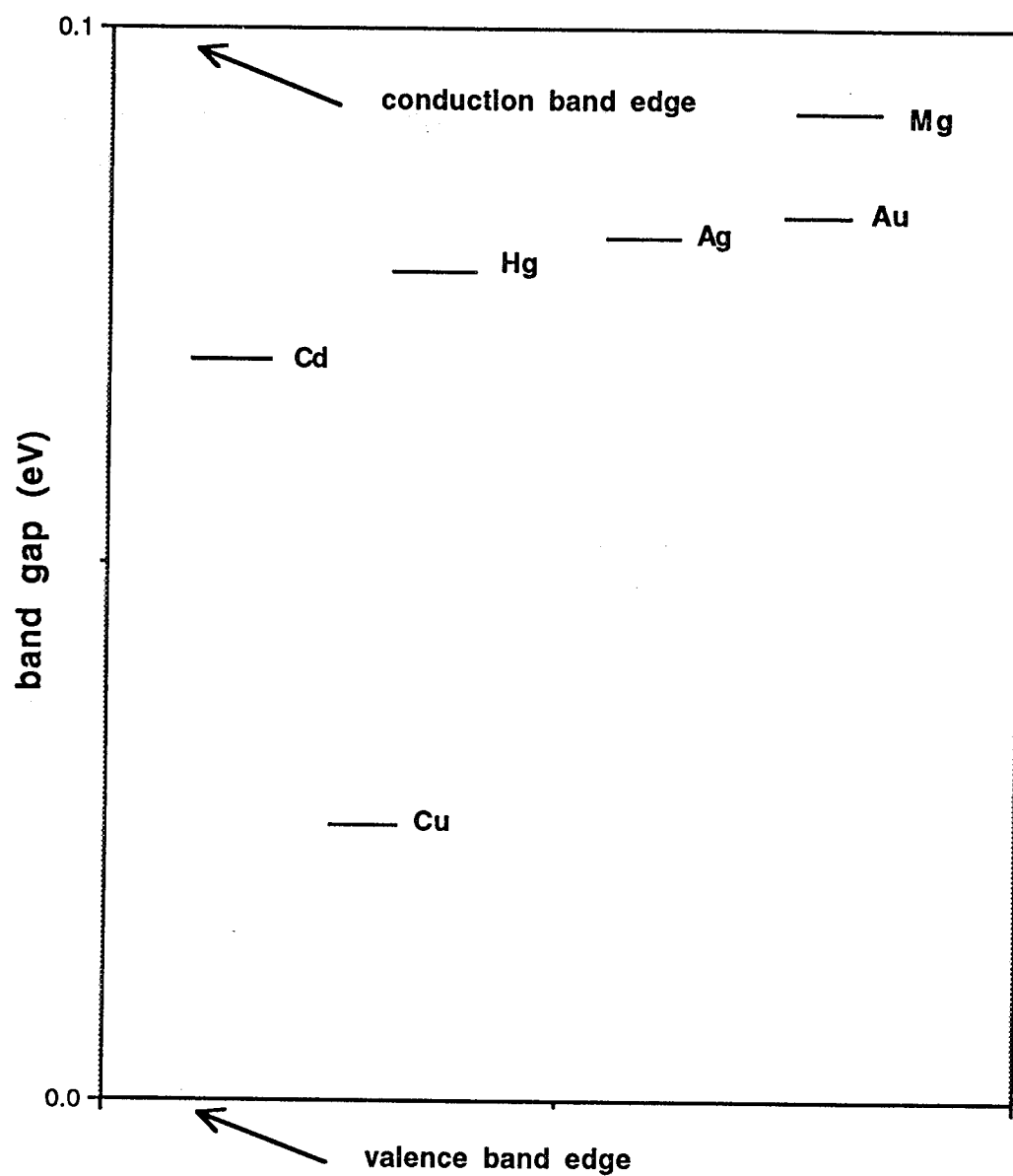


**TABLE I**  
**Narrow Gap III-V Materials**  
**and**  
**Room Temperature Bandgap**

	$E_g$
InAs	0.354 eV
InSb	0.180 eV
GaSb	0.70 eV

**TABLE II**  
**II-VI Materials**

MCT	HgCdTe	$\text{Hg}_{1-x}\text{Cd}_x\text{Te}$
MZT	HgZnTe	$\text{Hg}_{1-x}\text{Zn}_x\text{Te}$
MZS	HgZnSe	$\text{Hg}_{1-x}\text{Zn}_x\text{Se}$



**TABLE III**  
**Brief Properties of MCT**

1. A pseudo binary II-VI compound with structure isomorphic to zinc blende.
2.  $\text{Hg}_{1-x}\text{Cd}_x\text{Te}$  forms a continuous range of solid solutions between the semimetal  $\text{HgTe}$  and the semiconductor  $\text{CdTe}$ . The bandgap is tunable from 0 to about 1.6 eV as  $x$  carries from about 0.15 (at low temperature) to 1.0. The bandgap also depends on temperature, increasing linearly with temperature for a fixed value of  $x$ .
3. Useful as an infrared detector at liquid nitrogen temperature in the wavelength 8-12 microns which is an atmospheric window. A higher operating temperature than alternative materials and MCT has high detectivity, fast response, high sensitivity, IC compatible and low power.
4. The band structure involves mixing of unperturbed valence and conduction band wave function as derived by the Kane theory. They have non-parabolic bands which makes their analysis more difficult.
5. Typical carriers have small effective mass (about  $10^{-2}$  free electron mass) which implies large mobility and enhances their value as IR detectors.
6. At higher temperatures (well above 77K) the main electron scattering mechanism is the scattering by longitudinal optic modes. This scattering process is inelastic and it makes the calculation of electron mobility by the Boltzmann equation more difficult (non-iterated techniques for solving this equation do not work).
7. The small bandgap and relatively high concentration of carriers makes it necessary to include screening in the calculation of the scattering of carriers by several interactions.
8. Candidate for growth in microgravity in order to make a more perfect crystal.

**TABLE IV**  
**Some II-VI Compound Semiconductor Properties**

Atomic Number	Hg <sup>80</sup>	Cd <sup>48</sup>	Zn <sup>30</sup>	Te <sup>52</sup>
Outer Electron Configuration	5d <sup>10</sup> 6s <sup>2</sup>	4d <sup>10</sup> 5s <sup>2</sup>	3d <sup>10</sup> 4s <sup>2</sup>	5s <sup>2</sup> 5p <sup>4</sup>

	Atomic Weight	Density	Melting Point
Zn	65.38	7.14 g/cm <sup>3</sup>	693K
Cd	112.40	8.65	594K
Hg	200.59	13.6	234K
Te	127.60	6.24	723K

a in Å for unit cell

ZnTe	6.089
CdTe	6.481
HgTe	6.461

**TABLE V**

**Definition and Significance of Deep and Shallow Levels**

Shallow Levels are defect levels produced by the long range Coulomb potential of defect.

Deep Levels are defect levels produced by the central cell potential of defect.

	DEEP	SHALLOW
ENERGIES	May or May Not be Near Band Edge  Spectrum is Not Hydrogen Like	Near Band Edge  Spectrum is Hydrogen Like
TYPICAL PROPERTIES	Recombination Centers  Compensators  Electron-Hole Generators	Suppliers of Carriers

**TABLE VI**  
**Types of Deep Point Defects**

Substitutional Atoms

Interstitial Atoms

Vacancies

Antisite (Compound Semiconductors)